

A SWITCHED SYSTEMS APPROACH TO IMAGE-BASED ESTIMATION

By

ANUP PARIKH

A DISSERTATION PRESENTED TO THE GRADUATE SCHOOL  
OF THE UNIVERSITY OF FLORIDA IN PARTIAL FULFILLMENT  
OF THE REQUIREMENTS FOR THE DEGREE OF  
DOCTOR OF PHILOSOPHY

UNIVERSITY OF FLORIDA

2016

© 2016 Anup Parikh

To my parents, *Rita* and *Nilesh*, my brother, *Amit*, and my friends, for their invaluable support and encouragement

## ACKNOWLEDGMENTS

I would like to express sincere gratitude towards Dr. Warren E. Dixon, who not only provided excellent guidance in my research efforts as my academic advisor, but also mentored and shaped my career path. I would also like to extend my gratitude towards my committee members Dr. Prabir Barooah, Dr. Carl Crane, and Dr. Sean Meyn for their time and the valuable recommendations they have provided. I would also like to thank my colleagues at the University of Florida Nonlinear Controls and Robotics laboratory for the countless fruitful discussions that have helped shape the ideas in this dissertation, as well as for making my time as a graduate researcher an enjoyable and memorable one. I am also thankful for the support and encouragement provided by my family and my friends, without which this dissertation would not have been possible.

## TABLE OF CONTENTS

	<u>page</u>
ACKNOWLEDGMENTS . . . . .	4
LIST OF TABLES . . . . .	7
LIST OF FIGURES . . . . .	8
LIST OF ABBREVIATIONS . . . . .	11
ABSTRACT . . . . .	12
CHAPTER	
1 INTRODUCTION . . . . .	15
1.1 Motivation . . . . .	15
1.2 Literature Review . . . . .	16
1.3 Contributions . . . . .	21
2 SYSTEM MODEL . . . . .	24
2.1 Kinematic Motion Model . . . . .	24
2.2 Imaging Model . . . . .	29
3 STABILITY OF A CLASS OF IMAGE-BASED OBSERVERS DURING INTER- MITTENT MEASUREMENTS . . . . .	31
3.1 Structure Estimation Objective . . . . .	32
3.2 Stability Analysis . . . . .	33
3.3 Experiments . . . . .	41
3.4 Summary . . . . .	43
4 EXTENDED STABILITY RESULTS OF A CLASS OF IMAGE-BASED OB- SERVERS DURING INTERMITTENT MEASUREMENTS: STATE PREDIC- TION VIA A MOTION MODEL . . . . .	50
4.1 Structure Estimation Objective . . . . .	52
4.2 Stability Analysis . . . . .	53
4.3 Simulation . . . . .	58
4.4 Experiments . . . . .	60
4.5 Summary . . . . .	62
5 INTEGRAL CONCURRENT LEARNING: ADAPTIVE CONTROL WITH PA- RAMETER CONVERGENCE WITHOUT PE OR STATE DERIVATIVES . . . . .	81
5.1 Control Affine Dynamics . . . . .	81
5.1.1 Control Objective . . . . .	81
5.1.2 Stability Analysis . . . . .	84

5.2	Euler-Lagrange Dynamics . . . . .	86
5.2.1	Control Development . . . . .	86
5.2.2	Stability Analysis . . . . .	90
5.3	Simulation . . . . .	92
5.4	Summary . . . . .	94
6	ESTIMATION AND PREDICTION WITH MODEL LEARNING . . . . .	98
6.1	Estimation Objective . . . . .	99
6.2	Estimator Design . . . . .	101
6.2.1	Estimator . . . . .	102
6.2.2	Predictor . . . . .	103
6.3	Analysis . . . . .	103
6.4	Experiments . . . . .	108
6.5	Summary . . . . .	111
7	CONCLUSIONS . . . . .	127
	APPENDIX: AUGMENTED STATE OBSERVER . . . . .	130
	REFERENCES . . . . .	132
	BIOGRAPHICAL SKETCH . . . . .	144

LIST OF TABLES

<u>Table</u>	<u>page</u>
5-1 Average steady state RMS tracking and RMS parameter estimation errors across all simulations, for integral concurrent learning (ICL) and traditional derivative-based concurrent learning (DCL). . . . .	95

## LIST OF FIGURES

<u>Figure</u>	<u>page</u>
2-1 Reference frames and coordinate systems of a moving camera observing a moving target. . . . .	24
3-1 Representative illustration of the evolution of $W$ during the interval $[t_n^{on}, t_{n+1}^{on}]$ . . . . .	36
3-2 Evolution of the state estimates during the experiment. Vertical black lines denote switching times. . . . .	45
3-3 Evolution of the Euclidean coordinates estimate. Vertical black lines denote switching times. . . . .	46
3-4 Evolution of the estimation error. Vertical black lines denote switching times. Note the logarithmic scale. . . . .	47
3-5 Evolution of the estimation error for measurement unavailability dwell times of 0.5 to 2.5 seconds. Each plot shows three experiments (labeled A, B and C) for the listed dwell time. . . . .	48
3-6 Growth in the estimation error during each period of measurement unavailability. . . . .	49
4-1 Evolution of a Lyapunov-like function across multiple periods of losing and regaining visibility of the object. . . . .	54
4-2 True and estimated states, utilizing a predictor to evolve the state estimates when measurements are unavailable. Vertical lines represent switching times. . . . .	64
4-3 True and estimated states without a predictor. State estimates are held constant until measurements are available. Vertical lines represent switching times. . . . .	65
4-4 State estimates from the experiment with a static camera. Vertical black lines denote switches. . . . .	66
4-5 Reconstructed Euclidean coordinates of the target from the experiment with a static camera. Vertical black lines denote switches. . . . .	67
4-6 State estimation errors from the experiment with a static camera. Vertical black lines denote switches. . . . .	68
4-7 State estimates from the experiment with a moving camera. Vertical black lines denote switches. . . . .	69
4-8 Reconstructed Euclidean coordinates of the target from the experiment with a moving camera. Vertical black lines denote switches. . . . .	70
4-9 State estimation errors from the experiment with a moving camera. Vertical black lines denote switches. . . . .	71

4-10	Error growth magnitude as a function of the magnitude of the error, and corresponding bounds, for the experiment with a static camera. . . . .	72
4-11	Error growth magnitude as a function of the magnitude of the error, and corresponding bounds, for the experiment with a moving camera. . . . .	73
4-12	During one experiment, the target was commanded to follow this vector field. . . . .	74
4-13	State estimates from the experiment where the target followed a known vector field. Vertical black lines denote switches. . . . .	75
4-14	Reconstructed Euclidean coordinates of the target from the experiment where the target followed a known vector field. Vertical black lines denote switches. . . . .	76
4-15	State estimation errors from the experiment the target followed a known vector field. Vertical black lines denote switches. . . . .	77
4-16	State estimates from the experiment where the target followed a known vector field. Vertical black lines denote switches. . . . .	78
4-17	Reconstructed Euclidean coordinates of the target from the experiment where the target followed a known vector field. Vertical black lines denote switches. . . . .	79
4-18	State estimation errors from the experiment the target followed a known vector field. Vertical black lines denote switches. . . . .	80
5-1	Mean state trajectory tracking errors across all trials. . . . .	96
5-2	Mean parameter estimation errors across all trials. . . . .	97
6-1	During the first experiment, the target was commanded to follow a vector field of this form. . . . .	112
6-2	Relative position estimates for the first experiment with a stationary camera. . . . .	113
6-3	Relative orientation estimates for the first experiment with a stationary camera. . . . .	114
6-4	Evolution of the NN ideal weight estimates during the first experiment with a stationary camera. . . . .	115
6-5	Output of the NN compared with ground truth linear velocities for the first experiment with a stationary camera. . . . .	116
6-6	Output of the NN compared with ground truth orientation rates (i.e., $\frac{1}{2}B(q(t))\omega_q(t)$ ) for the first experiment with a stationary camera. . . . .	117
6-7	During the second experiment, both targets traveled along this network, randomly selecting turns at intersections . . . . .	118

6-8	Position estimates of target 1 expressed in world coordinates for the second experiment with a quadcopter observing two moving targets. . . . .	119
6-9	Orientation estimates of target 1 relative to the world coordinate system for the second experiment with a quadcopter observing two moving targets. . . . .	120
6-10	Output of the NN compared with ground truth linear velocities of target 1 for the second experiment with a quadcopter observing two moving targets. . . . .	121
6-11	Output of the NN compared with ground truth orientation rates (i.e., $\frac{1}{2}B(q(t))\omega_q(t)$ ) of target 1 for the second experiment with a quadcopter observing two moving targets. . . . .	122
6-12	Position estimates of target 2 expressed in world coordinates for the second experiment with a quadcopter observing two moving targets. . . . .	123
6-13	Orientation estimates of target 2 relative to the world coordinate system for the second experiment with a quadcopter observing two moving targets. . . . .	124
6-14	Output of the NN compared with ground truth linear velocities of target 2 for the second experiment with a quadcopter observing two moving targets. . . . .	125
6-15	Output of the NN compared with ground truth orientation rates (i.e., $\frac{1}{2}B(q(t))\omega_q(t)$ ) of target 2 for the second experiment with a quadcopter observing two moving targets. . . . .	126

## LIST OF ABBREVIATIONS

CL	Concurrent Learning
DOF	Degrees of Freedom
EKF	Extended Kalman Filter
FOV	Field of View
ICL	Integral Concurrent Learning
LTl	Linear Time Invariant
NCS	Network Control Systems
NN	Neural Network
PE	Persistent Excitation
SfM	Structure from Motion
SLAM	Simultaneous Localization and Mapping
ZOH	Zero-Order Hold

Abstract of Dissertation Presented to the Graduate School  
of the University of Florida in Partial Fulfillment of the  
Requirements for the Degree of Doctor of Philosophy

A SWITCHED SYSTEMS APPROACH TO IMAGE-BASED ESTIMATION

By

Anup Parikh

August 2016

Chair: Warren E. Dixon  
Major: Aerospace Engineering

With the advent of technological improvements in imaging systems and computational resources, as well as the development of image-based reconstruction techniques, it is necessary to understand algorithm performance when subject to real world conditions. Specifically, this dissertation focuses on the stability and performance of a class of image-based observers in the presence of intermittent measurements, caused by e.g., occlusions, limited FOV, feature tracking losses, communication losses, or finite frame rates.

Observers or filters that are exponentially stable under persistent observability may have unbounded error growth during intermittent sensing, even while providing seemingly accurate state estimates. In Chapter 3, dwell time conditions are developed to guarantee state estimation error convergence to an ultimate bound for a class of observers while undergoing measurement loss. Bounds are developed on the unstable growth of the estimation errors during the periods when the object being tracked is not visible. A Lyapunov-based analysis for the switched system is performed to develop an inequality in terms of the duration of time the observer can view the moving object and the duration of time the object is out of the field of view.

In Chapter 4, a motion model is used to predict the evolution of the states of the system while the object is not visible. This reduces the growth rate of the bounding function to an exponential and enables the use of traditional switched systems Lyapunov

analysis techniques. The stability analysis results in an average dwell time condition to guarantee state error convergence with a known decay rate. In comparison with the results in Chapter 3, the estimation errors converge to zero rather than a ball, with relaxed switching conditions, at the cost of requiring additional information about the motion of the feature.

In some applications, a motion model of the object may not be available. Numerous adaptive techniques have been developed to compensate for unknown parameters or functions in system dynamics; however, persistent excitation (PE) conditions are typically required to ensure parameter convergence, i.e., learning. Since the motion model is needed in the predictor, model learning is desired; however, PE is difficult to insure *a priori* and infeasible to check online for nonlinear systems. Concurrent learning (CL) techniques have been developed to use recorded data and a relaxed excitation condition to ensure convergence. In CL, excitation is only required for a finite period of time, and the recorded data can be checked to determine if it is sufficiently rich. However, traditional CL requires knowledge of state derivatives, which are typically not measured and require extensive filter design and tuning to develop satisfactory estimates. In Chapter 5 of this dissertation, a novel formulation of CL is developed in terms of an integral (ICL), removing the need to estimate state derivatives while preserving parameter convergence properties.

Using ICL, an estimator is developed in Chapter 6 for simultaneously estimating the pose of an object as well as learning a model of its motion for use in a predictor when the object is not visible. A switched systems analysis is provided to demonstrate the stability of the estimation and prediction with learning scheme. Dwell time conditions as well as excitation conditions are developed to ensure estimation errors converge to an arbitrarily small bound.

Experimental results are provided to illustrate the performance of each of the developed estimation schemes. The dissertation concludes with a discussion of the

contributions and limitations of the developed techniques, as well as avenues for future extensions.

## CHAPTER 1 INTRODUCTION

### 1.1 Motivation

Recent advances in imaging technology and computer hardware have enabled the use of vision sensors for recovering information about the operating environment for autonomous systems. Example applications include object tracking [1, 2], scene reconstruction and 3D modeling [3–5], object and location identification [6, 7], facial recognition [8–10], motion estimation [11, 12] and simultaneous localization and mapping (SLAM) [13–17]. Coupled with the development of nonlinear control theory, cameras are an ideal feedback sensor for various autonomous systems. However, several estimation and control challenges persist. Most of these challenges stem from the fact that full state feedback of observed features is not available: 3D coordinates of features cannot be immediately reconstructed since the imaging process involves the projection of the feature onto a 2D image plane (i.e., the range to any feature is lost). One method to compensate for the lack of range information is to use multiple overlapping images from multiple cameras (e.g., stereo vision). Depth information is derived from the parallax induced by the relative translation around a feature, however features farther away from the camera require larger relative translation to induce sufficient parallax. This introduces a drawback of requiring multiple cameras for depth recovery in that the cameras must be aligned for a specific range of targets, and for many applications it is challenging to separate the cameras sufficiently to provide a large enough baseline to accurately recover depth information. An alternate approach to multiple cameras is to use a single camera that acquires multiple images that can be compared, where the motion of the camera (e.g, in vehicular systems) provides sufficient parallax. This approach is often called Structure from Motion (SfM).

Two significant issues with using cameras for feedback are the intermittent loss of features (e.g., due to occlusions, feature tracking losses, limited camera field of

view, etc) and the slow sampling rate (which can be modeled as a periodic loss of features). In this dissertation, a switched systems framework is investigated to analyze the stability of observers during intermittent loss of feature observation. During periods in which the feature is outside the camera field of view (FOV) or in between frames of a video stream, the error dynamics are unstable, and although the estimation error may even be exponentially stable during the observable periods, the estimates may still diverge in the limit if the feature is unobservable for long periods of time. By using switched systems theory, sufficient conditions on the visibility time can be developed to guarantee convergence at a known rate. This analysis provides a condition for trusting the state estimates from the observer and an updated performance metric (via the error decay rate) based on the error growth rate during the unobservable periods. These conditions can also be used to ease trajectory generation constraints. For example, traditional visual servoing requires that the features remain in the camera FOV, which may be difficult for a camera mounted on a nonholonomic vehicle [18]. By relaxing this constraint (i.e., by allowing the target to temporarily leave the FOV), more efficient guidance laws may be designed.

## 1.2 Literature Review

Solutions to the SfM problem can be broadly classified as either batch or recursive methods. Batch (or offline) methods rely on epipolar constraints and employ a nonlinear optimization technique to determine both the relative camera pose between images and the 3D feature coordinates, up to an unknown scale [19–21]. Recursive (or online) techniques formulate a dynamic system to represent the relative motion of the feature with respect to the camera, and utilize state estimators or observers to reconstruct 3D feature coordinates. These online methods are more appropriate for real time applications since they only store current state estimates and generate new estimates using only the new image information. Examples of observers or filters for solving the SfM problem are provided in [22–28]. Observer based methods have also been applied

to the reverse problem of determining feature depth with a stationary camera and known feature motion [29–35]. In these cases, the feature motion is expressed as an affine dynamical system with partially unmeasurable states, expressed in coordinates relative to the fixed camera. Finally, observers have been used to recover the relative depth of a moving feature from a moving camera with known velocities [36]. In each of these cases, continuous observation of the features is assumed.

Removing the continuous observation requirement has been investigated for problems where the objective is to track the 2D image coordinates of features that undergo temporary occlusions. For example, authors in [37] construct autoregressive models for features while they are in view, and then use the models to predict the location of a feature of interest when it is occluded. Similarly, in [38, 39] Kalman or particle filters are used to estimate feature motion and predict feature coordinates while occluded. In contrast to using dynamic models, authors in [40–42] use visual context to increase the robustness of feature trackers to occlusions. All of these methods aid in tracking the target location on the image plane (i.e. only tracking feature points in images), and must be used in conjunction with SfM techniques to provide a continuous estimate of the full 3D target coordinates while undergoing intermittent observability loss. In [43], a SfM technique that is robust to occlusions or feature tracking losses is developed, but only the shape of the object is recovered due to the orthogonal projection model, and not the 3D position of the object relative to the camera.

Examples of filters that are robust to missing measurements are provided in [44–60]. In [44, 47–51, 54–58, 60–71], measurement loss is modeled as a random Bernoulli process with known probability. As a result, filter stability can only be shown in the stochastic sense, i.e. only the expected value of the estimation error is shown to asymptotically converge. In this dissertation, no assumption is made on the nature of switching; any switching sequence that meets certain dwell time conditions is shown to be stable. Furthermore, for some of the previous results (e.g., [44, 50, 55, 57, 61–66, 71]),

measurement loss is imperceptible, and measurements consisting of only noise are incorporated into the state estimates. For the machine vision applications discussed in this dissertation, loss of feature tracking is detectable, and therefore erroneous measurements are not incorporated into the state estimates.

Estimation and control with limited measurements has also been extensively studied in the networked control systems (NCS) literature [44, 72–77]. Typically, the problem is formulated as a sensor and decision maker separated from the estimator or controller by a wired or wireless network. In [72, 75–77], the sensor makes decisions on when to send sensor information to minimize the use of network bandwidth whereas in [73] and [74] data loss is due to the unreliable communication channel. In both cases, a model of the controlled system is used to propagate state estimates during the periods when sensor data is unavailable. The dwell time conditions arise from the requirement that a Lyapunov-like function must have an overall decreasing trend. This is less strict than other results where the function must decrease across repeated activations of every subsystem; in this work, the functions may increase for short durations. Also, in contrast to some NCS literature [72, 75–77], the results in this work are also applicable to cases when loss of observability is uncontrollable.

Many of the probabilistic approaches for SfM, or the associated SLAM problem, utilize a predictor or circumvent the intermittent sensing issue by only updating state estimates when new measurements are available (see [78] and [79] for an overview). However, these approaches are based on either linearizations of the nonlinear dynamics (e.g., [80–85]), and therefore only show local convergence, or are sample based (e.g., [86] and [87]), and therefore can only show optimal estimation in the limit as the number of samples approach infinity. Much of the recent literature on target tracking has focused on using suboptimal algorithms for tracking using simplified motion models (e.g., constant velocity, constant turn rate, etc.), with a focus on reduced complexity and improving practical performance, and do not analyze estimation error growth due

to model uncertainty or show estimation error convergence [88, 89]. Some methods explicitly handle occlusions, though they either assume availability of range measurements and only estimate position, therefore rendering the system linear, e.g., [90–92], or only estimate relative depth ordering and do not consider the pose estimation problem, e.g., [93]. Other methods attempt to learn a model of the target motion online using function approximation methods, e.g., [94–99], though do not provide a convergence analysis. Conversely, the full nonlinear dynamics are analyzed in this dissertation, and the proposed estimation framework has computing requirements that can be met by typical or low-end modern computers (e.g., see experimental results in the following chapters). Furthermore, convergence and consistency proofs of probabilistic estimators typically require knowledge of the probability distribution of the uncertainty in the system, and result in convergence in mean or in mean square. In comparison, analysis of deterministic observers typically assume boundedness and some level of smoothness of disturbances, and yield asymptotic or exponential convergence. The primary contribution of this work is in the development and analysis of a framework to show robustness to intermittent measurements when utilizing deterministic, image-based observers.

The inherent switching in the system caused by the loss of visibility of features prompts the use of Lyapunov-based, hybrid systems analysis techniques to examine the stability of the observers of interest. The systems considered in this dissertation are classified as switched systems, where the states of the system (i.e. the estimation error) are continuous functions of time while the time derivatives of the states are discontinuous with respect to time [100]. Switched systems are a subset of hybrid systems, where both the states and state derivatives are functions that can be discontinuous with respect to time. Although the true states and their derivatives are continuous in the systems considered in this work, the update law for the state estimates change based on whether the feature is visible to the camera, causing discontinuities in the estimation error derivatives, and the classification as a switched system

The overarching strategy for proving stability of switched systems is to first show stability of the individual subsystems through a traditional Lyapunov analysis, and then develop switching conditions upon which the overall system will remain stable. The latter is required because of the well known phenomenon that pathological switching between stable subsystems can cause instability [101]. One approach to demonstrating stability of switching is to use a common Lyapunov function for all subsystems. If the time derivative of the Lyapunov function can be upper bounded by a common negative definite function for all subsystems, the overall system is stable [101]. In some cases, one cannot determine a common Lyapunov function for every stable subsystem. For example, a common Lyapunov function cannot be developed for a set of linear systems, where the solution of the Lyapunov equation,  $P$ , is used in the quadratic Lyapunov function for stability and is dependent on the system matrix,  $A$ , of each subsystem. In these cases, the subsystem-specific Lyapunov function of the active subsystem is used to model the energy decay of the overall system, and switching between subsystems causes jumps in the overall energy storage function. Bounding the jumps and enforcing the requirement that every subsystem-specific Lyapunov function must decrease between successive activations of its respective subsystem results in conditions on when switching between subsystems may occur to guarantee stability. These conditions typically manifest as forward, reverse, or average subsystem dwell time requirements [101], i.e. conditions on how long subsystems must remain active before switching.

Complications arise when a subset of the subsystems are unstable. For the applications discussed in this dissertation, when the feature of interest is not visible to the camera, measurements are not available to estimate the state of the system, and the estimation errors grow. For linear time invariant (LTI) systems with stable and unstable subsystems, the authors in [102] develop an average dwell time condition to ensure stability. Since the subsystems are all LTI, state trajectories are exponential,

and a condition on the overall time spent in the stable and unstable systems can be developed based on the ratio of maximum unstable eigenvalues and minimum stable eigenvalues. Similar conditions were developed in [103] for nonlinear switched systems with exponentially stable and exponentially unstable subsystems. However, in Chapter 3, the unstable system is not exponentially unstable, and therefore algebraic simplifications cannot be determined that yield the less restrictive average dwell time conditions.

To relax dwell time conditions arising from the stability analysis, a predictor can be utilized to update state estimates when measurements are not available. However, prediction based on the state dynamics requires knowledge of a motion model of the target to generate target velocity signals. A number of adaptive methods have been developed to compensate for unknown functions or parameters in the dynamics, however, parameter estimates may not approach the true parameters without persistent excitation (PE) [104–106]. The PE condition cannot be guaranteed a priori for nonlinear systems, and is difficult to check online, in general. Recently, a technique known as concurrent learning (CL) was developed to use recorded data for online parameter estimation [107–109] without PE. In CL, input and state derivatives are recorded and used similar to recursive least squares to establish a negative definite parameter estimation error term in the Lyapunov analysis, and hence a negative definite Lyapunov derivative, provided a finite excitation condition is satisfied. However, state derivatives can be noisy, and require extensive filter design and tuning to yield satisfactory signals for use in CL. A novel formulation of CL is developed in Chapter 5 that removes the need for state derivatives while still maintaining convergence guarantees.

### **1.3 Contributions**

In Chapter 3, a class of image-based observers are analyzed to investigate stability and performance in the presence of intermittent measurements. In particular, a framework is constructed that utilizes an exponential observer when measurements are

available, and performs a zero order hold when measurements are unavailable. Bounds on the target velocity are used to bound the growth of the error during the unobservable periods and therefore the position of the target is bounded by a sphere that grows with time at a rate proportional to the maximum target velocity. Consequently, the Lyapunov-like function grows with a bound based on the trigonometric tangent function, resulting in a maximum contiguous duration in which the target can remain unobservable. The contribution of Chapter 3 is in the development of the dwell time and reverse dwell time requirements for estimator error convergence for uncertain nonlinear dynamics which exhibit finite escape time (i.e., faster than exponential) instabilities. Calculation of the dwell times only requires knowledge of the bounds of the target velocity. Experimental results are provided to illustrate the performance of this approach, and the effect of varying the amount of time measurements are unavailable.

A similar framework is constructed in Chapter 4, however a predictor is used to update the state estimates when measurements are not available. This results in an average dwell time condition and an average unmeasurability time condition, as opposed to the maximum time for each period of measurement unavailability. However, a motion model in the form of a feedback law is required to achieve these results. A contribution of Chapter 4 is the extension of one of the stability results in [103] to nonautonomous nonlinear switched systems by use of nonautonomous Lyapunov-like functions. An additional contribution of Chapter 4 is the development of an observer and predictor structure, and the application of the extended stability result to determine the performance of this combined estimator during intermittent switching. A comparison between the results in Chapters 3 and 4 demonstrate the tradeoff between the amount of information that is known about the target and the allowable flexibility in observation of the target for successful tracking. Experimental results are provided to demonstrate the performance of this approach as well as to compare with a similar probabilistic approach, namely an extended Kalman filter.

A stepping stone to removing the requirement of a known motion model in order to implement a predictor is provided in Chapter 5. A novel online adaptive update law that ensures parameter convergence, and hence, exponential convergence for adaptive controllers is developed in Chapter 5. Compared to other adaptive controllers that ensure parameter convergence, the ICL controller developed in this chapter does not require PE, and an eigenvalue procedure can be implemented to check if sufficient data has been collected for learning. A contribution of this chapter is that the CL technique is reformulated in terms of an integral, removing the need for state derivatives, while preserving convergence guarantees. Compared to traditional adaptive methods that utilize PE to ensure parameter convergence, and hence exponential convergence, CL and ICL only requires excitation for a finite period of time, and the excitation condition can be checked online. The ICL technique is formulated for both general control affine and Euler-Lagrange systems. Monte Carlo simulation results are provided to demonstrate the reduction in parameter estimation error as well as tracking error for an example system in the presence of measurement noise when compared to the traditional derivative-based CL.

In Chapter 6, a framework similar to Chapter 4 is developed to estimate the pose of a target in the presence of intermittent measurements. Similar to Chapter 4, a predictor is used when measurements are not available, thereby reducing the rate of estimation error growth when measurements are unavailable. Unlike Chapter 4, the motion model of the target is assumed unknown, and learned online using the techniques developed in Chapter 5. Further, the full 6 degree of freedom (DOF) pose of the target are estimated. The estimation errors are shown to converge to an arbitrarily small bound provided an average dwell time condition over a finite number of switches is satisfied. Experimental results are included to illustrate the performance of this approach.

## CHAPTER 2 SYSTEM MODEL

The development in this section is focused on the dynamics of the vision system of interest, as well as basic underlying assumptions, that will be used for the subsequent results in Chapters 3, 4 and 6.

### 2.1 Kinematic Motion Model

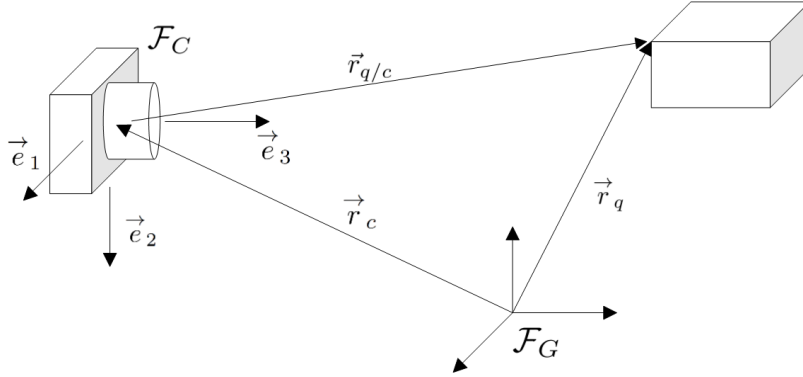


Figure 2-1. Reference frames and coordinate systems of a moving camera observing a moving target.

In the following development, the notation  $(\vec{\cdot})$  is used to denote geometric vectors, i.e. members of  $\mathbb{E}^3$ , and is distinguished from its  $\mathbb{R}^3$  expression in any particular reference frame. Figure 2-1 is used to develop the image kinematics. In Figure 2-1,  $\mathcal{F}_G$  denotes an inertial reference frame fixed with arbitrarily selected origin and Euclidean coordinate system and  $\mathcal{F}_C$  denotes a reference frame fixed to the camera. The right handed coordinate system attached to  $\mathcal{F}_C$  has an origin at the principle point of the camera,  $\vec{e}_3 \in \mathbb{E}^3$  axis pointing out and collinear with the optical axis of the camera,  $\vec{e}_1 \in \mathbb{E}^3$  axis aligned with the horizontal axis of the camera and  $\vec{e}_2 \triangleq \vec{e}_3 \times \vec{e}_1 \in \mathbb{E}^3$ . The vectors  $\vec{r}_q(t) \in \mathbb{E}^3$  and  $\vec{r}_c(t) \in \mathbb{E}^3$  represent the vectors from the origin of  $\mathcal{F}_G$  to the target and the camera principle point, respectively. The position of the target relative to the camera is then given by

$$\vec{r}_{q/c}(t) \triangleq \vec{r}_q(t) - \vec{r}_c(t) \in \mathbb{E}^3. \quad (2-1)$$

The vector  ${}^C\vec{v}_{q/c}(t) \in \mathbb{E}^3$  represents the relative velocity as viewed by an observer in the camera frame, defined as

$${}^C\vec{v}_{q/c}(t) \triangleq {}^C\frac{d}{dt}\vec{r}_{q/c}(t).$$

The relative velocity can be related to the time derivative with respect to the ground frame as

$${}^C\frac{d}{dt}\vec{r}_{q/c}(t) = {}^G\frac{d}{dt}\vec{r}_{q/c}(t) - {}^G\vec{\omega}^C(t) \times \vec{r}_{q/c}(t), \quad (2-2)$$

where  ${}^G\vec{\omega}^C(t) \in \mathbb{E}^3$  is the angular velocity of the camera frame with respect to the ground frame. Using (2-1),  ${}^G\frac{d}{dt}\vec{r}_{q/c}(t)$  can be expanded as

$${}^G\frac{d}{dt}\vec{r}_{q/c}(t) = {}^G\vec{v}_q(t) - {}^G\vec{v}_c(t), \quad (2-3)$$

where  ${}^G\vec{v}_q(t) \in \mathbb{E}^3$  is the linear velocity of the target as viewed by an observer in the ground frame, defined as  ${}^G\vec{v}_q(t) \triangleq {}^G\frac{d}{dt}\vec{r}_q(t)$ , and  ${}^G\vec{v}_c(t) \in \mathbb{E}^3$  is the linear velocity of the camera as viewed by an observer in the ground frame, defined as  ${}^G\vec{v}_c(t) \triangleq {}^G\frac{d}{dt}\vec{r}_c(t)$ .

Substituting (2-3) into (2-2) yields

$${}^C\frac{d}{dt}\vec{r}_{q/c}(t) = {}^G\vec{v}_q(t) - {}^G\vec{v}_c(t) - {}^G\vec{\omega}^C(t) \times \vec{r}_{q/c}(t). \quad (2-4)$$

In the following derivation, all vectors are expressed in the camera coordinate system, i.e. the basis fixed in  $\mathcal{F}_C$ . Let  $r_{q/c}(t)$ ,  ${}^Gv_q(t)$ ,  ${}^Gv_c(t)$ ,  ${}^G\omega^C(t) \in \mathbb{R}^3$  denote the expressions of  $\vec{r}_{q/c}(t)$ ,  ${}^G\vec{v}_q(t)$ ,  ${}^G\vec{v}_c(t)$  and  ${}^G\vec{\omega}^C(t)$  in the camera coordinate system, respectively, and be defined as

$$r_{q/c}(t) \triangleq \begin{bmatrix} X(t) & Y(t) & Z(t) \end{bmatrix}^T, \quad (2-5)$$

$${}^Gv_q(t) \triangleq \begin{bmatrix} v_{q1}(t) & v_{q2}(t) & v_{q3}(t) \end{bmatrix}^T, \quad (2-6)$$

$${}^Gv_c(t) \triangleq \begin{bmatrix} v_{c1}(t) & v_{c2}(t) & v_{c3}(t) \end{bmatrix}^T, \quad (2-7)$$

$${}^G\omega^C(t) \triangleq \begin{bmatrix} \omega_1(t) & \omega_2(t) & \omega_3(t) \end{bmatrix}^T, \quad (2-8)$$

where  $X(t), Y(t), Z(t) \in \mathbb{R}$  denote the Euclidean coordinates of the target position relative to the camera position,  $v_{q1}(t), v_{q2}(t), v_{q3}(t) \in \mathbb{R}$  denote the linear velocities of the target with respect to ground frame,  $v_{c1}(t), v_{c2}(t), v_{c3}(t) \in \mathbb{R}$  denote the linear velocities of the camera with respect to the ground frame and  $\omega_1(t), \omega_2(t), \omega_3(t) \in \mathbb{R}$  denote the angular velocity of the camera frame with respect to the ground frame.

Substituting (2-5), (2-6), (2-7), and (2-8) into (2-4) results in

$$\begin{aligned} \dot{X}(t) &= v_{q1}(t) - v_{c1}(t) + \omega_3(t)Y(t) - \omega_2(t)Z(t), \\ \dot{Y}(t) &= v_{q2}(t) - v_{c2}(t) + \omega_1(t)Z(t) - \omega_3(t)X(t), \\ \dot{Z}(t) &= v_{q3}(t) - v_{c3}(t) + \omega_2(t)X(t) - \omega_1(t)Y(t). \end{aligned} \quad (2-9)$$

To facilitate the subsequent analysis, the states of the system are defined as  $x(t) = [x_1(t), x_2(t), x_3(t)]^T = \left[ \frac{X(t)}{Z(t)}, \frac{Y(t)}{Z(t)}, \frac{1}{Z(t)} \right]^T \in \mathbb{R}^3$ . Formulating the kinematics in this way is common in observer-based structure from motion literature [23, 28–35].

Taking the time derivative of the state definition yields

$$\begin{aligned} \dot{x}_1(t) &= \frac{\dot{X}(t)}{Z(t)} - \frac{X(t)}{Z^2(t)}\dot{Z}(t), \\ \dot{x}_2(t) &= \frac{\dot{Y}(t)}{Z(t)} - \frac{Y(t)}{Z^2(t)}\dot{Z}(t), \\ \dot{x}_3(t) &= -\frac{\dot{Z}(t)}{Z^2(t)}. \end{aligned} \quad (2-10)$$

Substituting (2-9) into (2-10) and simplifying yields the perspective state dynamics  $\dot{x}(t) = g(t, x(t))$ , where  $g : [0, \infty) \times \mathbb{R}^3 \rightarrow \mathbb{R}^3$  is a nonlinear function that nonlinearly depends on the partially measurable states, and can be expressed as

$$\begin{aligned} \dot{x}_1(t) &= \Omega_1(t, x) + \xi_1(t, x) + v_{q1}(t)x_3(t) - x_1(t)v_{q3}(t)x_3(t), \\ \dot{x}_2(t) &= \Omega_2(t, x) + \xi_2(t, x) + v_{q2}(t)x_3(t) - x_2(t)v_{q3}(t)x_3(t), \\ \dot{x}_3(t) &= v_{c3}(t)x_3^2(t) - (\omega_2(t)x_1(t) - \omega_1(t)x_2(t))x_3(t) - v_{q3}(t)x_3^2(t), \end{aligned} \quad (2-11)$$

where  $\Omega_1, \Omega_2, \xi_1, \xi_2 : [0, \infty) \times \mathbb{R}^3 \rightarrow \mathbb{R}$  are defined as

$$\begin{aligned}\Omega_1(t, x) &= \omega_3(t) x_2(t) - \omega_2(t) - \omega_2(t) x_1^2(t) + \omega_1(t) x_1(t) x_2(t), \\ \Omega_2(t, x) &= \omega_1(t) - \omega_3(t) x_1(t) - \omega_2(t) x_1(t) x_2(t) + \omega_1(t) x_2^2(t), \\ \xi_1(t, x) &= (v_{c3}(t) x_1(t) - v_{c1}(t)) x_3(t), \\ \xi_2(t, x) &= (v_{c3}(t) x_2(t) - v_{c2}(t)) x_3(t).\end{aligned}\tag{2-12}$$

In Chapter 6, the orientation of the target will also be estimated. For that chapter, the quaternion parameterization will be used to represent orientation. Let  $\underline{q} \in \mathbb{H}$  be the unit quaternion parameterization of the orientation of the object with respect to the camera, which can be represented in the four dimensional vector space  $\mathbb{R}^4$  using the standard basis  $1, i, j, k$  as  $q(t) \triangleq \begin{bmatrix} q_0(t) & q_v^T(t) \end{bmatrix}^T \in \mathcal{S}^4$ , where  $\mathcal{S}^r \triangleq \{x \in \mathbb{R}^p | x^T x = 1\}$ , and  $q_0(t)$  and  $q_v(t)$  represent the scalar and vector components of  $q(t)$ . Based on this definition, a vector expressed in the object coordinate system,  $\xi_q \in \mathbb{R}^3$ , can be related to the same vector expressed in the camera coordinate system,  $\xi_c \in \mathbb{R}^3$ , as  $\xi_c = q \cdot \xi_q \cdot \bar{q}$ , where  $(\bar{\cdot}) : \mathcal{S}^4 \rightarrow \mathcal{S}^4$  represents the unit quaternion inverse operator defined as  $\bar{q} \triangleq \begin{bmatrix} q_0 & -q_v^T \end{bmatrix}^T$  with identity  $\bar{q} \cdot q = q \cdot \bar{q} = \begin{bmatrix} 1 & 0 & 0 & 0 \end{bmatrix}^T$ , and  $(\cdot) : \mathbb{R}^4 \times \mathbb{R}^4 \rightarrow \mathbb{R}^4$  represents the Hamilton product<sup>1</sup>, with property  $q_a \cdot q_b \in \mathcal{S}^4$  for  $q_a, q_b \in \mathcal{S}^4$ . The Hamilton product can be expressed in block matrix notation as

$$q_a \cdot q_b = \begin{bmatrix} q_{a0} & -q_{av}^T \\ q_{av} & q_{a0}I_3 + q_{av}^\times \end{bmatrix} q_b$$

---

<sup>1</sup> For brevity, a slight abuse of notation will be utilized throughout the dissertation. For  $v_1, v_2 \in \mathbb{R}^3$  and  $q \in \mathcal{S}^4$ , the equation  $v_2 = q \cdot v_1 \cdot \bar{q}$  can be written precisely as  $q_{v2} = q \cdot q_{v1} \cdot \bar{q}$ , where  $q_{v1} \triangleq \begin{bmatrix} 0 & v_1^T \end{bmatrix}^T$  and  $q_{v2} \triangleq \begin{bmatrix} 0 & v_2^T \end{bmatrix}^T$ . In other words, an  $\mathbb{R}^4$  quaternion,  $q_{v1}$ , is derived from an  $\mathbb{R}^3$  vector,  $v_1$ , by setting the scalar part of  $q_{v1}$  to zero and setting the vector part of  $q_{v1}$  as equal to  $v_1$ . Similarly, the resulting vector,  $v_2$ , is derived from the vector component of  $q_{v2}$ .

where  $I_g \in \mathbb{R}^{g \times g}$  is the identity matrix. The kinematics for the relative orientation of the object with respect to the camera are (see [110, Chapter 3.4] or [111, Chapter 3.6])

$$\dot{q}(t) = \frac{1}{2} B(q(t)) (\omega_q(t) - \bar{q}(t) \cdot \omega_c(t) \cdot q(t)) \quad (2-13)$$

where  $B : \mathcal{S}^4 \rightarrow \mathbb{R}^{4 \times 3}$  is defined as

$$B(\xi) \triangleq \begin{bmatrix} -\xi_v^T \\ \xi_0 I_3 + \xi_v^\times \end{bmatrix}$$

and has the pseudoinverse property  $B(\xi)^T B(\xi) = I_3$  (see [110, Chapter 3.4]).

**Assumption 2.1.** The state  $x(t)$  is bounded, i.e.  $x(t) \in \mathcal{X}$ , where  $\mathcal{X} \subset \mathbb{R}^3$  is a convex, compact set.

*Remark 2.1.* For the state estimates to converge to the states while remaining bounded, the states themselves must remain bounded (analogous to the requirement that desired trajectories must remain bounded for trajectory tracking control problems). During periods in which the target is observable, bounds on the states are a result of the physical constraints on the imaging system. For image formation, the target must remain in front of the camera principle point by an arbitrarily small amount,  $\epsilon \in \mathbb{R}$ . This provides an arbitrarily small lower bound on  $Z(t)$  and therefore an arbitrarily large upper bound on  $x_3(t)$ . Similarly, a feature with infinite range lower bounds  $x_3(t)$  by zero. In addition, boundedness of the pixel coordinates of the target and boundedness of the camera intrinsic parameter matrix (see the imaging model in the next section) result in boundedness of  $x_1(t)$  and  $x_2(t)$ . During the periods in which the target is unobservable, these physical constraints no longer apply. However, Assumption 2.1 requires that the target does not exhibit finite escape, even during the unobservable periods. This restricts the relative motion of the target with respect to the camera; the target cannot move behind the camera, even during the unobservable periods, else the state  $x_3(t)$  will pass through infinity.

**Assumption 2.2.** The motion of the camera is known and bounded in the sense that  $v_{c1}(t)$ ,  $v_{c2}(t)$ ,  $v_{c3}(t)$ ,  $\omega_1(t)$ ,  $\omega_2(t)$  and  $\omega_3(t)$  are known and bounded.

## 2.2 Imaging Model

Using projective geometry, the image coordinates of the feature point,  $p(t) = \begin{bmatrix} u(t) & v(t) & 1 \end{bmatrix}^T \in \mathbb{R}^3$ , where  $u(t)$ ,  $v(t) \in \mathbb{R}$ , are related to the normalized Euclidean coordinates,  $m(t) \triangleq \begin{bmatrix} \frac{X(t)}{Z(t)} & \frac{Y(t)}{Z(t)} & 1 \end{bmatrix}^T \in \mathbb{R}^3$ , by

$$p(t) = Am(t),$$

where  $A \in \mathbb{R}^{3 \times 3}$  is the known, invertible, camera intrinsic parameter matrix [112].

Since  $A$  is invertible, the states  $x_1(t)$  and  $x_2(t)$  are measurable when the target is in the camera FOV.

**Assumption 2.3.** The target is uniquely identifiable from image projections, even across periods of unobservability.

*Remark 2.2.* Algorithms such as the Kanade–Lucas–Tomasi (KLT) [113] feature tracker have been developed to track image features in consecutive frames of a video stream, however these may not be sufficient for object tracking if the object temporarily leaves the FOV or becomes occluded; these feature trackers typically do not differentiate between new features and features that have been tracked previously and therefore cannot track an object continuously through intermittent measurements, where continuity or small deviation assumptions may not hold. Other feature descriptors, such as SIFT [114] and SURF [115], have been used to match objects across affine transformations, and therefore may be more robust to temporary loss of sight. Recently, machine learning techniques have been used to recognize and localize objects in images [116, 117]. A combination of these techniques can be used to track a feature through multiple periods of intermittent visibility. See [1] and [118] for a survey of feature trackers and [116] for examples and performance of modern object localization algorithms.

**Assumption 2.4.** An observer for the state  $x(t)$  is used so that when the states  $x_1(t)$  and  $x_2(t)$  are measurable, the state estimation error is globally exponentially convergent at a rate of  $\lambda_{on} \in \mathbb{R}_{>0}$ , i.e.  $\|e(t)\| \leq C \|e(t_0)\| \exp[-\lambda_{on}(t - t_0)]$  for any initial condition  $e(t_0)$ , with  $t_0 \in \mathbb{R}_{\geq 0}$  and some positive constant  $C \in \mathbb{R}$ .

*Remark 2.3.* Exponentially convergent observers for image-based structure estimation that satisfy Assumption 2.4 are available from results such as [30, 31, 119–122]. Many of these results utilize an excitation condition as well as gain conditions to yield exponential convergence. Any conditions required by the observer are also inherited here. Also, in some cases (e.g., [122]), only the unmeasurable state,  $x_3(t)$ , is estimated. In these cases, the observer can be augmented as exemplified in the Appendix to maintain continuity of the state estimates as is required in the following stability analysis (i.e., to guarantee the system is a switched system as opposed to a hybrid system with discontinuous states).

## CHAPTER 3 STABILITY OF A CLASS OF IMAGE-BASED OBSERVERS DURING INTERMITTENT MEASUREMENTS

In this chapter, the robustness of a class of image-based observers to intermittent measurements is analyzed. During periods in which the feature is not visible, the growth of a Lyapunov-like function is bounded using the dynamics developed in Chapter 2 and the velocity bounds in Assumption 3.1 below. Combined with the exponential decay of a Lyapunov function during periods in which the feature is observable, one can examine the value of these functions after every cycle of losing and regaining observability of the feature. Analyzing the limit of a sequence of cycles demonstrates the stability of the system.

**Assumption 3.1.** Bounds for the camera and target velocities exist and are known, i.e. the following inequalities are satisfied

$$\begin{aligned} \begin{bmatrix} |v_{q1}(t)| & |v_{q2}(t)| & |v_{q3}(t)| \end{bmatrix}^T &\leq \begin{bmatrix} \bar{v}_{q1} & \bar{v}_{q2} & \bar{v}_{q3} \end{bmatrix}^T \\ \begin{bmatrix} |v_{c1}(t)| & |v_{c2}(t)| & |v_{c3}(t)| \end{bmatrix}^T &\leq \begin{bmatrix} \bar{v}_{c1} & \bar{v}_{c2} & \bar{v}_{c3} \end{bmatrix}^T \\ \begin{bmatrix} |\omega_1(t)| & |\omega_2(t)| & |\omega_3(t)| \end{bmatrix}^T &\leq \begin{bmatrix} \bar{\omega}_1 & \bar{\omega}_2 & \bar{\omega}_3 \end{bmatrix}^T \end{aligned}$$

where  $\bar{v}_{q1}, \bar{v}_{q2}, \bar{v}_{q3}, \bar{v}_{c1}, \bar{v}_{c2}, \bar{v}_{c3}, \bar{\omega}_1, \bar{\omega}_2, \bar{\omega}_3 \in \mathbb{R}$  are known non-negative constants.

*Remark 3.1.* Conservative bounds on the target velocities can easily be established.

For example, the velocities of observed vehicular systems can readily be upper bounded with some domain knowledge.

To facilitate the subsequent stability analysis, the unknown nonlinear functions in (2–12) can be bounded as

$$\begin{aligned} \xi_1(t, x) &\leq \bar{v}_{c1} \|x(t)\| + \bar{v}_{c3} \|x(t)\|^2, \\ \xi_2(t, x) &\leq \bar{v}_{c2} \|x(t)\| + \bar{v}_{c3} \|x(t)\|^2, \end{aligned} \tag{3–1}$$

$$\begin{aligned}\Omega_1(t, x) &\leq \bar{\omega}_2 + \bar{\omega}_3 \|x(t)\| + (\bar{\omega}_1 + \bar{\omega}_2) \|x(t)\|^2, \\ \Omega_2(t, x) &\leq \bar{\omega}_1 + \bar{\omega}_3 \|x(t)\| + (\bar{\omega}_1 + \bar{\omega}_2) \|x(t)\|^2.\end{aligned}\tag{3-2}$$

Substituting (3-1) and (3-2) into (2-11) and bounding the remaining terms yields the following inequalities:

$$\begin{aligned}\dot{x}_1(t) &\leq \bar{\omega}_2 + (\bar{v}_{c1} + \bar{\omega}_3 + \bar{v}_{q1}) \|x(t)\| + (\bar{v}_{c3} + \bar{\omega}_1 + \bar{\omega}_2 + \bar{v}_{q3}) \|x(t)\|^2, \\ \dot{x}_2(t) &\leq \bar{\omega}_1 + (\bar{v}_{c2} + \bar{\omega}_3 + \bar{v}_{q2}) \|x(t)\| + (\bar{v}_{c3} + \bar{\omega}_1 + \bar{\omega}_2 + \bar{v}_{q3}) \|x(t)\|^2, \\ \dot{x}_3(t) &\leq (\bar{v}_{c3} + \bar{\omega}_1 + \bar{\omega}_2 + \bar{v}_{q3}) \|x(t)\|^2.\end{aligned}\tag{3-3}$$

### 3.1 Structure Estimation Objective

To quantify the structure estimation objective, let the state estimate error,  $e \in \mathbb{R}^3$ , be defined as

$$e(t) = x(t) - \hat{x}(t),$$

where  $\hat{x} \in \mathbb{R}^3$  denotes the state estimate determined from an observer. The evolution of  $e$  is defined by the family of systems

$$\dot{e}(t) = f_p(t, x(t), \hat{x}(t))\tag{3-4}$$

where  $f_p : [0, \infty) \times \mathbb{R}^3 \times \mathbb{R}^3 \rightarrow \mathbb{R}^3$ ,  $p \in \{s, u\}$ ,  $s$  is an index referring to the system in which the target is observable, and  $u$  is an index referring to the system in which the target is unobservable. When the target is in view, the states  $x_1(t)$  and  $x_2(t)$  are measurable, and the closed-loop error dynamics are given by

$$f_s(t, x(t), \hat{x}(t)) = g(t, x(t)) - \dot{\hat{x}}(t),\tag{3-5}$$

where  $\dot{\hat{x}}(t)$  is defined by an observer based on Assumption 2.4. However, when the target is out of the camera FOV, the state estimates cannot be updated (i.e.,  $\dot{\hat{x}}(t) = 0$ ),

and the error dynamics are given by

$$f_u(t, x(t), \hat{x}(t)) = g(t, x(t)). \quad (3-6)$$

### 3.2 Stability Analysis

In the following development, the switching signal  $\sigma : [0, \infty) \rightarrow \{s, u\}$  indicates the active subsystem. Also, let  $t_n^{\text{on}} \in \mathbb{R}$  denote the time of the  $n^{\text{th}}$  instance at which the target enters the camera FOV and  $t_n^{\text{off}} \in \mathbb{R}$  denote the time of the  $n^{\text{th}}$  instance at which the target exits the camera FOV, where  $n \in \mathbb{N}$ . The dwell time in the  $n^{\text{th}}$  activation of subsystem  $s$  and  $u$  is denoted by  $\Delta t_n^{\text{on}} \triangleq t_n^{\text{off}} - t_n^{\text{on}} \in \mathbb{R}$  and  $\Delta t_n^{\text{off}} \triangleq t_{n+1}^{\text{on}} - t_n^{\text{off}} \in \mathbb{R}$ , respectively. Finally,  $\Delta t_{\min}^{\text{on}} \triangleq \inf_{n \in \mathbb{N}} \{\Delta t_n^{\text{on}}\} \in \mathbb{R}$  and  $\Delta t_{\max}^{\text{off}} \triangleq \sup_{n \in \mathbb{N}} \{\Delta t_n^{\text{off}}\} \in \mathbb{R}$  denote the minimum dwell time in subsystem  $s$  and maximum dwell time in subsystem  $u$ , respectively, for all  $n$ .

Based on Assumption 2.4, the estimation error will converge when measurements are available. However, when measurements are unavailable, the estimation error is expected to grow since the camera and target may move while the estimate is held constant. Therefore, a quadratic Lyapunov-like function based on the estimation error is expected to evolve as shown in Figure 3-1. In Theorem 3.1, it is shown that the asymptotic behavior of the Lyapunov-like function, and hence the estimation error, is bounded, provided measurements are available for a sufficient amount of time, and the duration of time that measurements are not available is relatively small. To prove this, bounds on the Lyapunov-like functions when each subsystem is active are developed. From the bounds, a recursive relation between successive cycles of losing and regaining measurements is developed (i.e., a bound on  $W_{n+1}^{\text{on}}$  based on  $W_n^{\text{on}}$  in Figure 3-1). The recursive relation is then used to define a sequence, and conditions in which the sequence converges are determined. Conditions for convergence of the sequence lead to dwell time conditions, as well as a relation for the limit of the sequence, which is used to bound the ultimate estimation error.

**Theorem 3.1.** *The switched system generated by (3–4) and switching signal  $\sigma$  is asymptotically regulated to a ball of arbitrary size provided the switching signal and the initial condition satisfy the following conditions:*

$$\Delta t_{\max}^{\text{off}} < \frac{\pi}{2\beta},$$

$$\Delta t_{\min}^{\text{on}} \geq -\frac{1}{\lambda_s} \ln \frac{1}{\mu^2}, \quad (3-7)$$

$$\frac{1 - \mu^2 \exp(-\lambda_s \Delta t_{\min}^{\text{on}})}{2\mu \exp(-\frac{\lambda_s}{2} \Delta t_{\min}^{\text{on}})} > \tan(\beta \Delta t_{\max}^{\text{off}}), \quad (3-8)$$

$$c_2 \|e(0)\|^2 < \bar{d}, \quad (3-9)$$

where the constants  $\beta, \lambda_s, \mu, \bar{d}, c_2 \in \mathbb{R}$  are known positive bounding constants.

*Proof.* The existence of an exponentially tracking state observer from Assumption 2.4 implies the existence of a Lyapunov function  $V_s : [0, \infty) \times \mathbb{R}^3 \rightarrow \mathbb{R}$  that satisfies

$$c_1 \|e(t)\|^2 \leq V_s(t, e(t)) \leq c_2 \|e(t)\|^2 \quad (3-10)$$

$$\frac{\partial V_s}{\partial t} + \frac{\partial V_s}{\partial e} (\dot{e}(t)) \leq -c_3 \|e(t)\|^2 \quad (3-11)$$

$$\left\| \frac{\partial V_s}{\partial e} \right\| \leq c_4 \|e(t)\|$$

for some positive scalar constants  $c_1, c_2, c_3, c_4 \in \mathbb{R}$ , during the periods in which the target is observable (see the converse Lyapunov theorem in [123, Theorem 4.14]). From (3–10) and (3–11) it is clear that

$$\dot{V}_s \leq -\lambda_s V_s \quad (3-12)$$

when the target is in view, where  $\lambda_s = \frac{c_3}{c_2}$ .

Consider a Lyapunov-like function  $V_u : [0, \infty) \times \mathbb{R}^3 \rightarrow \mathbb{R}$  defined as

$$V_u(t, e(t)) = c_5 e(t)^T e(t) \quad (3-13)$$

where  $c_5 \in \mathbb{R}$  is selected so that  $c_1 \leq c_5 \leq c_2$ . From (3-10) and (3-13) it is clear that

$$V_p(t, e(t)) \leq \frac{c_2}{c_1} V_q(t, e(t)), \quad \forall p, q \in \{s, u\}, p \neq q \quad (3-14)$$

i.e., for any value of  $t$ , the functions  $V_s(t, e(t))$  and  $V_u(t, e(t))$  are within a factor  $\mu \triangleq \frac{c_2}{c_1} \in \mathbb{R}$  of each other. Taking the time derivative of  $V_u(t, e(t))$ , and substituting (3-4), (3-6), and (3-3), yields

$$\dot{V}_u(t, e(t)) \leq 2c_5 (c_6 \|e(t)\| + c_7 \|e(t)\|^2 + c_8 \|e(t)\|^3)$$

where  $c_6, c_7, c_8 \in \mathbb{R}$  denote known positive constants based on the upper bounds on the camera and target velocities and an upper bound on  $\|\hat{x}(t)\|$  from Assumption 2.1. From (3-13),  $\|e(t)\|$  can be upper bounded by  $\sqrt{\frac{V_u}{c_5}}$ , resulting in

$$\dot{V}_u(t, e(t)) \leq \beta (V_u^2 + 1) \quad (3-15)$$

where  $\beta$  is a known, bounded, positive constant.

Let the function  $W : [0, \infty) \rightarrow \mathbb{R}$  be defined such that  $W(t) \triangleq V_{\sigma(t)}(t, e(t))$ . From (3-12) and (3-15)

$$\dot{W}(t) \leq \begin{cases} -\lambda_s W(t) & t \in [t_n^{\text{on}}, t_n^{\text{off}}) \\ \beta (W(t)^2 + 1) & t \in [t_n^{\text{off}}, t_{n+1}^{\text{on}}) \end{cases}, \quad \forall n. \quad (3-16)$$

The second inequality in (3-16) indicates that  $W(t)$  can grow unbounded in finite time when the target is unobservable. However, from the first inequality,  $W(t)$  is regulated to zero when the target is observable. This suggests that if the target is observed for a long enough duration, and the target is out of the FOV for a short enough duration, the net change in  $W(t)$  will be negative over a cycle where observability is lost and regained, and consequently the estimation error will decrease. A representative illustration of the evolution of  $W(t)$  if these conditions are satisfied is depicted in Fig. 3-1.

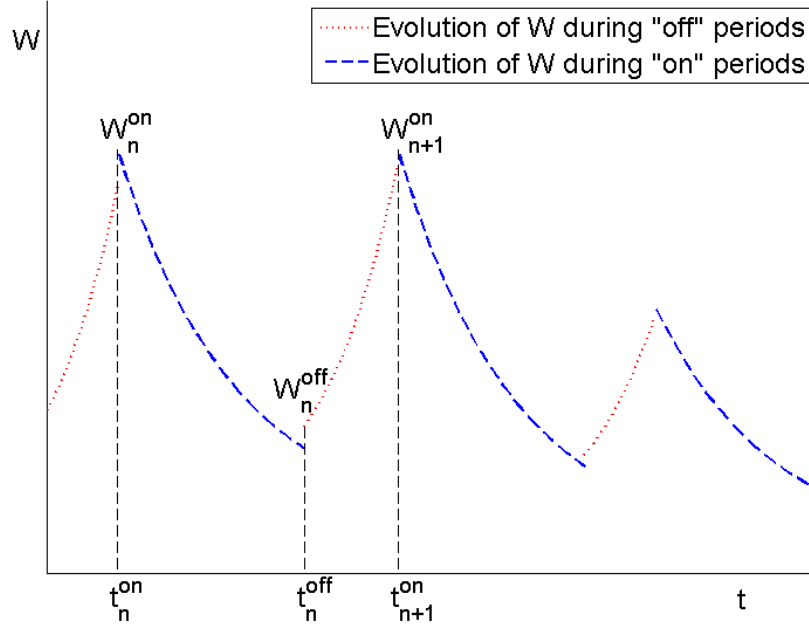


Figure 3-1. Representative illustration of the evolution of  $W$  during the interval  $[t_n^{\text{on}}, t_{n+1}^{\text{on}}]$ .

Utilizing the Comparison Lemma in [123, Lemma 3.4], (3–16) can be integrated, yielding

$$W(t) \leq \begin{cases} W_n^s(t) & t \in [t_n^{\text{on}}, t_n^{\text{off}}) \\ W_n^u(t) & t \in [t_n^{\text{off}}, t_{n+1}^{\text{on}}) \end{cases}, \quad \forall n \quad (3-17)$$

where the functions  $W_n^s : [t_n^{\text{on}}, t_n^{\text{off}}) \rightarrow \mathbb{R}$  and  $W_n^u : [t_n^{\text{off}}, t_{n+1}^{\text{on}}) \rightarrow \mathbb{R}$  are defined as

$$W_n^s(t) \triangleq W_n^{\text{on}} \exp(-\lambda_s(t - t_n^{\text{on}})), \quad (3-18)$$

$$W_n^u(t) \triangleq \tan(\beta(t - t_n^{\text{off}}) + \arctan(W_n^{\text{off}})), \quad (3-19)$$

$W_n^{\text{on}}$  denotes  $W(t_n^{\text{on}})$  and  $W_n^{\text{off}}$  denotes  $W(t_n^{\text{off}})$ . From (3–14), the discontinuities in  $W$  are related as

$$\begin{aligned} W(t_n^{\text{off}}) &\leq \mu W(t_n^{\text{off}-}), \\ W(t_{n+1}^{\text{on}}) &\leq \mu W(t_{n+1}^{\text{on}-}), \end{aligned}$$

where <sup>1</sup>  $W(t_n^{\text{off}-}) \triangleq \lim_{t \nearrow t_n^{\text{off}}} W(t)$  and  $W(t_{n+1}^{\text{on}-}) \triangleq \lim_{t \nearrow t_{n+1}^{\text{on}}} W(t)$ . Therefore, the change in  $W(t)$  over a cycle of losing and regaining observability is

$$W_{n+1}^{\text{on}} \leq \mu \tan(\beta \Delta t_n^{\text{off}} + \arctan(\mu W_n^{\text{on}} e^{-\lambda_s \Delta t_n^{\text{on}}}), \quad \forall n.$$

Considering the worst case scenario of minimum time of observability and maximum unobservability

$$W_{n+1}^{\text{on}} \leq \mu \tan(\beta \Delta t_{\max}^{\text{off}} + \arctan(\mu W_n^{\text{on}} e^{-\lambda_s \Delta t_{\min}^{\text{on}}}), \quad (3-20)$$

for all  $n$ . The right hand side of (3-20) can be rewritten using a trigonometric identity as

$$\mu \tan(\beta \Delta t_{\max}^{\text{off}} + \arctan(\mu W_n^{\text{on}} \exp(-\lambda_s \Delta t_{\min}^{\text{on}}))) = \mu \frac{\tan(\beta \Delta t_{\max}^{\text{off}}) + \mu W_n^{\text{on}} \exp(-\lambda_s \Delta t_{\min}^{\text{on}})}{1 - [\tan(\beta \Delta t_{\max}^{\text{off}})] [\mu W_n^{\text{on}} \exp(-\lambda_s \Delta t_{\min}^{\text{on}})]}$$

resulting in

$$W_{n+1}^{\text{on}} \leq \mu \frac{A + B W_n^{\text{on}}}{1 - A B W_n^{\text{on}}},$$

where

$$A = \tan(\beta \Delta t_{\max}^{\text{off}}),$$

$$B = \mu \exp(-\lambda_s \Delta t_{\min}^{\text{on}}).$$

The elements of the sequence  $\{W_n^{\text{on}}\}$  are upper bounded as

$$W_n^{\text{on}} \leq z_n, \quad \forall n$$

where the sequence  $\{z_n\}$  is defined as

$$\begin{aligned} z_0 &= W_0^{\text{on}}, \\ z_{n+1} &= \mu \frac{A + B z_n}{1 - A B z_n}. \end{aligned} \quad (3-21)$$

---

<sup>1</sup> The notation  $\lim_{t \nearrow t^*} W(t)$  refers to the one-sided limit of  $W(t)$  as  $t$  approaches  $t^*$  from below (i.e., the left handed limit given in [124, Definition 4.25]).

Since the elements of the sequence  $\{W_n^{\text{on}}\}$  are lower bounded by zero due to the definition of  $W$ , the squeeze theorem [124, Theorem 3.19] can be used to show that  $\{W_n^{\text{on}}\}$  converges to a ball upper bounded by  $\lim_{n \rightarrow \infty} z_n$ . The sequence  $\{z_n\}$  will converge if it is bounded and monotonically decreases. The following two conditions arise from the requirement that  $z_n$  remain upper bounded over every iteration from  $n$  to  $n + 1$  (i.e., the right hand side of (3–21) remains bounded):

$$\Delta t_{\text{max}}^{\text{off}} < \frac{\pi}{2\beta}, \quad (3-22)$$

$$ABz_n < 1. \quad (3-23)$$

For decaying convergence, the sequence is monotonically decreasing for all  $n$  if  $z_{n+1} \leq z_n$ , resulting in the condition

$$ABz_n^2 - (1 - \mu B)z_n + \mu A \leq 0. \quad (3-24)$$

Since  $A$  and  $B$  are positive for all positive values of  $\Delta t_{\text{min}}^{\text{on}}$  and  $\Delta t_{\text{max}}^{\text{off}}$ , the inequality in (3–24) can only be satisfied for various values of  $z_n$  if  $1 - \mu B \geq 0$ , resulting in the condition

$$-\frac{1}{\lambda_s} \ln \frac{1}{\mu^2} \leq \Delta t_{\text{min}}^{\text{on}}. \quad (3-25)$$

Note that since  $\mu \geq 1$ , the left hand side of (3–25) is always greater than or equal to zero.

Since the left hand side of (3–24) is a convex parabola, the condition

$$\underline{d} \leq z_n < \bar{d},$$

must also be satisfied in addition to the condition in (3–25), to satisfy the inequality in (3–24), where  $\underline{d}$  and  $\bar{d}$  are solutions to the quadratic equation

$$ABz_n^2 - (1 - \mu B)z_n + \mu A = 0 \quad (3-26)$$

and are given by

$$\underline{d} \triangleq \frac{1 - \mu B - \sqrt{(1 - \mu B)^2 - 4\mu A^2 B}}{2AB}, \quad (3-27)$$

$$\bar{d} \triangleq \frac{1 - \mu B + \sqrt{(1 - \mu B)^2 - 4\mu A^2 B}}{2AB}. \quad (3-28)$$

The roots,  $\underline{d}$  and  $\bar{d}$ , are real and distinct if

$$(1 - \mu B)^2 - 4\mu A^2 B > 0, \\ \implies \frac{1 - \mu^2 \exp(-\lambda_s \Delta t_{\min}^{\text{on}})}{2\mu \exp(-\frac{\lambda_s}{2} \Delta t_{\min}^{\text{on}})} > \tan(\beta \Delta t_{\max}^{\text{off}}). \quad (3-29)$$

If the conditions in (3-22), (3-25) and (3-29) are satisfied and if the initial conditions satisfy (3-23), the sequence is monotonically decreasing. Since the function  $\phi : \mathbb{R} \rightarrow \mathbb{R}$ ,  $\phi(z) \triangleq \mu \frac{A+Bz}{1-ABz}$ , where  $z$  is a dummy variable representing the argument of  $\phi$ , is an increasing function on the interval  $(-\infty, \frac{1}{AB}]$ , and  $\underline{d}$  and  $\bar{d}$  are both upper bounded by  $\frac{1}{AB}$ ,

$$z_n \in [\underline{d}, \bar{d}] \implies \phi(\underline{d}) \leq \phi(z_n) \implies \underline{d} \leq z_{n+1}.$$

Consequently, if the initial condition  $z_0$  is in the interval  $[\underline{d}, \bar{d}]$ , the sequence is lower bounded and monotonically decreasing, and therefore converges. The limit of the sequence is given by

$$L \triangleq \lim_{n \rightarrow \infty} z_n.$$

Using the definition of the sequence in (3-21)

$$\lim_{n \rightarrow \infty} z_{n+1} = \mu \frac{A + B \lim_{n \rightarrow \infty} z_n}{1 - AB \lim_{n \rightarrow \infty} z_n} \\ \implies L = \mu \frac{A + BL}{1 - ABL}$$

which results in an equation similar to (3–26) with solutions

$$L = \frac{1 - \mu B \pm \sqrt{(1 - \mu B)^2 - 4\mu A^2 B}}{2AB}.$$

However, since  $z_n$  monotonically decreases in the interval  $[d, \bar{d}]$ , if  $z_0 \in [d, \bar{d}]$ , the sequence  $\{z_n\}$  converges to the lesser solution, i.e.  $\underline{d}$ , and not  $\bar{d}$ .

A similar procedure can be used to show that  $z_n$  monotonically increases outside the interval  $[d, \bar{d}]$ . Again, since  $\phi$  is an increasing function,

$$z_n \in [0, \underline{d}] \implies \phi(z_n) \leq \phi(\underline{d}) \implies z_{n+1} \leq \underline{d}.$$

Therefore, if  $z_0 \in [0, \underline{d}]$ ,  $\{z_n\}$  monotonically increases and is upper bounded by  $\underline{d}$ .

Applying the limit as above, it can be shown that  $\{z_n\}$  then converges to  $\underline{d}$ . Thus, if  $z_0 \in [0, \bar{d}]$  (and therefore automatically satisfies (3–23)), the elements of the sequence  $\{z_n\}$  continue to satisfy (3–23) and the sequence converges to  $\underline{d}$ . Consequently, the sequence  $\{W_n^{\text{on}}\}$  converges via the squeeze theorem [124, Theorem 3.19] to the set

$$0 \leq \lim_{n \rightarrow \infty} W_n^{\text{on}} \leq \underline{d}.$$

From (3–17), (3–18), and (3–19) it is clear that  $W(t) \leq W_n^{\text{on}}, \forall t \in [t_n^{\text{on}}, t_{n+1}^{\text{on}}), \forall n$  if conditions (3–22), (3–25) and (3–29) are satisfied. Therefore,

$$\limsup_{t \rightarrow \infty} W(t) \leq \underline{d}.$$

Using (3–10), (3–13) and the definition of  $W$ , the estimation error converges to the ultimate bound

$$\limsup_{t \rightarrow \infty} \|e(t)\|^2 \leq \frac{\underline{d}}{c_1}.$$

□

*Remark 3.2.* The observer initial condition,  $\hat{x}(0)$ , and the state bounds from Assumption 2.1 can be used to bound the initial error to check the condition in (3–9) without any

additional information. However, satisfying this condition using this initial error bound may require an overly large  $\bar{d}$  and therefore overly conservative forward and reverse dwell times (i.e.  $\Delta t_{\min}^{\text{on}}$  and  $\Delta t_{\max}^{\text{off}}$ ). Any additional domain knowledge that can be used to restrict  $\|e(0)\|$  is helpful in allowing a larger set of dwell times.

*Remark 3.3.* The stability conditions in (3–7) and (3–8) are functions of the error decay rate,  $\lambda_s$ . The implication of increasing the decay rate of the Lyapunov-like function, i.e. increasing the observer gains, is that the target has to remain in the FOV for less time. The size of the ultimate bound can also be decreased, either by increasing the dwell time in the observable region or increasing  $\lambda_s$ . However, this is only effective up to a limit. Re-examining (3–27) and using L'Hôpital's rule, in the limit as  $B \rightarrow 0$  (i.e.  $\lambda_s \rightarrow \infty$  or  $\Delta t_{\min}^{\text{on}} \rightarrow \infty$ ),  $\underline{d} \rightarrow \mu A$ , which is equivalent to the growth in  $W$  during the period in which the target is out of the camera FOV in the case when the estimation error is initially zero. Similarly, from (3–28),  $\bar{d} \rightarrow \infty$  as  $B \rightarrow 0$ , allowing an arbitrarily large initial error.

### 3.3 Experiments

Experiments were performed to verify the theoretical results. The overall goal of the experiment was to simulate the scenario of tracking the Euclidean position of a cooperative mobile vehicle in a GPS-denied environment via a camera. For example, a common scenario in GPS-denied environments could be one where the object of interest is a cooperative ground vehicle, which is being observed by a high altitude aerial vehicle with an active GPS signal [125, 126], or when multiple cooperative agents are each observing each other to reduce the overall position uncertainty growth rate [127–130]. Specifically, the objective was to demonstrate convergence of the relative position estimation errors despite intermittent measurements if a class of image-based observers is used when the mobile vehicle is visible, and a zero-order hold (ZOH) of the position estimate is used when the mobile vehicle is not visible. An IDS UI-1580SE camera with 2-pixel binning enabled and a lens with a 90 FOV was

used to capture 1280x960 pixel resolution images at a rate of approximately 15 frames per second. A Clearpath Robotics TurtleBot 2 with a Kobuki base was utilized as a GPS-denied mobile vehicle simulant. An augmented version of the observer in [122] provided range estimates while the mobile robot was visible (details are given in the Appendix). A fiducial marker with a corresponding tracking software library (see [131] and [132]) was used to repeatably track the image feature pixel coordinates and the 3D orientation of the mobile robot while it was in view. Although the library is capable of utilizing marker scale information to reconstruct the fully scaled relative Euclidean position between the camera and the marker, the scale information was not necessary for implementation, and was not used in the experiment. The optic flow signals (i.e., derivatives of the measurable states) required for the observer were approximated via finite difference.

A NaturalPoint, Inc. OptiTrack motion capture system was used to record the ground truth pose of the camera and target at a rate of 360 Hz. The pose provided by the motion capture system was also used to estimate the linear and angular velocities of the camera necessary for the range observer, where the current camera velocity estimates were taken to be the slope of the linear regression of the 20 most recent pose data points. The wheel encoders and rate gyroscope onboard the mobile robot provided estimates of the linear and angular velocity of the robot, expressed in the robot body coordinate system, for input into the range observer. Velocities of both the camera and target are necessary to resolve the well known speed-depth scale ambiguity in vision systems [112, Chapter 5.4.4], and these quantities would be available in a real world implementation of the scenario considered in this experiment. When the robot was in the camera FOV, the fiducial marker tracking algorithm orientation estimate was used to rotate the linear and angular velocities of the robot into the camera frame,  $\mathcal{F}_C$ . When the robot was outside the camera FOV, the relative orientation between the camera and robot was estimated via dead-reckoning with the onboard rate gyroscope. For simplicity,

the camera was mounted on a stationary tripod, while the TurtleBot was driven via remote control in an unstructured path.

The results of the experiment are shown in Figures 3-2 through 3-4, with vertical lines denoting switching times. Specifically, the first vertical line represents the time when the robot would leave the camera FOV and was no longer visible, and a zero-order hold was initiated with the last state estimate from the estimator. The second vertical line represents the time when the robot reentered the camera FOV and the estimator was restarted with the previous state estimate. From the results, it is clear that the estimation errors remain bounded.

To examine how the duration of time that measurements are unavailable (i.e.,  $\Delta t_n^{\text{off}}$ ) affects the ultimate estimation error, a number of experiments were performed with  $\Delta t_n^{\text{off}}$  ranging from 0.5 to 2.5 seconds, in increments of 0.5 seconds. During these experiments,  $\Delta t_n^{\text{on}}$  was held constant at 4 seconds, and the Turtlebot was sent constant forward and angular velocity commands, resulting in an approximately circular path. The experiment was performed three times (labeled A, B and C in Figure 3-5) for each set of dwell times. The evolution of the norm of the estimation error for all three runs and across all dwell times is shown in Figure 3-5, with the growth of the estimation norm after each period of measurement unavailability shown in Figure 3-6 against  $\Delta t_n^{\text{off}}$ . Compared to the bound based on the trigonometric tangent function that was used in the stability analysis, the estimation error in the experiments does not seem to grow unbounded for finite dwell times. This exemplifies the conservative nature of the bounds derived in the theory, as is typical in Lyapunov-based analysis.

### 3.4 Summary

Sufficient observation conditions are developed to guarantee convergence to an ultimate bound of the position estimation error from a vision based observer with intermittent sensing. Evaluation of the conditions only require conservative bounds on the target and camera velocities, bounds on the target range and bearing, and

bounds on the dwell times in which the target is in and out of the FOV. Solutions to the dynamics,  $\dot{W}(t)$ , of a Lyapunov-like function during both the period when the target is in view and the period when it is out of the FOV were utilized to bound the decay and growth of the estimation errors and therefore relate dwell times to a decay in  $W(t)$ .

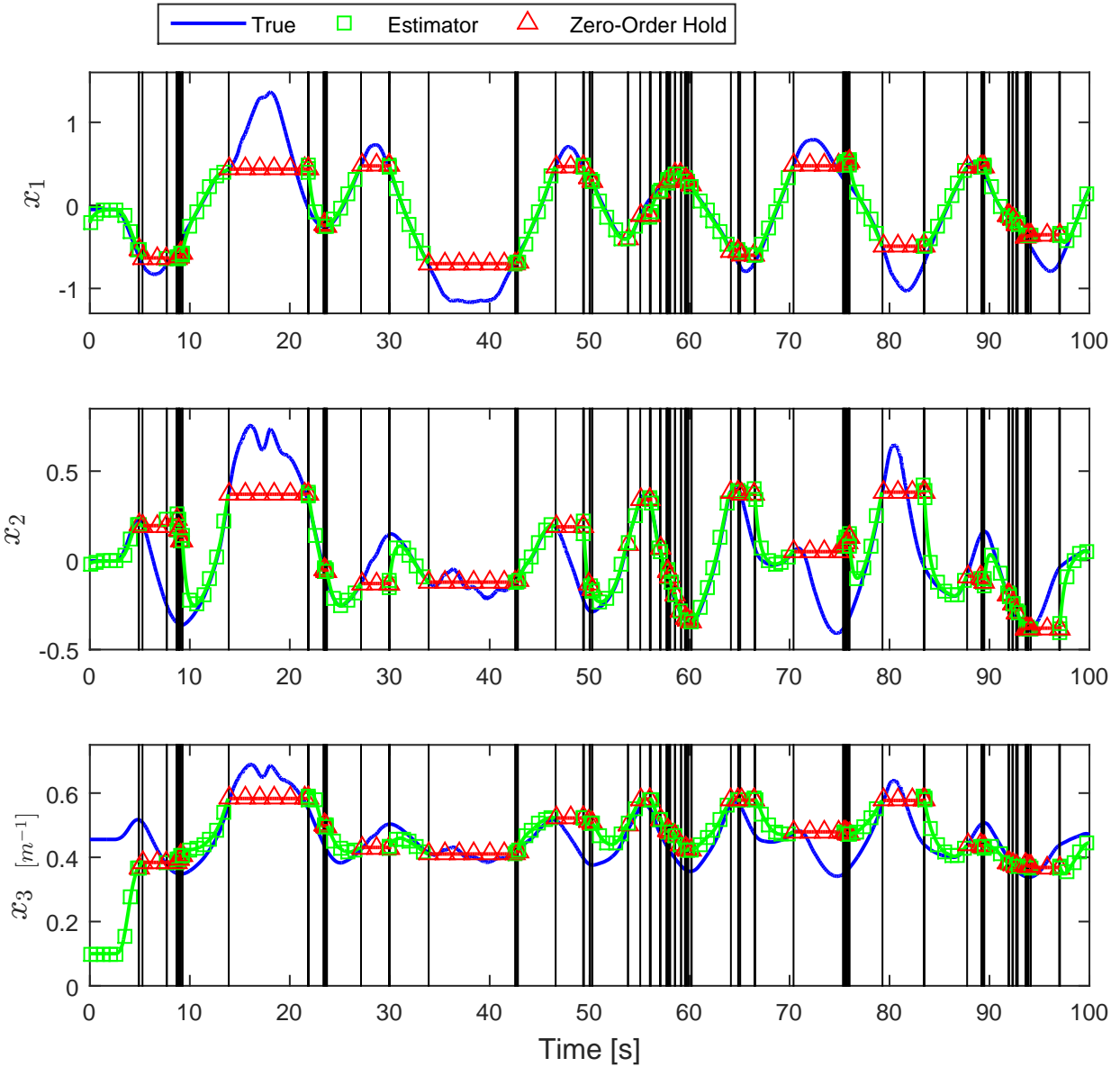


Figure 3-2. Evolution of the state estimates during the experiment. Vertical black lines denote switching times.

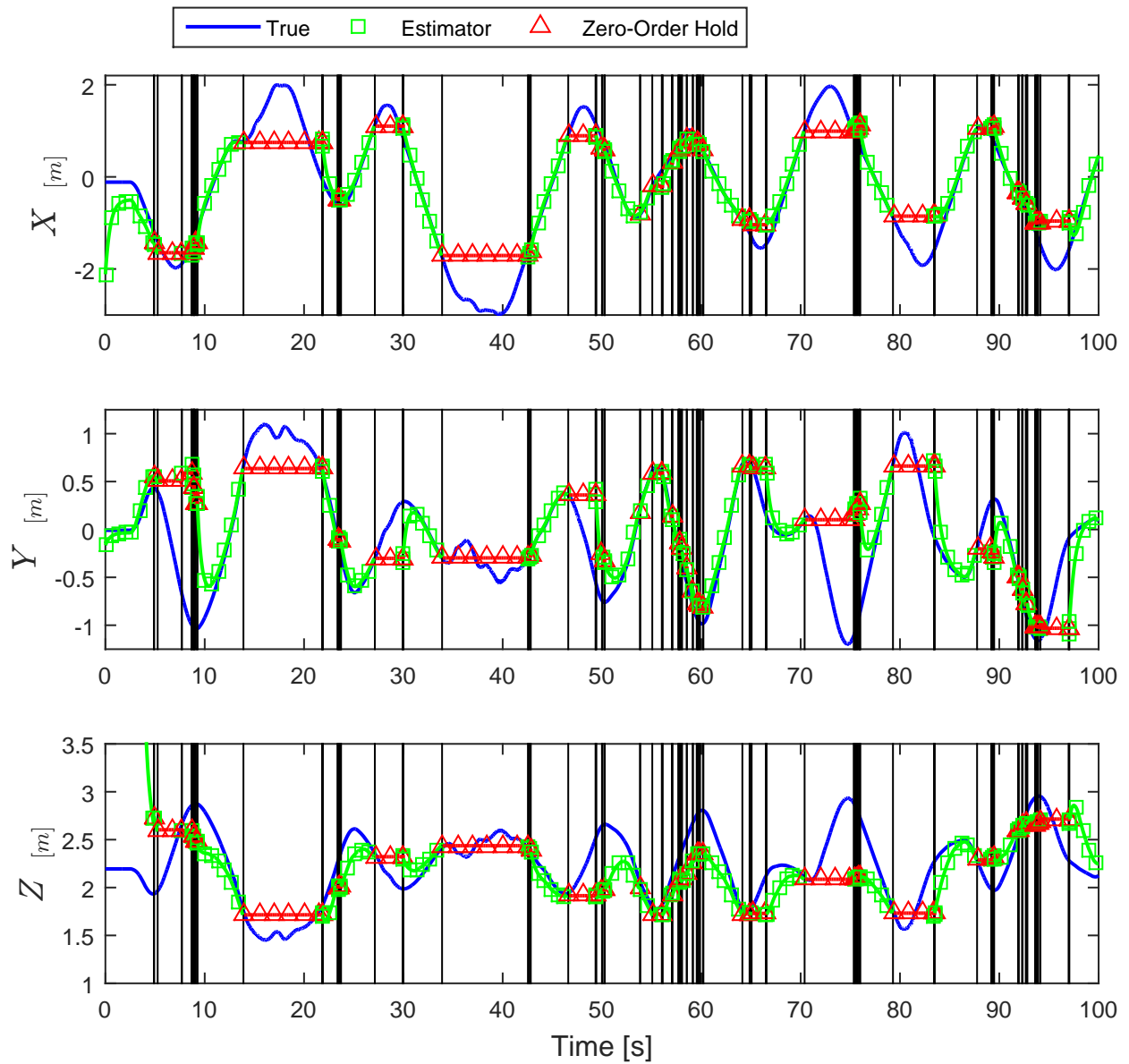


Figure 3-3. Evolution of the Euclidean coordinates estimate. Vertical black lines denote switching times.

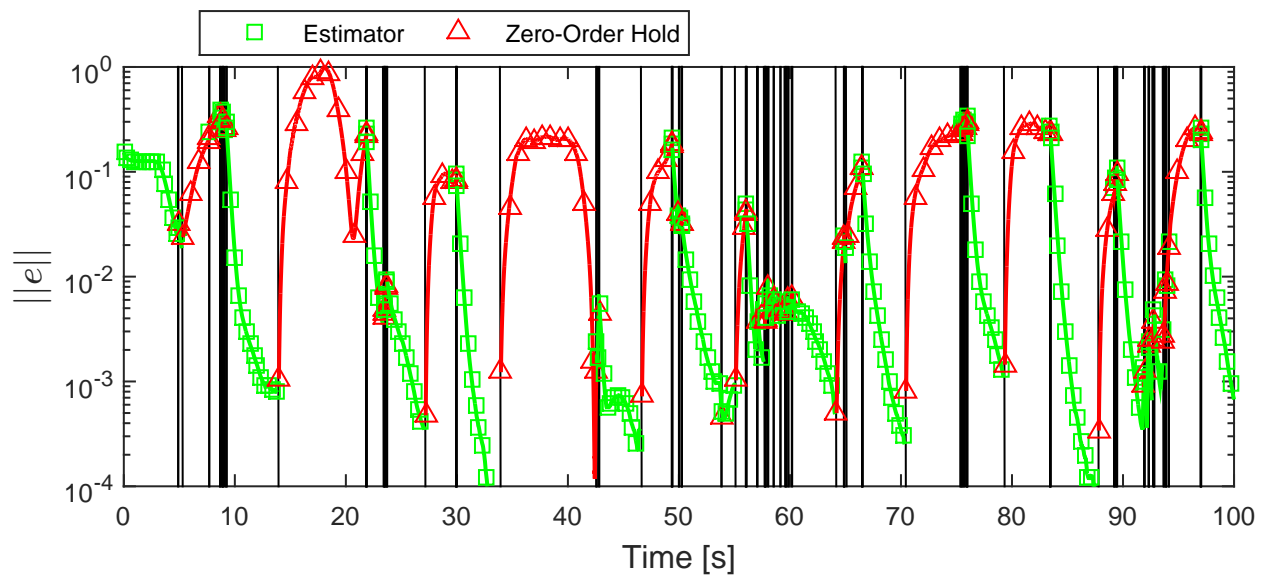


Figure 3-4. Evolution of the estimation error. Vertical black lines denote switching times. Note the logarithmic scale.

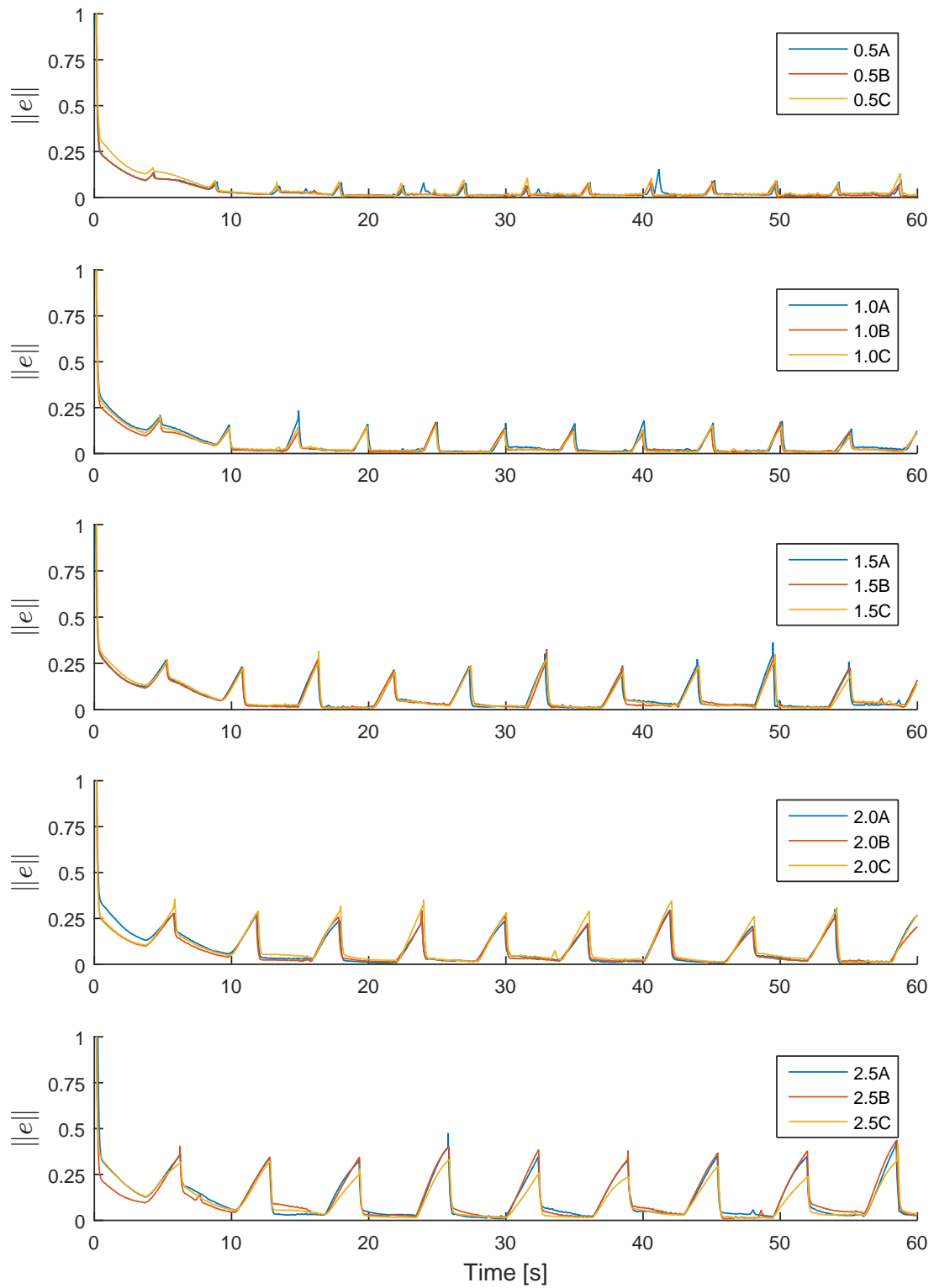


Figure 3-5. Evolution of the estimation error for measurement unavailability dwell times of 0.5 to 2.5 seconds. Each plot shows three experiments (labeled A, B and C) for the listed dwell time.

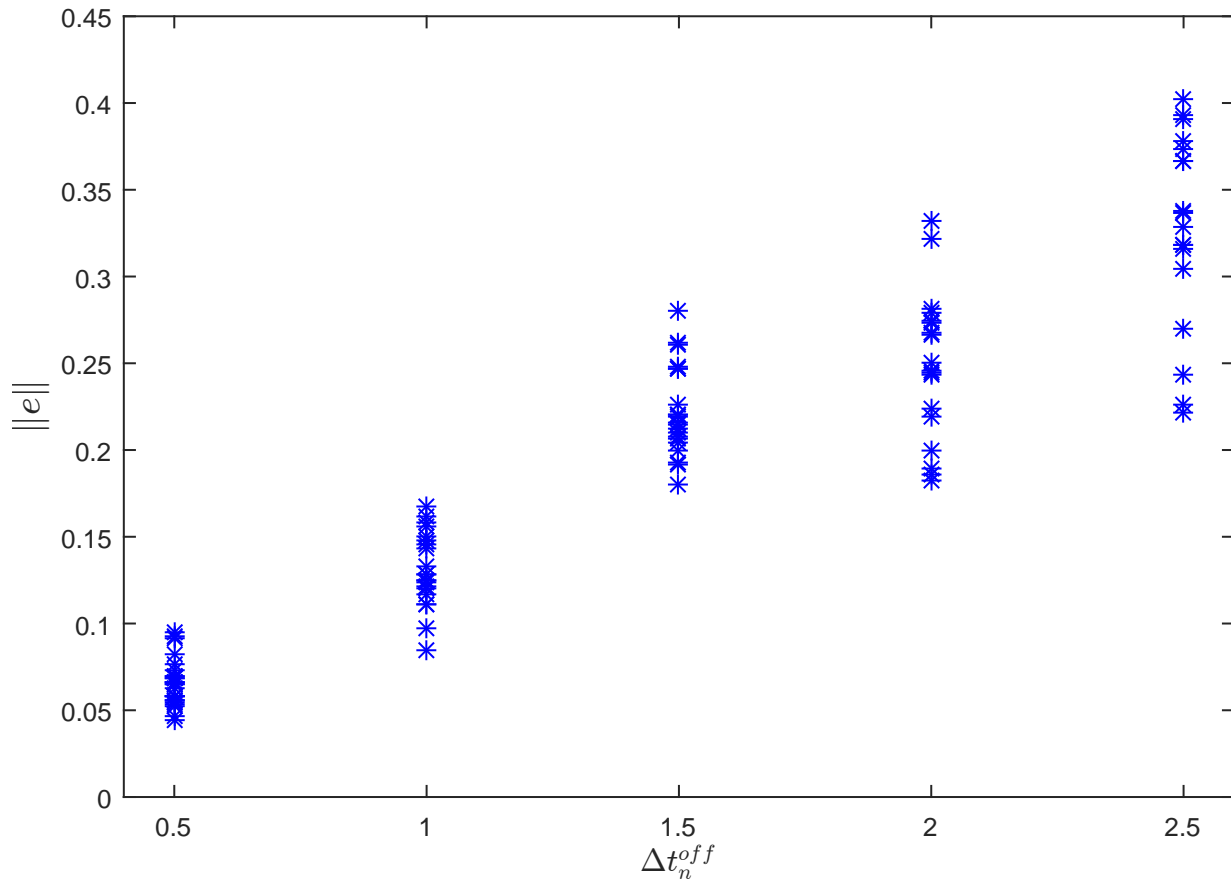


Figure 3-6. Growth in the estimation error during each period of measurement unavailability.

CHAPTER 4  
EXTENDED STABILITY RESULTS OF A CLASS OF IMAGE-BASED OBSERVERS  
DURING INTERMITTENT MEASUREMENTS: STATE PREDICTION VIA A MOTION  
MODEL

In this chapter, additional information about the feature of interest is used to relax the dwell time constraints of Chapter 3. Specifically, a motion model of the form described in Assumption 4.1 below is utilized to estimate the velocity of the feature during periods in which the feature is not observable. Exploiting the last state estimate before the feature leaves the FOV and the estimated feature velocity, the dynamics in (2–11) can be integrated forward in time to continue to provide state estimates. By using the state prediction, and the locally Lipschitz property of (2–11), the growth of the Lyapunov like function is bounded by an exponentially increasing function during periods in which the feature is unobservable, as opposed to the tangential function with finite escape in Chapter 3. Combined with the exponential decay during the observable periods, the overall system is exponentially convergent provided that an average dwell time condition and an average unobservable time condition are met.

**Assumption 4.1.** A motion model of the moving target is known and bounded, in the sense that either the target velocity,  $v_q(t) \triangleq \begin{bmatrix} v_{q1}(t) & v_{q2}(t) & v_{q3}(t) \end{bmatrix}^T \in \mathbb{R}^3$ , is known and bounded or the target velocities are given by  $v_q(t) = \phi(x(t))$ , where the known, continuous function  $\phi : \mathbb{R}^3 \rightarrow \mathbb{R}^3$  is locally Lipschitz on  $\mathcal{X}$ .

*Remark 4.1.* An analytical expression for target velocities as a function of time is not required to generate the necessary signals  $v_{q1}(t)$ ,  $v_{q2}(t)$  and  $v_{q3}(t)$ . For example, a feedback law in the form of

$$\dot{r}_q(t) = \phi_G(r_q(t)) \tag{4–1}$$

is sufficient to generate  $v_q(t)$ , where  $\phi_G : \mathbb{R}^3 \rightarrow \mathbb{R}^3$  is Lipschitz and  $r_q(t)$  is the expression of  $\vec{r}_q(t)$  in the coordinate system attached to the inertial frame  $\mathcal{F}_G$ . However, in this case, the position and orientation of the camera is required to transform state estimates in the camera frame to position estimates in the ground frame. From (4–1),

the signal,  $v_q(t)$ , is given by

$$v_q(t) = [\phi_1(x(t)), \phi_2(x(t)), \phi_3(x(t))]^T \triangleq R^T(t) \phi_G(R(t) r_{q/c}(t) + r_c(t)), \quad (4-2)$$

where  $\phi_1, \phi_2, \phi_3 : \mathbb{R}^3 \rightarrow \mathbb{R}$ ,  $r_c(t) \in \mathbb{R}^3$  is the expression of the camera position in the coordinate system attached to the inertial frame  $\mathcal{F}_G$ ,  $R(t) \in \mathbb{R}^{3 \times 3}$  denotes the orientation of the camera in the sense that premultiplying by  $R(t)$  rotates a vector expressed in the camera coordinate system to a vector expressed in the ground coordinate system, and  $r_{q/c}(t)$  is related to the states by

$$r_{q/c}(t) = \begin{bmatrix} \frac{x_1(t)}{x_3(t)} & \frac{x_2(t)}{x_3(t)} & \frac{1}{x_3(t)} \end{bmatrix}^T.$$

Substituting (4-2) into (2-11) yields a new expression for  $g(t, x(t))$  given as

$$\begin{aligned} \dot{x}_1(t) &= \Omega_1(t, x) + \xi_1(t, x) + \phi_1(x(t)) x_3(t) - x_1(t) \phi_3(x(t)) x_3(t), \\ \dot{x}_2(t) &= \Omega_2(t, x) + \xi_2(t, x) + \phi_2(x(t)) x_3(t) - x_2(t) \phi_3(x(t)) x_3(t), \\ \dot{x}_3(t) &= v_{c3}(t) x_3^2(t) - (\omega_2(t) x_1(t) - \omega_1(t) x_2(t)) x_3(t) - \phi_3(x(t)) x_3^2(t). \end{aligned}$$

Although the target motion model,  $\phi(x(t)) \triangleq [\phi_1(x(t)), \phi_2(x(t)), \phi_3(x(t))]^T$ , is assumed to be known, the states are unknown and therefore the estimated target velocity,  $\hat{v}_q(t) \in \mathbb{R}^3$  is given by

$$\hat{v}_q(t) = \phi(\hat{x}(t)).$$

A wide variety of object motions can be described by a feedback law in the form of (4-2). For example, consider the scenario of a vehicle moving with a known constant nominal speed. In this case, the velocity of the vehicle,  $\hat{v}_q(t)$ , is determined based on the location of the vehicle (e.g., based on whether the vehicle is traveling on an East/West road or North/South road, and which side of the road the vehicle is on). The state estimates can also be used to determine if the vehicle is at an intersection, and  $\hat{v}_q(t)$  can be adjusted based on that information. A model of the form in (4-1) can also be generated in cases where the object is undergoing projectile or orbital motion. In

these cases, the object velocity is a function of the object position. Similarly, in eye-to-hand image based visual servoing, a control law of the form in (4-1) is designed, and therefore known.

In applications where the object and camera are cooperative, the object can directly communicate its velocities to the camera. This is a common scenario in GPS-denied environments, where the object of interest might be a ground vehicle, which is being observed by a high altitude aerial vehicle with an active GPS signal [125, 126], or when multiple cooperative agents are each observing each other to reduce the overall position uncertainty growth rate [127–130]. Once the relative position vector is estimated, the geographic coordinates of the ground vehicle can be determined and continuously estimated even if the camera intermittently loses line of sight.

#### 4.1 Structure Estimation Objective

Similar to Chapter 3, to quantify the structure estimation objective, let the state estimation error,  $e(t) \in \mathbb{R}^3$ , be defined as

$$e(t) = x(t) - \hat{x}(t),$$

where  $\hat{x}(t) \in \mathbb{R}^3$  denotes the continuous state estimate. Consider the family of systems defined in (3-4) and repeated here

$$\dot{e}(t) = f_p(t, x(t), \hat{x}(t)). \quad (4-3)$$

When the target is in view, the states  $x_1$  and  $x_2$  are measurable, and the error dynamics are given by (3-5), i.e.,

$$f_s = g(t, x) - \dot{\hat{x}}. \quad (4-4)$$

In contrast to Chapter 3, when the target is outside the camera FOV, the state estimates are updated using a target motion model described in Assumption 4.1 and a predictor of

the form

$$\dot{\hat{x}} = \text{proj}(g(t, \hat{x}(t))),$$

resulting in the error dynamics

$$f_u(t, x(t), \hat{x}(t)) = g(t, x(t)) - \text{proj}(g(t, \hat{x}(t))), \quad (4-5)$$

where  $\text{proj}(\cdot)$  is a smooth projection operator (see [133], Remark 3.7 in [134] or §4.4 in [104]) with bounds based on the state bounds of Assumption 2.1 and the velocity bounds in Assumptions 2.2 and 4.1. Since  $g(t, x(t))$  is continuously differentiable with respect to  $x(t)$  on the compact set  $\mathcal{X}$ , the mean value theorem can be invoked to bound the error dynamics during the unobservable periods as

$$\|f_u(t, x(t), \hat{x}(t))\| \leq K \|e(t)\|, \quad (4-6)$$

where  $K \in \mathbb{R}$  is a bounded constant.

## 4.2 Stability Analysis

To facilitate the following development, let  $T^u(t, \tau)$  denote the total time the subsystem  $u$  is active in the time interval  $[\tau, t]$ , where  $0 \leq \tau \leq t$ . Also, let  $N_\sigma(t, \tau) \in \mathbb{N}$  denote the number of switches of the switching signal  $\sigma : [0, \infty) \rightarrow \{s, u\}$  during the time interval  $(\tau, t)$ . Then, using the definition from [135], the switching signal  $\sigma$  is said to have an average dwell time  $\tau_a$  if there exists constants  $N_0, \tau_a \in \mathbb{R}_{>0}$  such that

$$N_\sigma(t, \tau) \leq N_0 + \frac{t - \tau}{\tau_a}, \quad \forall t \geq \tau \geq 0.$$

Finally, let  $\mathcal{P}$  be an index set with partition  $\{\mathcal{P}_s, \mathcal{P}_u\}$  for the family of systems

$$\dot{\eta} = \phi_p(\eta, t), \quad \forall p \in \mathcal{P} \quad (4-7)$$

where  $\eta(t) \in \mathbb{R}^n$ ,  $t \in [0, \infty)$  and  $\phi_p : \mathbb{R}^n \rightarrow \mathbb{R}^n$ .

Based on Assumption 2.4, the state estimate errors will converge to zero when measurements are available. Similarly, when measurements are unavailable, the growth

of the estimation errors are bounded by an exponential based on (4-3) and (4-6). Hence, a quadratic Lyapunov-like function is expected to evolve similar to Figure 4-1 across multiple instances of losing and regaining measurement availability. The goal is to show that, despite intermittent growth in the Lyapunov-like function, the overall trend is convergence to zero, and therefore convergence of the estimation errors. Lemma 4.1 shows that for a set of exponentially stable and exponentially unstable Lyapunov-like functions, the overall trend is convergence to zero if more time is spent in stable systems (proportional to the decay and growth rates of the stable and unstable systems, respectively) and if switching between systems does not occur too often, on average. Using this result, Theorem 4.1 indicates that the vision based estimation approach developed in this chapter is exponentially stable by developing Lyapunov-like functions that satisfy the hypotheses of Lemma 4.1.

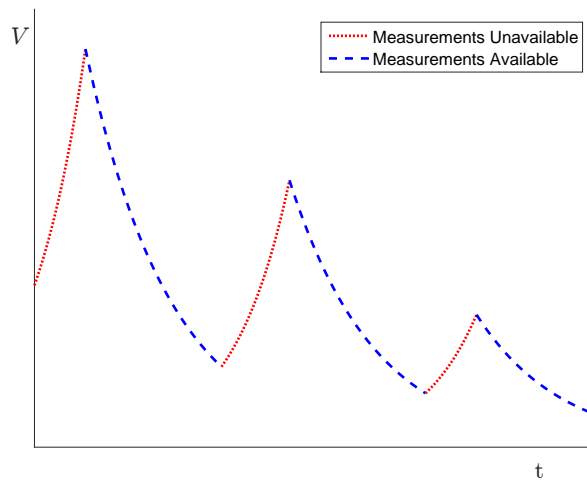


Figure 4-1. Evolution of a Lyapunov-like function across multiple periods of losing and regaining visibility of the object.

**Lemma 4.1.** *Consider the family of systems in (4-7). Suppose there exists continuously differentiable functions  $V_p : \mathbb{R}^n \times [0, \infty) \rightarrow \mathbb{R}$ , strictly positive constants  $c_1, c_2, \lambda_s, \lambda_u \in \mathbb{R}_{>0}$  and constant  $\mu \in \mathbb{R}$  greater than 1 such that*

$$c_1 \|\eta(t)\|^2 \leq V_p(\eta(t), t) \leq c_2 \|\eta(t)\|^2$$

$$\begin{aligned}\frac{\partial V_p}{\partial t} + \frac{\partial V_p}{\partial \eta} \phi_p(\eta(t), t) &\leq -\lambda_s V_p(\eta(t), t), \quad \forall p \in \mathcal{P}_s \\ \frac{\partial V_p}{\partial t} + \frac{\partial V_p}{\partial \eta} \phi_p(\eta(t), t) &\leq \lambda_u V_p(\eta(t), t), \quad \forall p \in \mathcal{P}_u \\ V_p(\eta(t), t) &\leq \mu V_q(\eta(t), t), \quad \forall p, q \in \mathcal{P}.\end{aligned}$$

If there exists positive constants  $\rho, T_0 \in \mathbb{R}_{\geq 0}$  such that

$$\rho < \frac{\lambda_s}{\lambda_s + \lambda_u}$$

$$T^u(t, \tau) \leq T_0 + \rho(t - \tau), \quad \forall t \geq \tau \geq 0$$

and if  $\sigma : [0, \infty) \rightarrow \mathcal{P}$  is a piecewise constant, right continuous switching signal with average dwell time

$$\tau_a > \frac{\ln \mu}{\lambda_s(1 - \rho) - \lambda_u \rho}$$

then the switched system

$$\dot{\eta}(t) = \phi_{\sigma}(\eta(t), t)$$

is globally exponentially stable.

*Proof.* Lemma 4.1 is an extension to Theorem 2 in [103] for nonautonomous systems with nonautonomous functions  $V_p(\eta(t), t)$ . The majority of the proof is omitted here as it is identical to the proof of Lemma 1 in [103]. However, in this case, the functions  $\alpha_1, \alpha_2 \in \mathcal{K}_{\infty}$  are quadratic and the trajectory of the switched system can be reduced to

$$\|\eta(t)\| \leq \frac{c_2}{c_1} \mu^{N_0} \exp((\lambda_s + \lambda_u) T_0) \exp(-\lambda(t - t_0)) \|\eta(0)\|$$

where  $\lambda \triangleq \frac{1}{2} \left( \lambda_s - (\lambda_s + \lambda_u) \rho - \frac{\ln \mu}{\tau_a} \right) \in (0, (1 - \rho) \lambda_s + \rho \lambda_u) \subset \mathbb{R}_{>0}$ . □

**Theorem 4.1.** *The switched system*

$$\dot{e}(t) = f_{\sigma}(t, x(t), \hat{x}(t))$$

generated by the family of systems described by (4-3), (4-4), and (4-5) and piecewise constant, right continuous switching signal  $\sigma : [0, \infty) \rightarrow \{s, u\}$  is globally exponentially

stable provided that the switching signal  $\sigma$  satisfies the total unstable activation time condition

$$T^u(t, \tau) \leq T_0 + \rho(t - \tau), \quad \forall t \geq \tau \geq 0 \quad (4-8)$$

and average dwell time condition

$$\tau_a > \frac{\ln \mu}{\lambda_s(1 - \rho) - \lambda_u \rho}, \quad (4-9)$$

where  $T_0 \in \mathbb{R}$  is an arbitrary positive constant and  $\rho, \lambda_s, \lambda_u, \mu \in \mathbb{R}$  are known positive constants that satisfy  $\mu \geq 1$  and  $\rho < \frac{\lambda_s}{\lambda_s + \lambda_u}$ .

*Proof.* Via the Converse Lyapunov Theorem in [123, Theorem 4.14], the existence of an exponential state tracking observer from Assumption 2.4 implies the existence of a Lyapunov function  $V_s : [0, \infty) \times \mathbb{R}^3 \rightarrow \mathbb{R}$  that satisfies

$$c_1 \|e(t)\|^2 \leq V_s(t, e(t)) \leq c_2 \|e(t)\|^2 \quad (4-10)$$

$$\begin{aligned} \frac{\partial V_s}{\partial t} + \frac{\partial V_s}{\partial e}(\dot{e}(t)) &\leq -c_3 \|e(t)\|^2 \\ \left\| \frac{\partial V_s}{\partial e} \right\| &\leq c_4 \|e(t)\| \end{aligned} \quad (4-11)$$

for some positive scalar constants  $c_1, c_2, c_3, c_4 \in \mathbb{R}$ , during the periods in which the target is observable. From (4-10) and (4-11), it is clear that

$$\dot{V}_s(t, e(t)) \leq -\lambda_s V_s(t, e(t))$$

when the target is in view, where  $\lambda_s \triangleq \frac{c_3}{c_2}$ . Consider a continuously differentiable, Lyapunov-like function,  $V_u : [0, \infty) \times \mathbb{R}^3 \rightarrow \mathbb{R}$  defined as

$$V_u(t, e(t)) \triangleq c_5 \|e(t)\|^2$$

where  $c_5 \in \mathbb{R}$  is bounded by  $c_1 \leq c_5 \leq c_2$ . Using (4–6), the growth of  $V_u(t, e(t))$  during the periods in which the target is outside the camera FOV can be bounded as

$$\dot{V}_u(t, e(t)) \leq 2c_5 \|e(t)\| (K \|e(t)\|) \leq \lambda_u V_u(t, e(t)),$$

where  $\lambda_u \triangleq 2K$ . From (4–10) and 4.2, the functions  $V_s(t, e(t))$  and  $V_u(t, e(t))$  can be related by

$$V_p(t, e(t)) \leq \mu V_q(t, e(t)), \quad \forall p, q \in \{s, u\},$$

where  $\mu \triangleq \frac{c_2}{c_1}$ . Using Lemma 4.1, the system is globally exponentially stable for any switching signal that satisfies (4–8) and (4–9) with trajectory

$$\|e(t)\| \leq \|e(0)\| C \exp(-\lambda(t - t_0)),$$

decay rate  $\lambda \triangleq \frac{1}{2} \left( \lambda_s - (\lambda_s + \lambda_u) \rho - \frac{\ln \mu}{\tau_a} \right) \in (0, (1 - \rho) \lambda_s + \rho \lambda_u) \subset \mathbb{R}_{>0}$  and positive constant  $C \triangleq \frac{c_2}{c_1} \mu^{N_0} \exp((\lambda_s + \lambda_u) T_0) \in \mathbb{R}_{>0}$ . □

*Remark 4.2.* In application, the constraint on the unstable activation time (i.e. (4–8)) is trivially satisfied. An arbitrarily large amount of time can be spent in the unstable system (i.e., measurements are unavailable), and  $T_0$  can be increased to compensate. This condition is only relevant in the limit as  $t \rightarrow \infty$ , where, on average, more time needs to be spent in the stable system (i.e., measurements are available) based on the relative convergence and divergence rates of the two systems. However, by increasing  $T_0$  to satisfy stability conditions for large unstable activation times  $T^u(t, \tau)$ , the bounding envelope on the estimation error increases exponentially. This highlights the importance of increasing the duration in which the object is visible, even in the short term.

*Remark 4.3.* The average dwell time,  $\tau_a$ , and the total allowable invisibility time in (4–8), are functions of the error decay and growth rates of the observer and predictor. As the observer convergence rate increases or the predictor divergence rate decreases, the upper bound on the allowable  $\rho$  increases, increasing the total allowable time duration

in which the object can remain outside of the camera FOV. In addition, increasing  $\rho$  decreases the lower bound on the allowable average dwell time, enabling the use of a larger set of switching signals. However, increasing  $\rho$  decreases the convergence rate of the switched system; by allowing longer durations in which measurements are unavailable (from (4–8)), the error of the switched system is slower to converge. Conversely, as  $\rho \rightarrow 0$ , the allowable amount of time without measurements decreases and the convergence rate of the switched system increases. The limiting case where  $\rho = 0$  denotes the case when measurements are available for all time after a finite number of switches. Finally, switching signals with larger average dwell times also increase the switched system convergence rate since the jumps in the Lyapunov-like functions occur less frequently.

*Remark 4.4.* The average dwell time conditions in Lemma 4.1 and Theorem 4.1 come as a result of the possibility that the Lyapunov-like functions for each subsystem may differ, even though they all satisfy a common quadratic bound. However, in some cases (e.g., [31, 122]), the constants  $c_1$  and  $c_2$  are equal, and  $c_5$  can be chosen as  $c_5 = c_1 = c_2$ . Therefore,  $\mu = 1$  and the average dwell time condition reduces to the trivial condition  $\tau_a > 0$ .

### 4.3 Simulation

Simulations were performed using MATLAB to verify the robustness to measurement loss of the proposed observer and predictor estimation scheme. The observer in [119] was used to satisfy Assumption 2.4 and estimate the states when measurements were available, while the predictor in (6–10) was used when measurements were unavailable. Camera and object velocities,  $v_c(t) = \begin{bmatrix} 2 & 1 & 0.5 \cos(t/2) \end{bmatrix}^T$  m/s,

$\omega(t) = \begin{bmatrix} 0 & 0 & 1 \end{bmatrix}^T$  rad/s and  $v_q(t) = \begin{bmatrix} 0.5 & 0 & 0 \end{bmatrix}^T$  m/s and observer matrices,

$$A = \begin{bmatrix} 0 & -1 & 2 \\ 1 & 0 & 1 \\ 0 & 0 & 0 \end{bmatrix}, C = \begin{bmatrix} 1 & 0 & 0 \\ 0 & 1 & 0 \end{bmatrix}, D = \begin{bmatrix} 1 \\ 0 \\ 0 \end{bmatrix},$$

$$K = \begin{bmatrix} 0.8278 & 0 \\ 0 & 0.8278 \\ -1.5374 & 0 \end{bmatrix}, Y = \begin{bmatrix} 0 & 0 \\ 0 & -1 \\ 0 & -1.5374 \end{bmatrix}$$

were set to match the simulation parameters in [119]. The switching signal,  $\sigma$ , was generated with randomly selected dwell times. The dwell times were selected from a uniform random distribution between 0 and 5 seconds, and 0 and 2 seconds for the  $s$  and  $u$  subsystems, respectively. Simulation results are shown in Figure 4-2 with the switching times shown as vertical lines where the first vertical line represents the time when the object is no longer visible (i.e., the predictor is started with the last state estimate from the estimator), and the next vertical line represents the time when the object is in view again and the estimator is restarted with the state estimate from the predictor, etc.

An ad hoc approach for state estimation while undergoing intermittent measurements would be to implement a ZOH during periods in which measurements are unavailable, as in Chapter 3. For comparison, a simulation using the approach described in Chapter 3 was also performed. As shown in Figure 4-3, using the same switching signal and observer as in the previous simulation, the performance greatly degrades, with no indication of convergence. The results from Figure 4-2 and Figure 4-3 indicate that the predictor not only provides accurate state estimates when measurements are unavailable, but also aids in observer convergence when measurements are available by reinitializing the observer with a more accurate initial state estimate. This demonstrates the tradeoff mentioned in the introduction: by utilizing more information (i.e., velocity

information of the object when it is not in view), a predictor can be utilized to relax dwell time conditions and ensure estimator convergence in the presence of a wider class of switching signals. However, if velocity information is not available, the more stringent conditions described in Chapter 3 must be satisfied to ensure convergence.

#### 4.4 Experiments

Experiments were also performed to verify the theoretical results. The overall goal of the experiment was to represent the scenario of tracking the Euclidean position of a cooperative mobile vehicle in a GPS-denied environment via a camera. Specifically, the objective was to demonstrate the convergence of the relative position estimation errors when the estimator and predictor structure described in Section 4.1 is implemented. The experimental setup for these experiments were the same as the setup described in Chapter 3.

Four experiments were performed. In the first experiment, the camera was mounted on a stationary tripod, while the mobile robot was driven via remote control in an arbitrary motion, including leaving and entering the camera FOV. In the second experiment, the camera was moved by hand in an arbitrary motion, while the TurtleBot was sent constant forward velocity and angular turn rate commands, resulting in an approximately circular path. In the second experiment, the intermittent measurements were caused by both the TurtleBot leaving the camera FOV, and an object placed directly in front of the camera lens, completely occluding the scene<sup>1</sup>. The resulting evolution of the state estimates and the reconstructed Euclidean coordinates of the target are shown in Figures 4-4 and 4-5 for the first experiment, and Figures 4-7 and 4-8 for the second experiment. In both cases, the estimates track the true values despite the intermittent visibility of

---

<sup>1</sup> A supplementary video with a representative sample of the motion of the mobile robot and the camera during the first two experiments is available at <https://www.youtube.com/watch?v=daSZAYXmt-g>

the mobile robot. As can be seen in the Figures 4-6 and 4-9, during periods when the object is not visible, the estimation error grows since there is no feedback from image measurements, though, exponential error growth would manifest as lines with constant positive slope on the log scale plots, indicating the estimation error growth bounds used in the stability analysis in Section 4.2 are conservative.

To analyze the growth of the estimation error during periods when measurements are unavailable, the Mean Value Theorem was used to develop a linear bound on  $f_u$ , as shown in (4-6). However, based on the quadratic terms in (2-11), the bounding constant  $K$  may need to be extremely large to bound  $f_u$  throughout the bounded set  $\mathcal{X}$ . Since only bounds on the states and velocities are available, the calculated value of  $K$  may also be larger than the smallest constant that bounds  $f_u$  during a specific application. To investigate the conservativeness of  $K$ , and therefore the conservativeness of the exponential bound developed in Theorem 4.1, Figures 4-10 and 4-11 show the error and its corresponding time derivative during the each experiment, as well as the linear best fit line, minimum bounding line, and bounding line calculated based on the known quantities in Assumptions 2.1 and 2.2. For the experiment with a static camera, the best fit line (blue) had a slope of 0.1862, the minimum bound (green) had a slope of 0.5098 and the calculated  $K$  (red) was 8.987. For the experiment with the moving camera, these values were 0.7337, 2.357 and 22.54, respectively. In both cases, the calculated bounds were an order of magnitude greater than the ideal bound; however, this is expected due to the conservative nature of Lyapunov analysis.

A third experiment was performed using a motion model of the target (as described in Assumption 4.1 and the proceeding explanation) rather than directly communicated velocities. In this experiment, a velocity field of the form shown in Figure 4-12 was prescribed in the world coordinate system, and a low level controller was implemented to have the mobile robot follow the velocity field, though it should be noted that the robot did not follow the velocity field exactly due to the nonholonomic constraints of the

robot and limits on the wheel velocity. The velocity field was rotated into the camera coordinate system and used as a velocity estimate of the robot in the predictor. For simplicity, camera feedback was artificially blocked at set intervals. The results of this experiment are shown in Figures 4-13 through 4-15. Despite the actual target velocities being unknown, the state estimates generated by the observer/predictor framework successfully track the true states, with steady state performance similar to that of the first two experiments, as seen in Figure 4-15, and as compared to Figures 4-6 and 4-9.

Finally, an extended Kalman filter (EKF) was implemented as an example of a typical probabilistic approach, where the robustness to intermittent measurements is inherent to predictor-corrector structure of these types of approaches. For this implementation, the covariance matrices were set based on an estimated 1 pixel uncertainty in the measurements, and 0.1 m/s uncertainty in the velocity information used in the dynamic model. The results of this experiment are shown in Figures 4-16 through 4-18, where it is apparent that convergence of the state estimate generated by the EKF is much slower compared to the nonlinear observer implemented in the first two experiments. However, in many applications, the covariance matrices are used as tuning parameters rather than selected based on the actual uncertainty in the system, and therefore estimation convergence performance may be improved through tuning.

#### **4.5 Summary**

An analysis is performed to demonstrate the robustness of a class of observers to intermittent loss of sensing. The analysis is applicable to any exponentially convergent, image-based observer. From signals generated via a known motion model of the target, a predictor is used in conjunction with the observer to provide state estimates during the periods when the target is unobservable. The predictor also aids in the stability analysis by bounding the error growth with an exponential during the unobservable periods. The system in Chapter 3 does not use a predictor, and the resulting error is bounded by a tangent function, with finite escape time, leading to hard constraints on the maximum

allowable dwell time in the unobservable system. In contrast, the result in this chapter leads to the more relaxed average dwell time and total activation time conditions in (4–8) and (4–9). If feature loss is uncontrollable, the average dwell time and total unstable activation time can be calculated and checked against (4–8) and (4–9) to verify the convergence of state estimates and therefore their trustworthiness. These conditions can also be used to relax trajectory constraints for camera motion. Simulation results confirm the improvements in stability and performance that the analyses suggest are a consequence of the use of a predictor as opposed to the ZOH approach.

Experiments were performed to demonstrate the stability and performance of the proposed estimator-predictor scheme in two common scenarios. The experimental results are compared to the theoretically developed bounds to elucidate how conservative Lyapunov analysis can be. In addition, an extended Kalman filter is implemented for the SfM problem as a comparison to the approach developed in this chapter. An example of how a common observer design that only recovers partial states can be augmented for full state estimation and therefore can be used during periods of target visibility is provided.

The novelty of the developed approach is the ability to reconstruct relative Euclidean measurements of a target viewed by intermittent camera observations using any exponentially convergent observer. This contribution is enabled by using switched systems methods to analyze the stability of the state estimate when constructed by switching between the observer and the predictor. However, the current predictor is limited to applications where target velocity information is measurable or available, either directly or through a known motion model. Further investigation is required to circumvent this requirement, either by changing the predictor structure, or learning a motion model online while the target is visible.

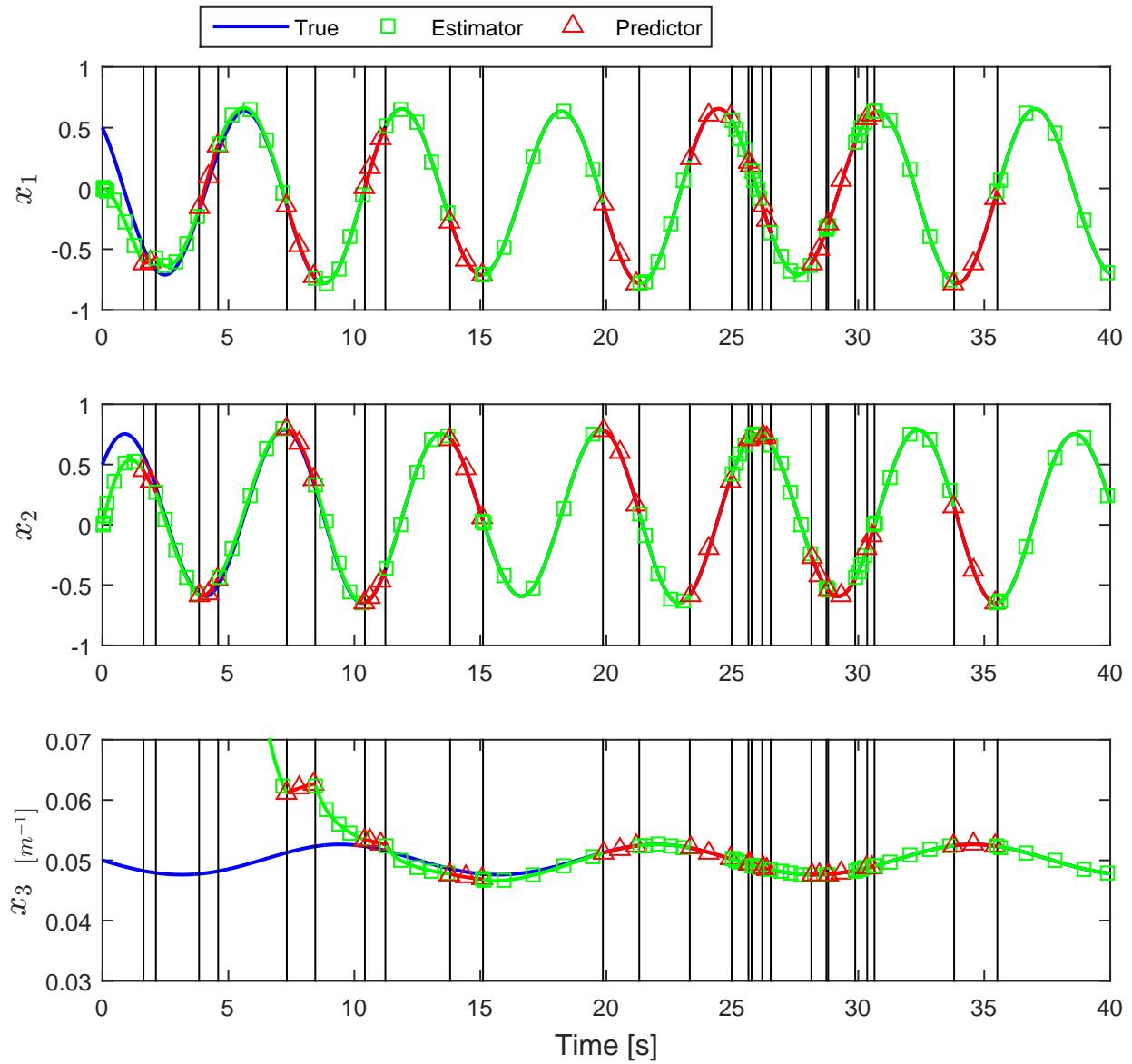


Figure 4-2. True and estimated states, utilizing a predictor to evolve the state estimates when measurements are unavailable. Vertical lines represent switching times.

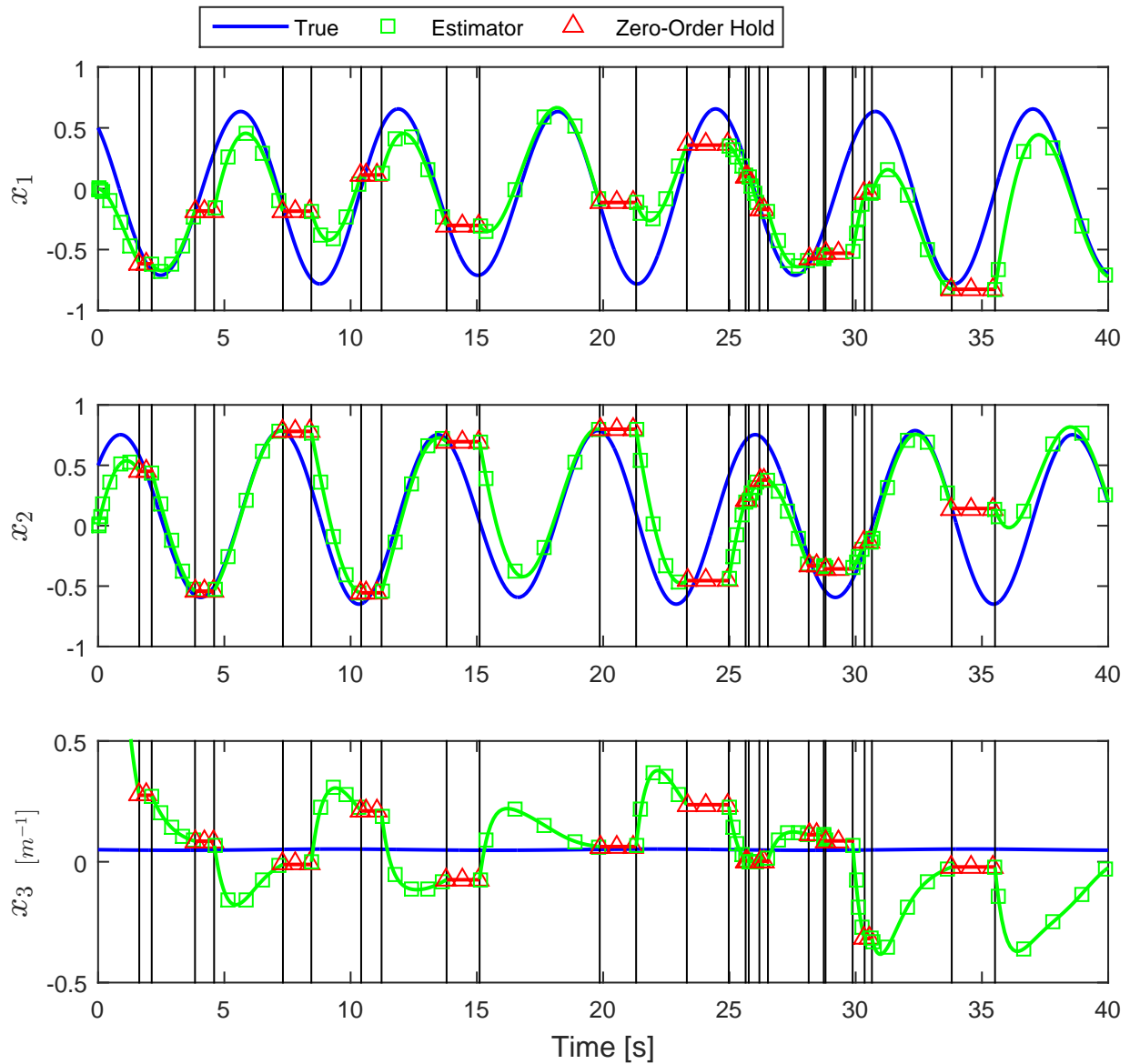


Figure 4-3. True and estimated states without a predictor. State estimates are held constant until measurements are available. Vertical lines represent switching times.

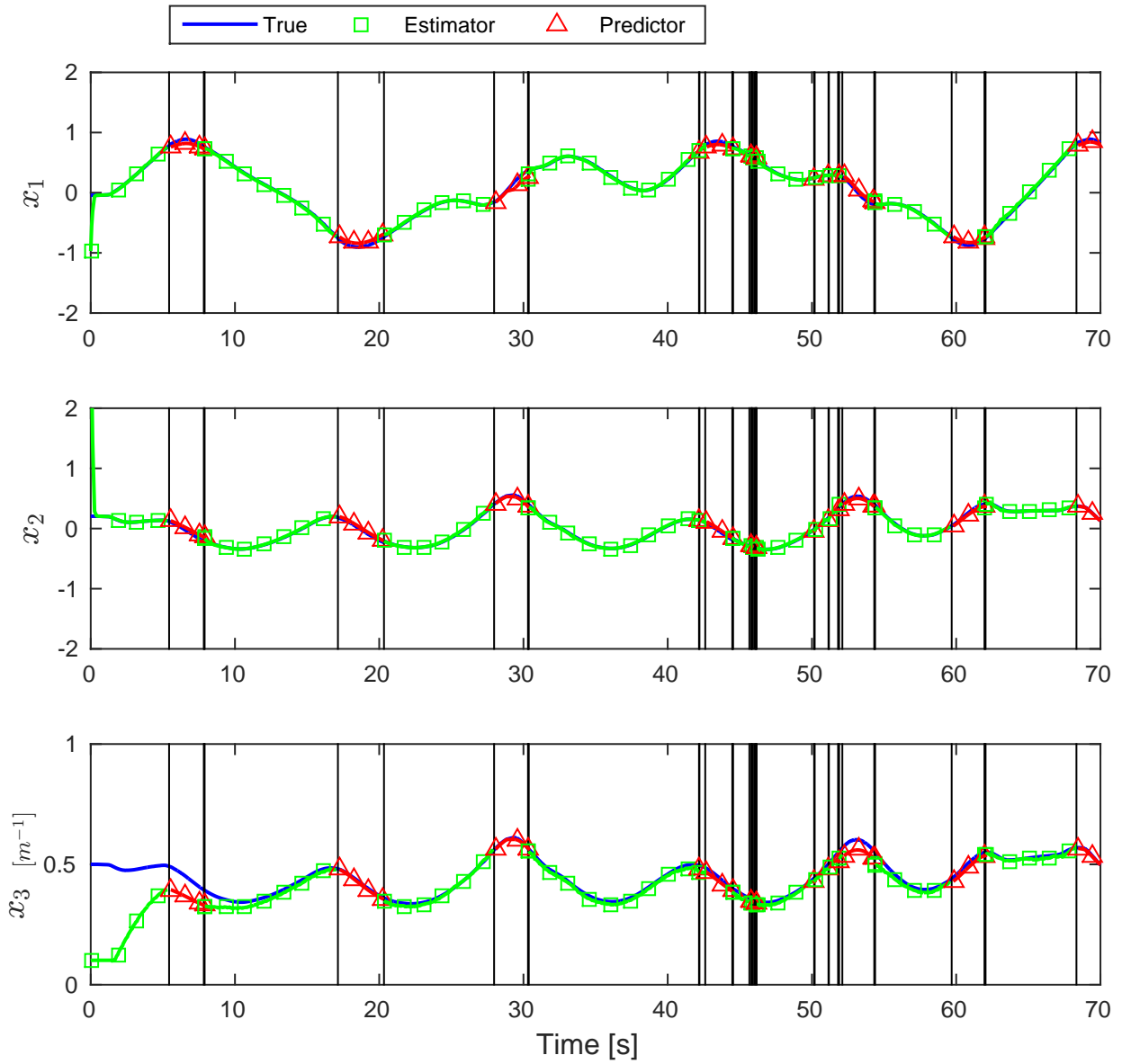


Figure 4-4. State estimates from the experiment with a static camera. Vertical black lines denote switches.

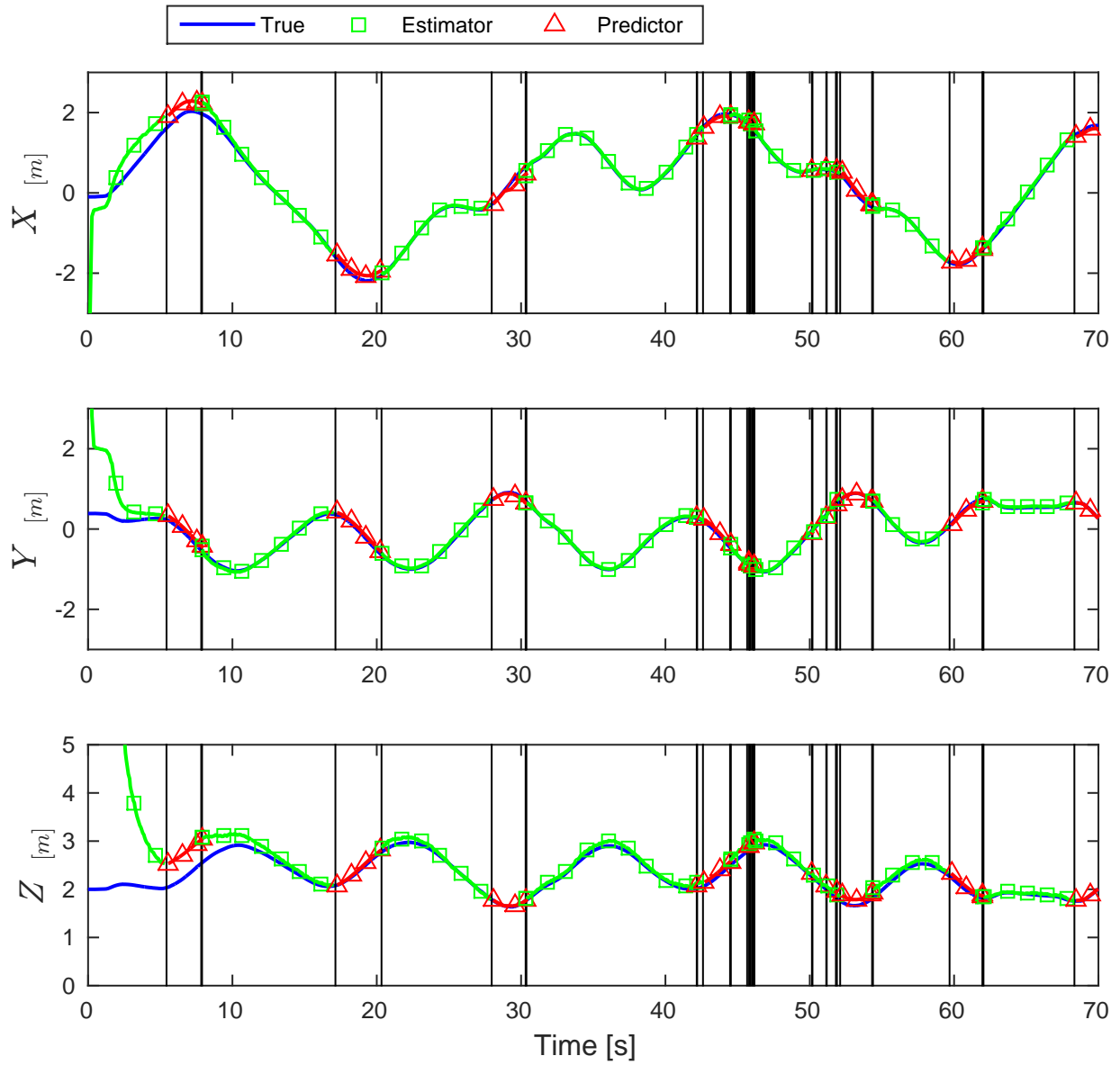


Figure 4-5. Reconstructed Euclidean coordinates of the target from the experiment with a static camera. Vertical black lines denote switches.

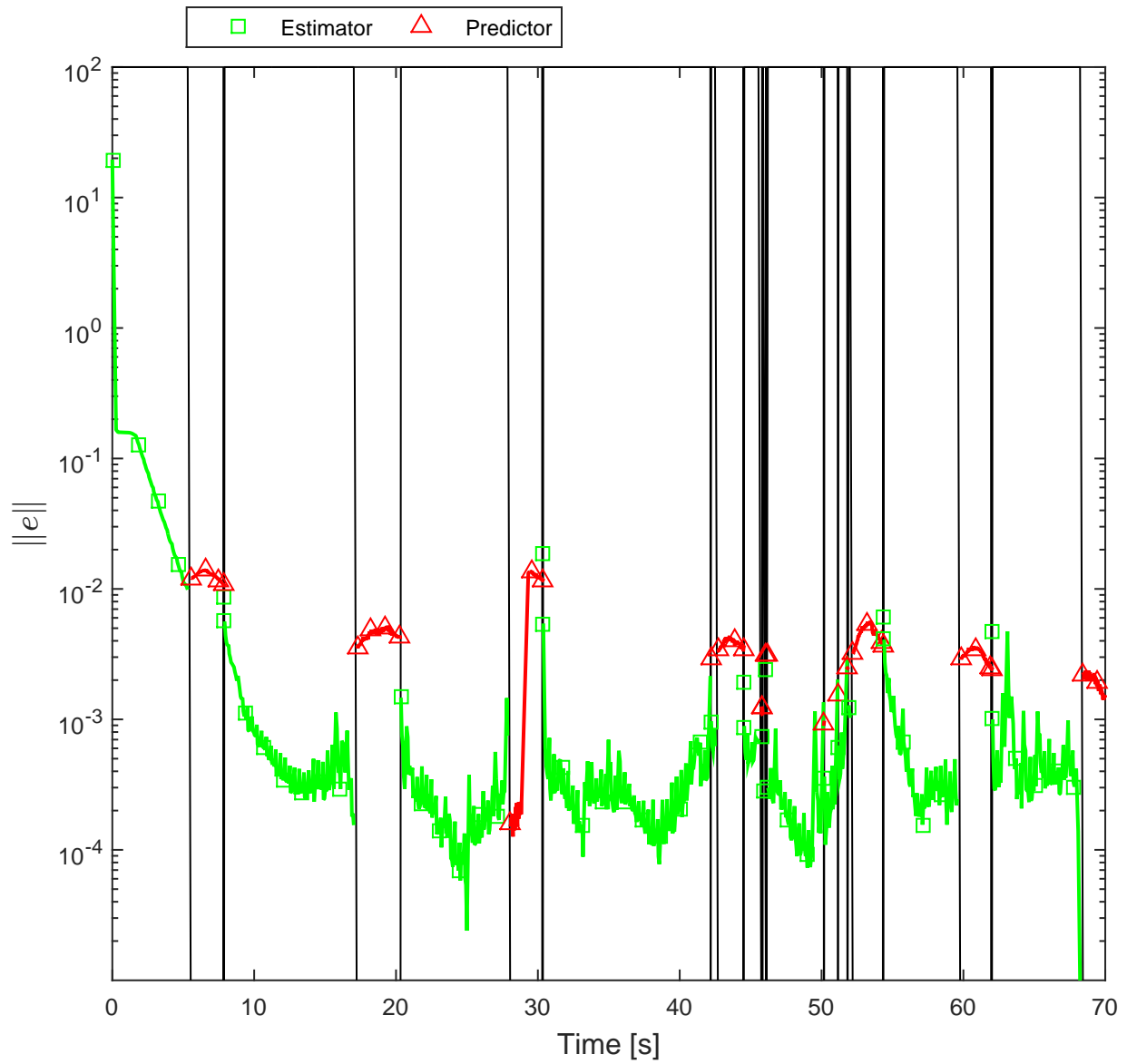


Figure 4-6. State estimation errors from the experiment with a static camera. Vertical black lines denote switches.

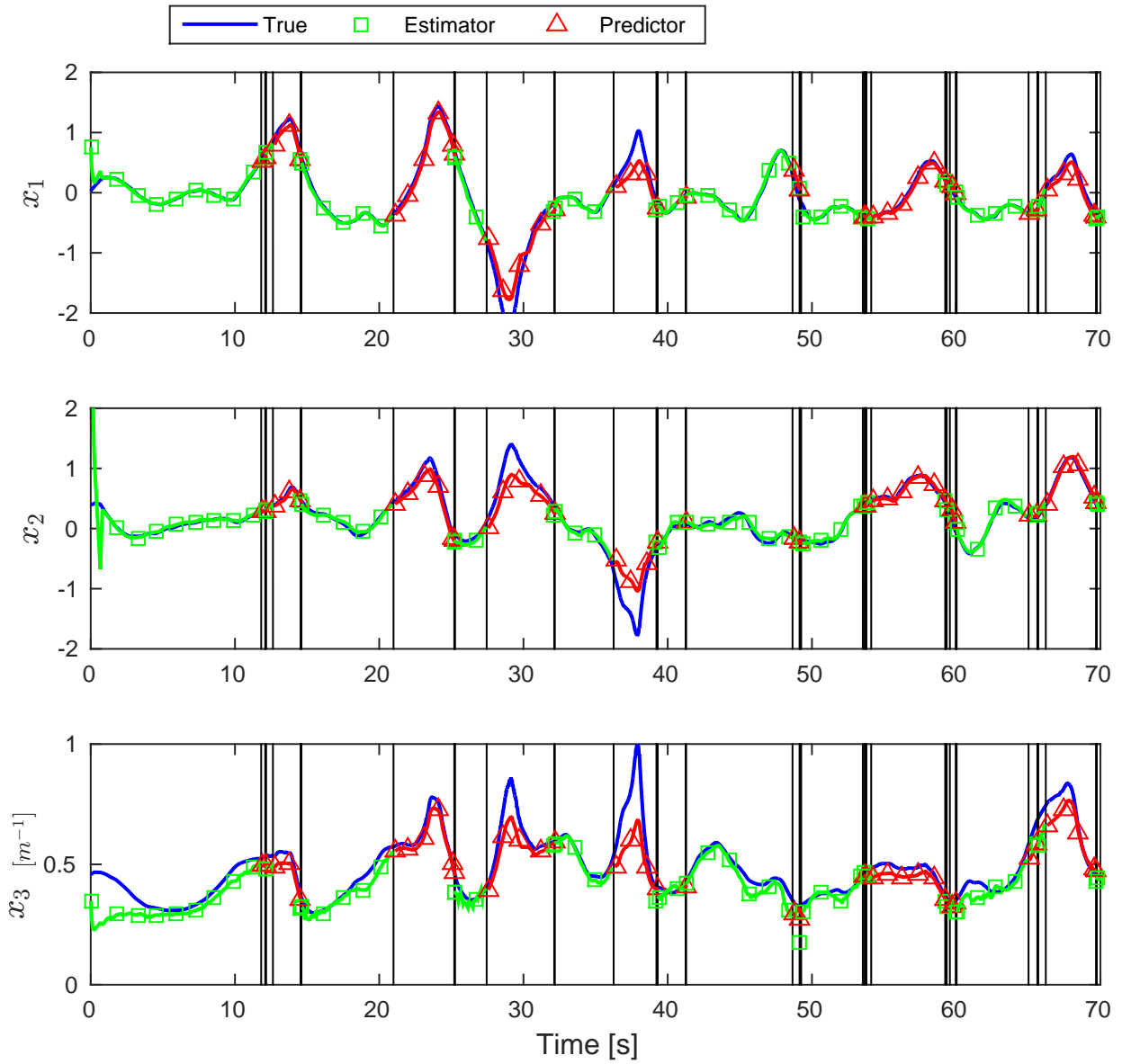


Figure 4-7. State estimates from the experiment with a moving camera. Vertical black lines denote switches.

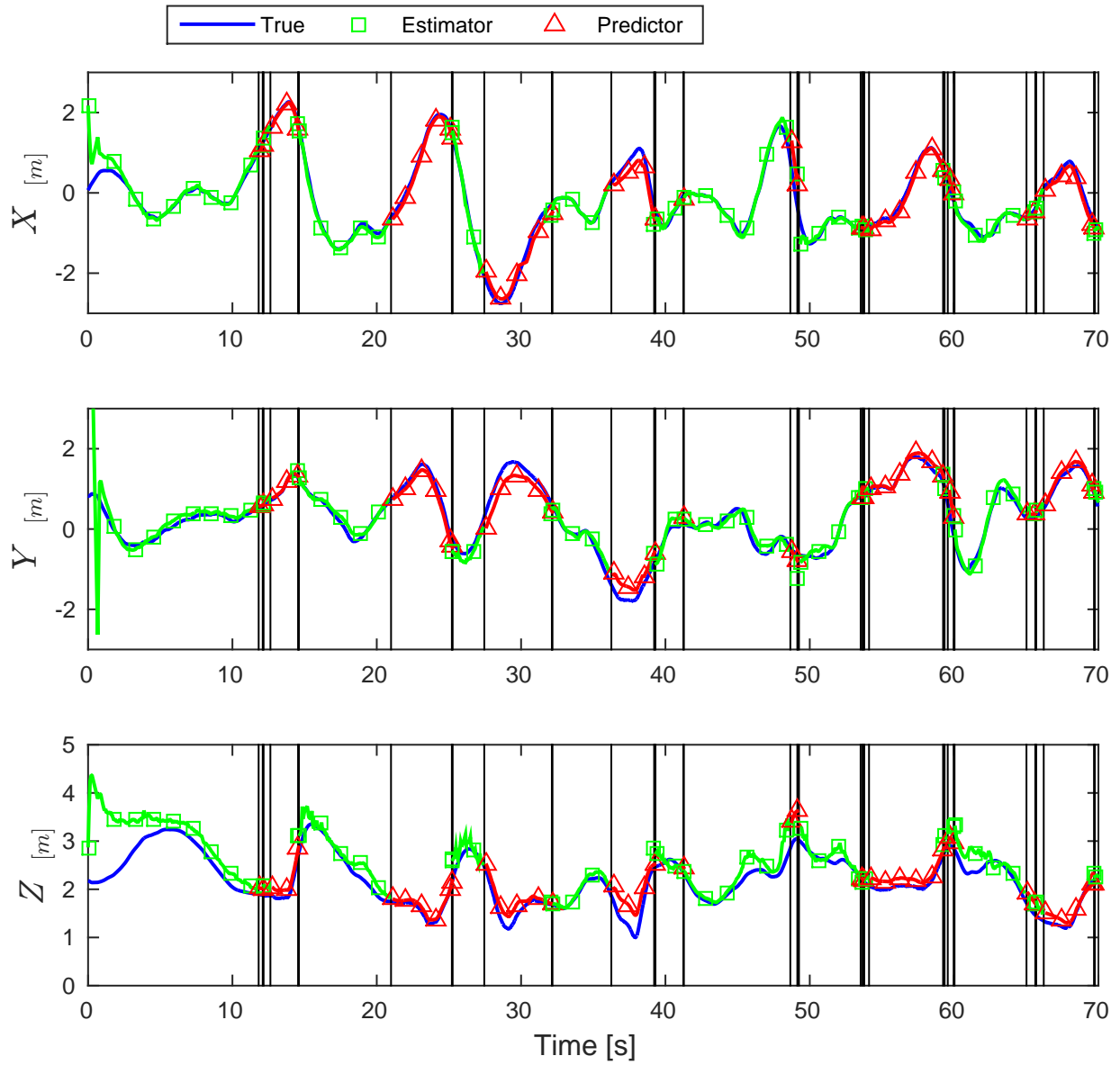


Figure 4-8. Reconstructed Euclidean coordinates of the target from the experiment with a moving camera. Vertical black lines denote switches.

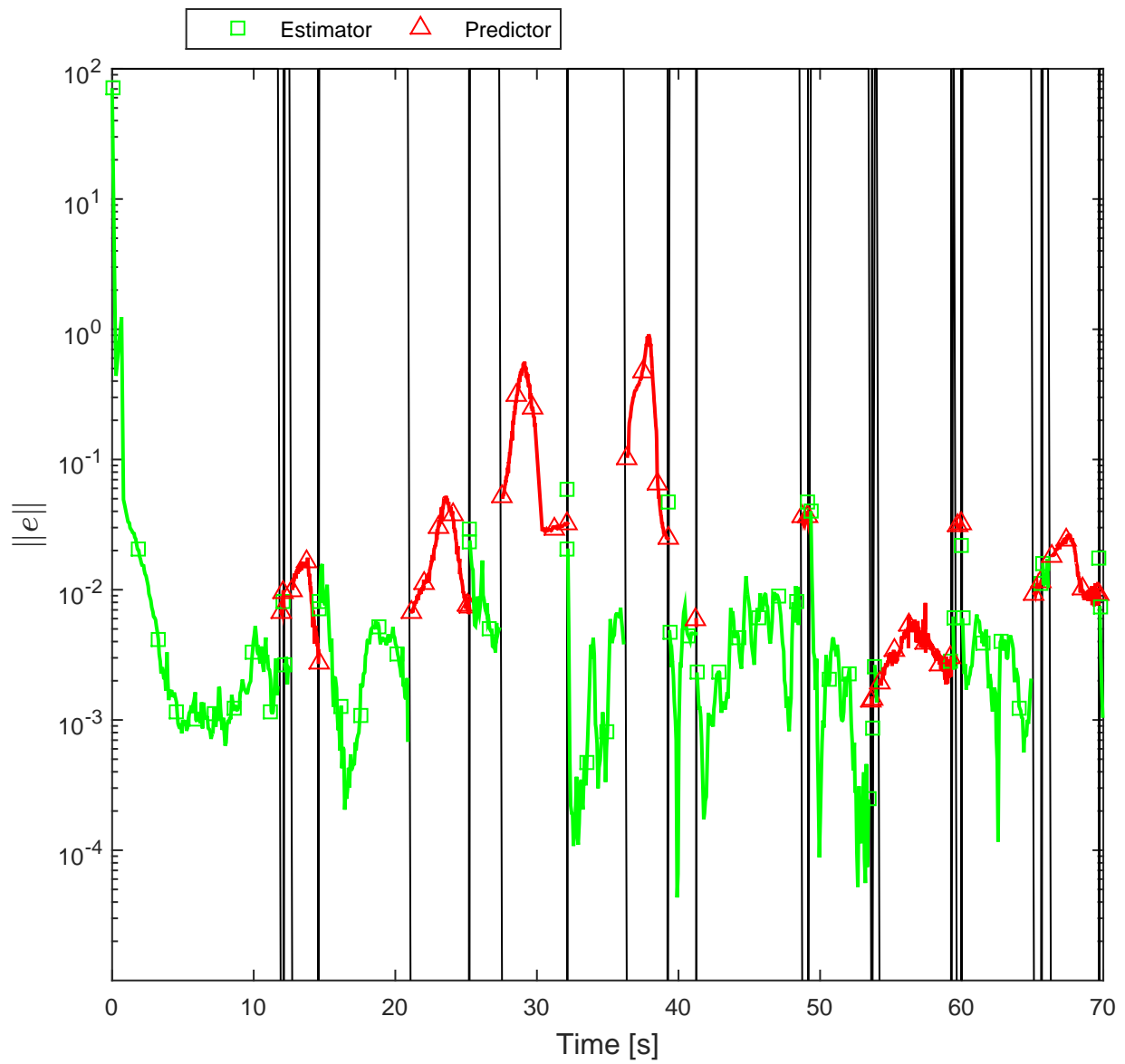


Figure 4-9. State estimation errors from the experiment with a moving camera. Vertical black lines denote switches.

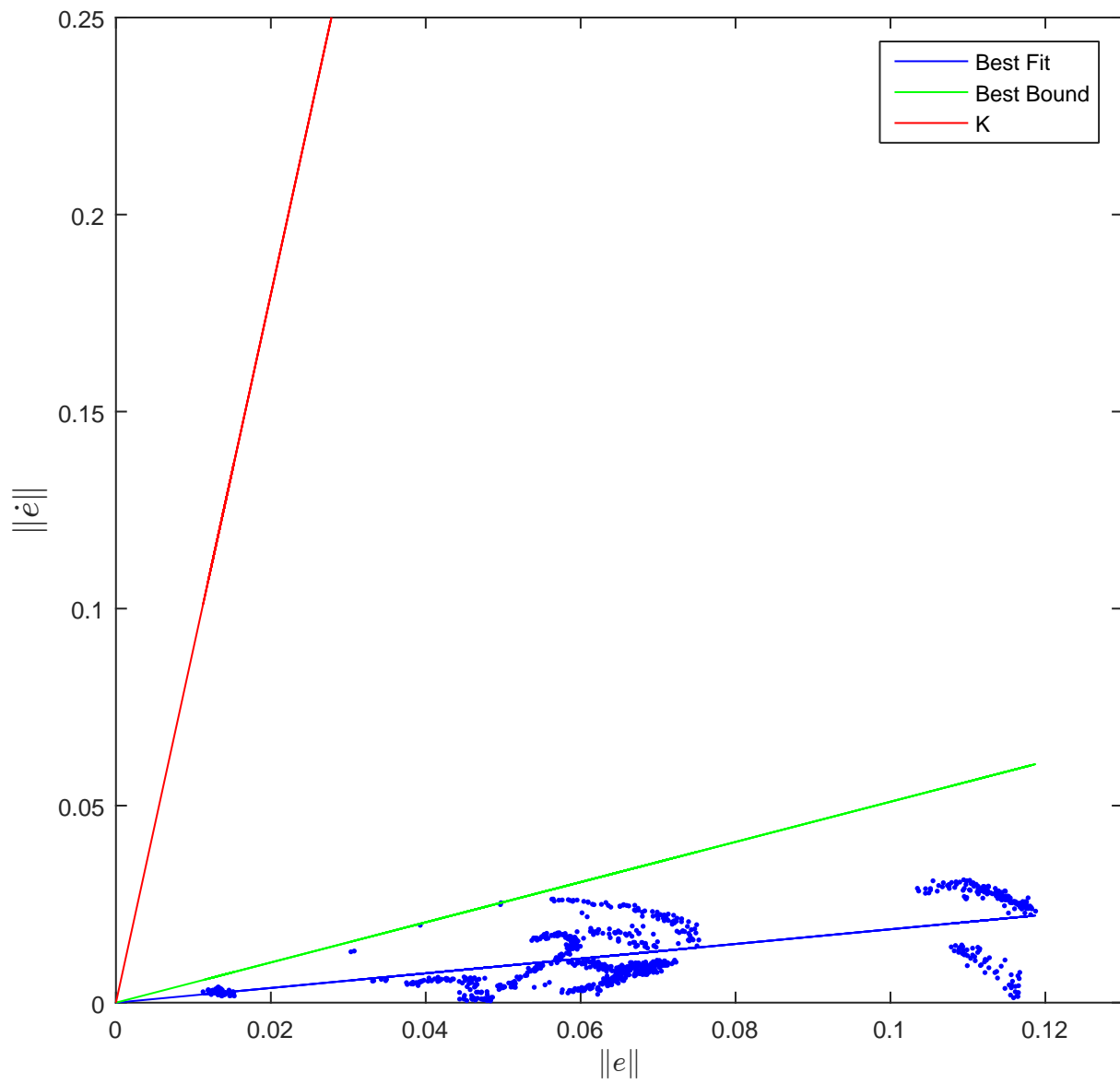


Figure 4-10. Error growth magnitude as a function of the magnitude of the error, and corresponding bounds, for the experiment with a static camera.

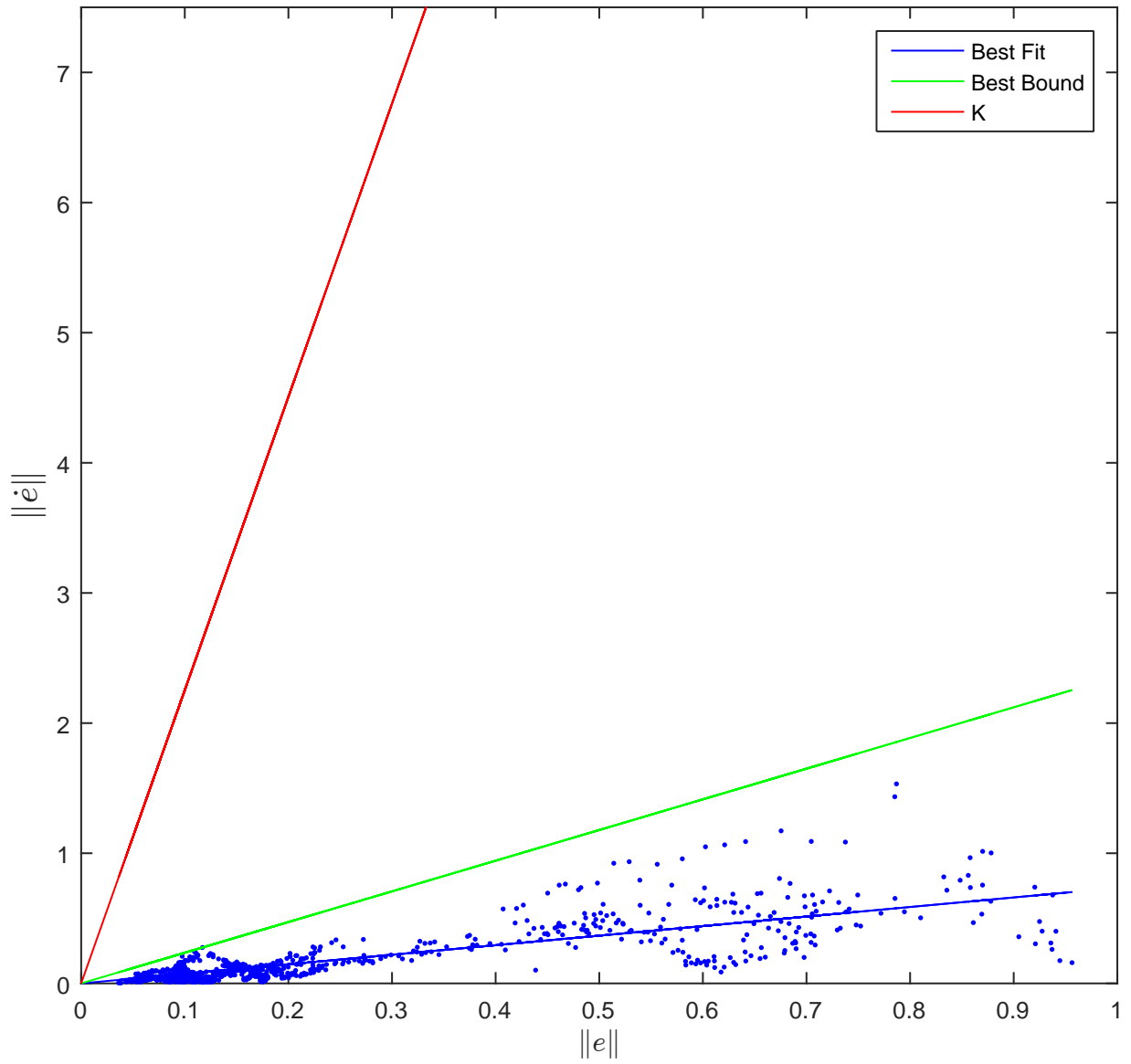


Figure 4-11. Error growth magnitude as a function of the magnitude of the error, and corresponding bounds, for the experiment with a moving camera.

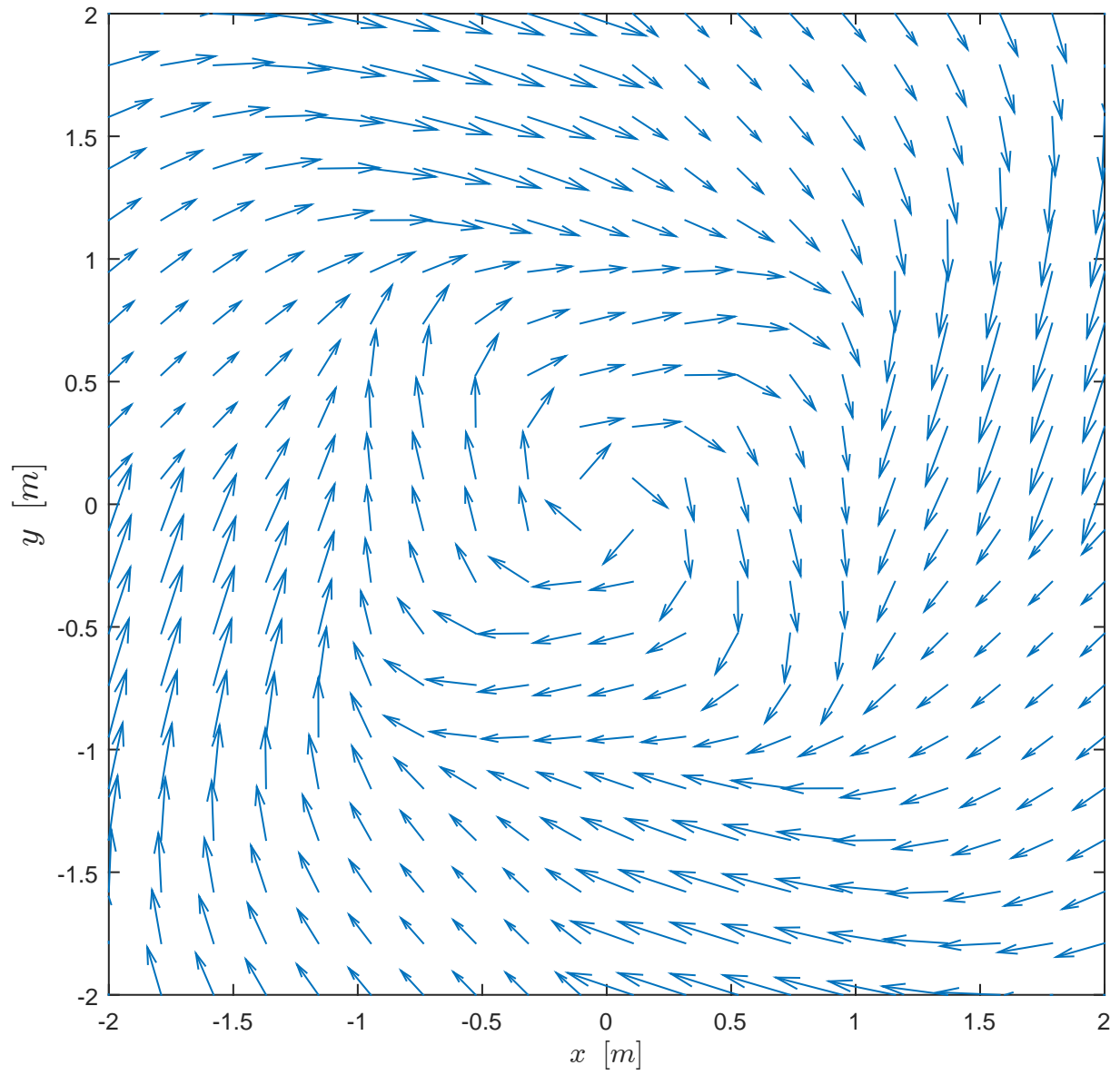


Figure 4-12. During one experiment, the target was commanded to follow this vector field.

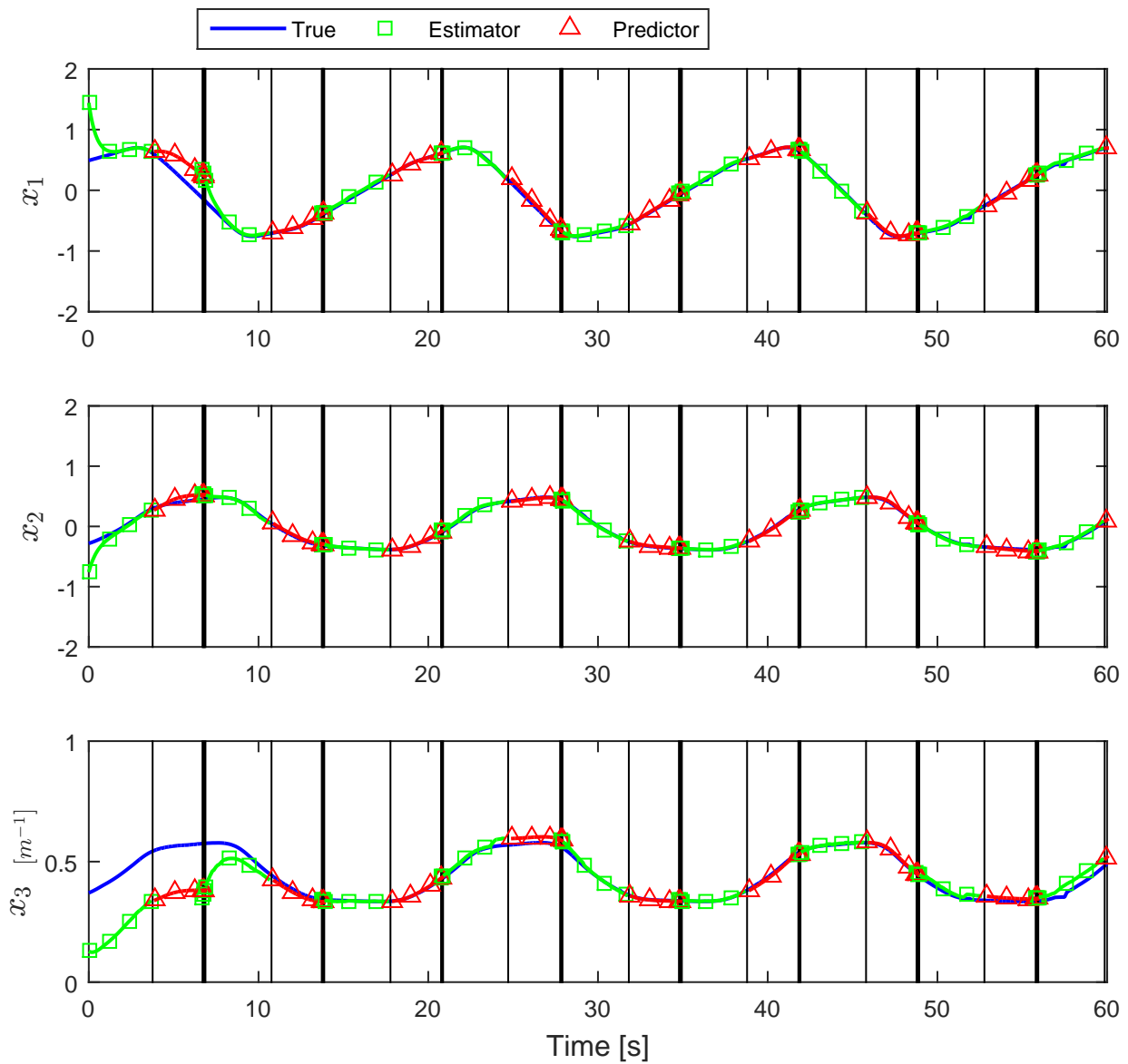


Figure 4-13. State estimates from the experiment where the target followed a known vector field. Vertical black lines denote switches.

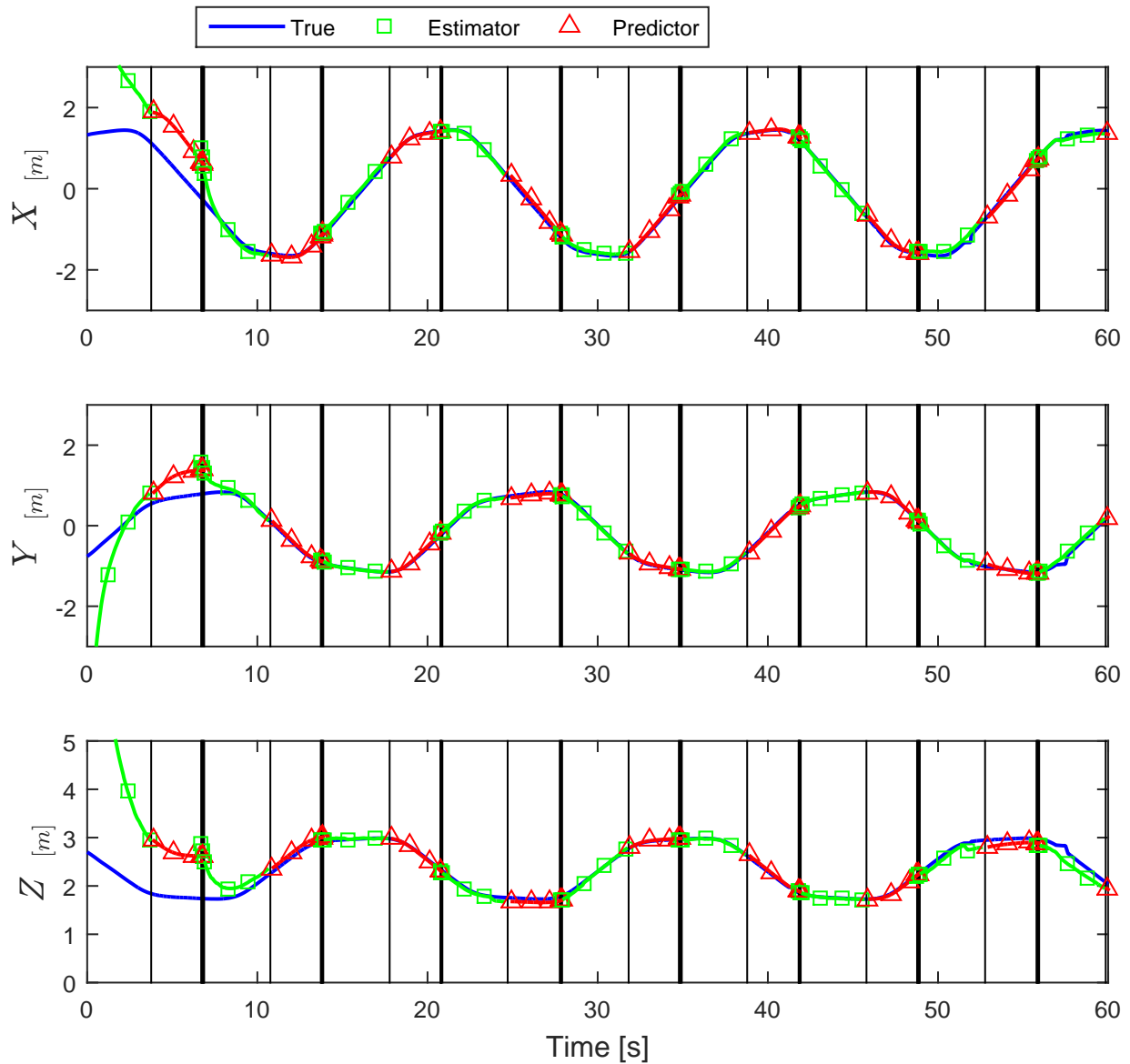


Figure 4-14. Reconstructed Euclidean coordinates of the target from the experiment where the target followed a known vector field. Vertical black lines denote switches.

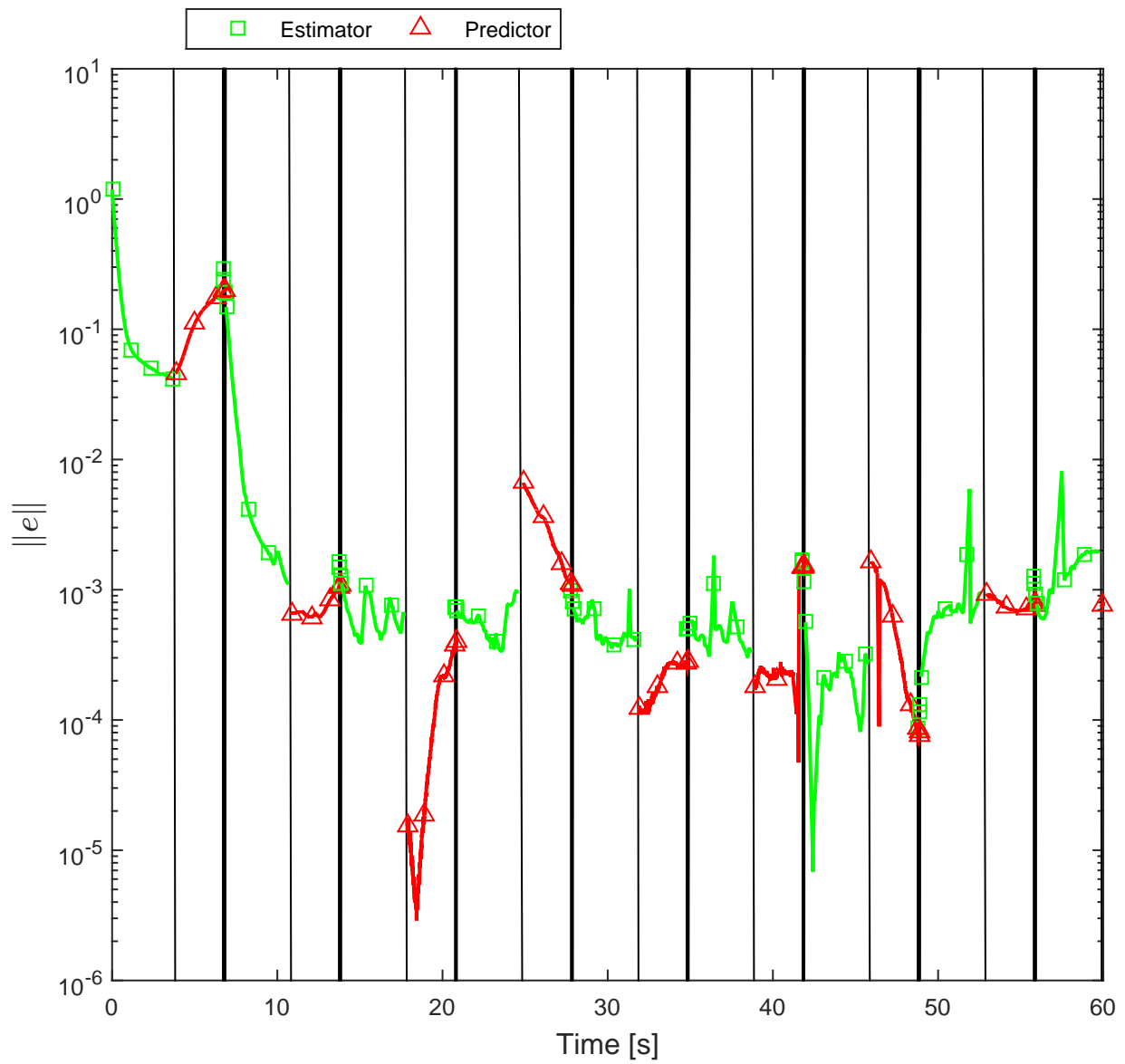


Figure 4-15. State estimation errors from the experiment the target followed a known vector field. Vertical black lines denote switches.

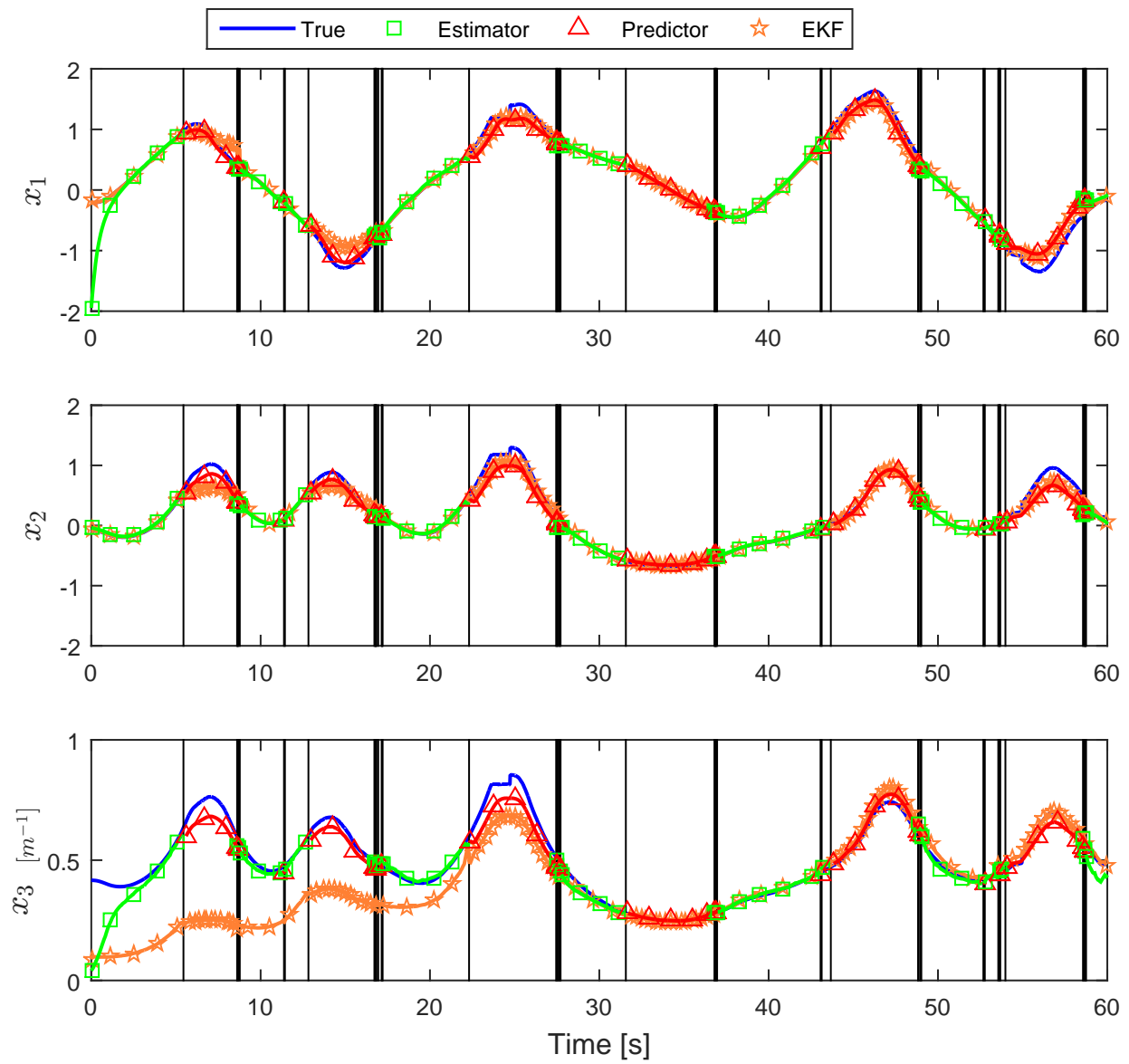


Figure 4-16. State estimates from the experiment where the target followed a known vector field. Vertical black lines denote switches.

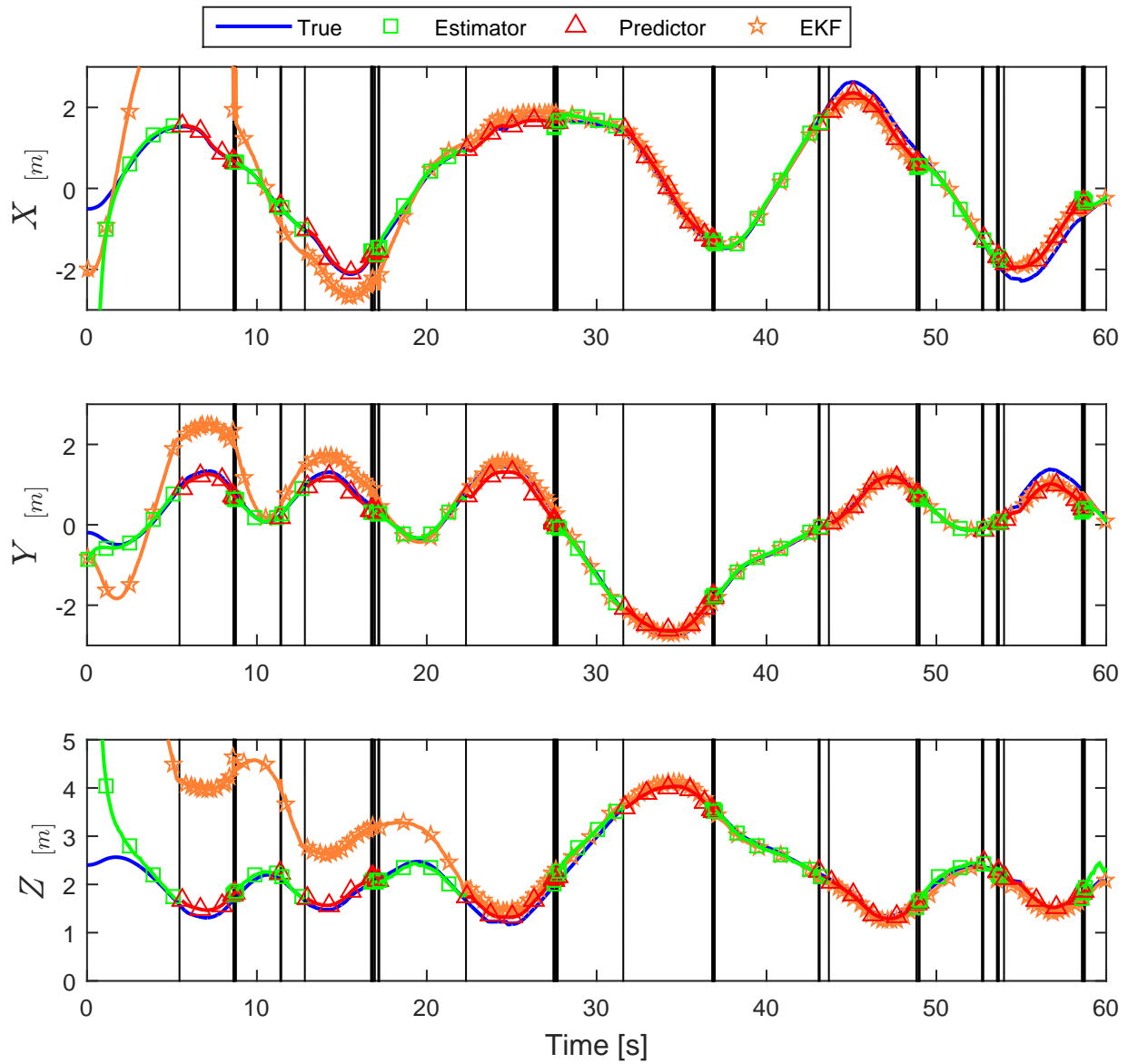


Figure 4-17. Reconstructed Euclidean coordinates of the target from the experiment where the target followed a known vector field. Vertical black lines denote switches.

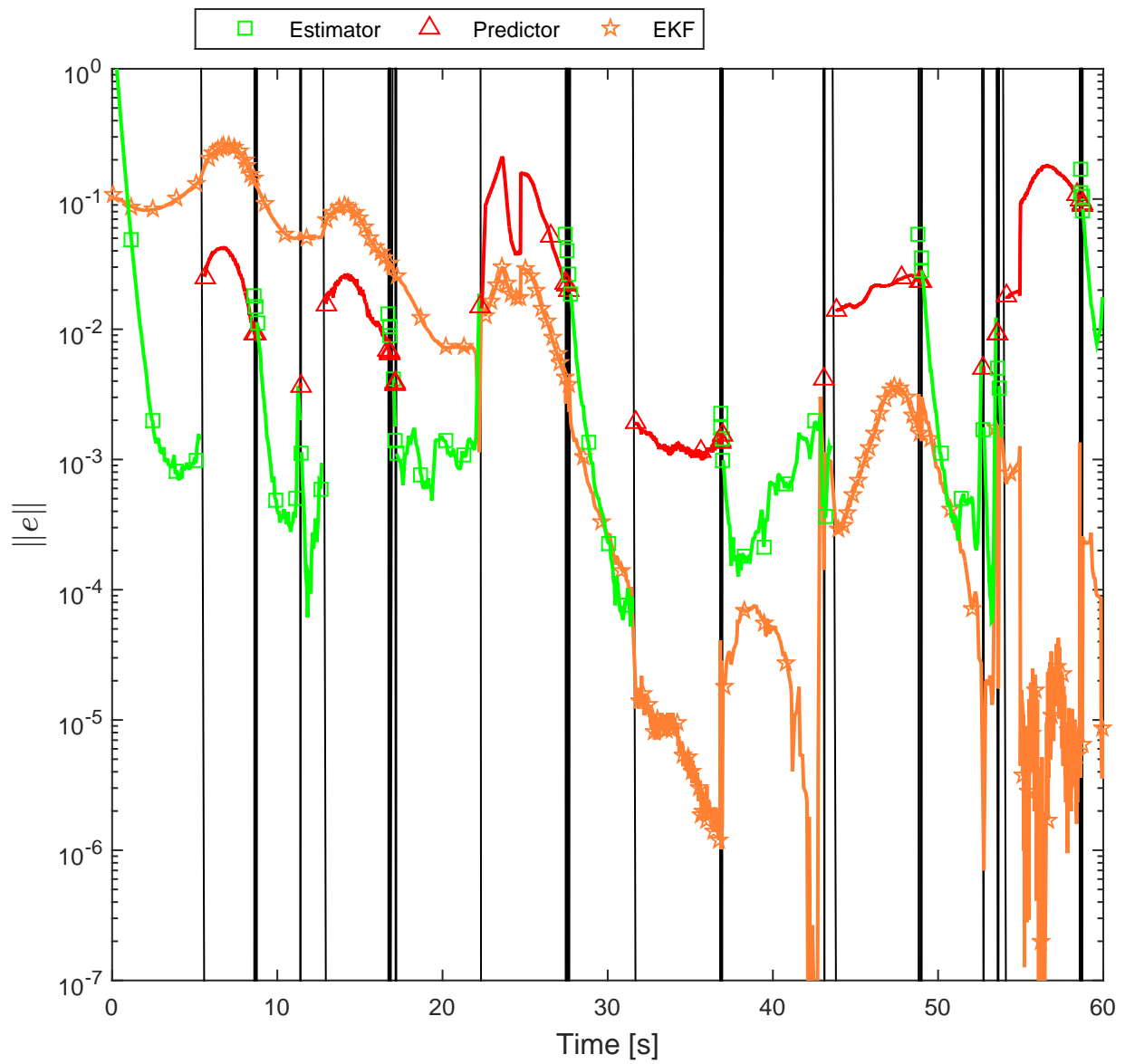


Figure 4-18. State estimation errors from the experiment the target followed a known vector field. Vertical black lines denote switches.

CHAPTER 5  
INTEGRAL CONCURRENT LEARNING: ADAPTIVE CONTROL WITH PARAMETER  
CONVERGENCE WITHOUT PE OR STATE DERIVATIVES

In this chapter, a novel adaptive update law is developed to ensure parameter convergence without PE or state derivatives. Whereas traditional gradient based or least-squares adaptive update laws do not yield parameter convergence without PE, CL enables the use of recorded data to develop a negative definite bound on the Lyapunov derivative, and hence exponential convergence of tracking and parameter estimation errors. The novelty in this chapter is a reformulation of CL in terms of an integral, therefore removing the need to measure or estimate state derivatives as is required in traditional CL. With this approach, parameter convergence is ensured provided a finite excitation condition is satisfied, and the finite excitation condition can be evaluated online, whereas the PE condition is difficult to verify for general nonlinear systems. In the following, the ICL technique will be developed for both control affine dynamics as well as Euler-Lagrange dynamics.

## 5.1 Control Affine Dynamics

### 5.1.1 Control Objective

To illustrate the integral CL method, consider an example dynamic system modeled as

$$\dot{x}(t) = f(x(t), t) + u(t) \quad (5-1)$$

where  $t \in [0, \infty)$ ,  $x : [0, \infty) \rightarrow \mathbb{R}^n$  are the measurable states,  $u : [0, \infty) \rightarrow \mathbb{R}^n$  is the control input and  $f : \mathbb{R}^n \times [0, \infty) \rightarrow \mathbb{R}^n$  represents the locally Lipschitz drift dynamics, with some unknown parameters. In the following development, as is typical in adaptive control,  $f$  is assumed to be linearly parametrized in the unknown parameters, i.e.,

$$f(x, t) = Y(x, t) \theta \quad (5-2)$$

where  $Y : \mathbb{R}^n \times [0, \infty) \rightarrow \mathbb{R}^{n \times m}$  is a regressor matrix and  $\theta \in \mathbb{R}^m$  represents the constant, unknown system parameters. To quantify the state tracking and parameter estimation

objective of the adaptive control problem, the tracking error and parameter estimate error are defined as

$$e(t) \triangleq x(t) - x_d(t) \quad (5-3)$$

$$\tilde{\theta}(t) \triangleq \theta - \hat{\theta}(t) \quad (5-4)$$

where  $x_d : [0, \infty) \rightarrow \mathbb{R}^n$  is a known, continuously differentiable desired trajectory and  $\hat{\theta} : [0, \infty) \rightarrow \mathbb{R}^m$  is the parameter estimate.

To achieve the control objective, the following controller is commonly used:

$$u(t) \triangleq \dot{x}_d(t) - Y(x(t), t)\hat{\theta}(t) - Ke(t) \quad (5-5)$$

where  $K \in \mathbb{R}^{n \times n}$  is a positive definite constant control gain. Taking the time derivative of (5-3) and substituting for (5-1), (5-2), and (5-5), yields the closed-loop error dynamics

$$\begin{aligned} \dot{e}(t) &= Y(x(t), t)\theta + \dot{x}_d(t) - Y(x(t), t)\hat{\theta}(t) - Ke(t) - \dot{x}_d(t) \\ &= Y(x(t), t)\tilde{\theta}(t) - Ke(t) \end{aligned} \quad (5-6)$$

The parameter estimation error dynamics are determined by taking the time derivative of (5-4), yielding

$$\dot{\tilde{\theta}}(t) = -\dot{\hat{\theta}}(t). \quad (5-7)$$

An integral CL-based update law for the parameter estimate is designed as

$$\begin{aligned} \dot{\hat{\theta}}(t) &\triangleq \Gamma Y(x(t), t)^T e(t) \\ &+ k_{CL}\Gamma \sum_{i=1}^N \mathcal{Y}_i^T \left( x(t_i) - x(t_i - \Delta t) - \mathcal{U}_i - \mathcal{Y}_i \hat{\theta}(t) \right) \end{aligned} \quad (5-8)$$

where  $k_{CL} \in \mathbb{R}$  and  $\Gamma \in \mathbb{R}^{m \times m}$  are constant, positive definite control gains,  $N \in \mathbb{Z}^+$  is a positive constant,  $t_i \in [0, t]$  are time points between the initial time and the current time,

$$\mathcal{Y}_i \triangleq \mathcal{Y}(t_i), \mathcal{U}_i \triangleq \mathcal{U}(t_i),$$

$$\mathcal{Y}(t) \triangleq \begin{cases} 0_{n \times m} & t \in [0, \Delta t] \\ \int_{t-\Delta t}^t Y(x(\tau), \tau) d\tau & t > \Delta t \end{cases} \quad (5-9)$$

$$\mathcal{U}(t) \triangleq \begin{cases} 0_{n \times 1} & t \in [0, \Delta t] \\ \int_{t-\Delta t}^t u(\tau) d\tau & t > \Delta t \end{cases} \quad (5-10)$$

$0_{n \times m}$  denotes an  $n \times m$  matrix of zeros, and  $\Delta t \in \mathbb{R}$  is a positive constant denoting the size of the window of integration. The concurrent learning term (i.e., the second term) in (5-8) represents saved data. The principal idea behind this design is to utilize recorded input-output data generated by the dynamics to further improve the parameter estimate. See [108] for a discussion on how to choose data points to record. In short, the data points should be selected to maximize the minimum eigenvalue of  $\sum_{i=1}^N \mathcal{Y}_i^T \mathcal{Y}_i$  since the minimum eigenvalue bounds the rate of convergence of the parameter estimation errors, as shown in the subsequent stability analysis.

The integral CL-based adaptive update law in (5-8) differs from traditional state derivative based CL update laws given in, e.g., [107–109]. Specifically, the state derivative, control, and regressor terms, i.e.,  $\dot{x}$ ,  $u$ , and  $Y$ , respectively, used in [107–109] are replaced with the integral of those terms over the time window  $[t - \Delta t, t]$ .

Substituting (5-2) into (5-1), and integrating yields

$$\int_{t-\Delta t}^t \dot{x}(\tau) d\tau = \int_{t-\Delta t}^t Y(x(\tau), \tau) \theta d\tau + \int_{t-\Delta t}^t u(\tau) d\tau,$$

$\forall t > \Delta t$ . Using the Fundamental Theorem of Calculus and the definitions in (5-9) and (5-10),

$$x(t) - x(t - \Delta t) = \mathcal{Y}(t) \theta + \mathcal{U}(t) \quad (5-11)$$

$\forall t > \Delta t$ , where the fact that  $\theta$  is a constant was used to pull it outside the integral.

Rearranging (5–11) and substituting into (5–8) yields

$$\dot{\hat{\theta}}(t) = \Gamma Y(x(t), t)^T e(t) + k_{CL} \Gamma \sum_{i=1}^N \mathcal{Y}_i^T \mathcal{Y}_i \tilde{\theta}(t), \quad \forall t > \Delta t. \quad (5-12)$$

### 5.1.2 Stability Analysis

To facilitate the following analysis, let  $\eta : [0, \infty) \rightarrow \mathbb{R}^{n+m}$  represent a composite vector of the system states and parameter estimation errors, defined as

$\eta(t) \triangleq \begin{bmatrix} e^T(t) & \tilde{\theta}^T(t) \end{bmatrix}^T$ . Also, let  $\lambda_{\min}\{\cdot\}$  and  $\lambda_{\max}\{\cdot\}$  represents the minimum and maximum eigenvalues of  $\{\cdot\}$ , respectively.

**Assumption 5.1.** The system is sufficiently excited over a finite duration of time.

Specifically,  $\exists \underline{\lambda} > 0, \exists T > \Delta t : \forall t \geq T, \lambda_{\min} \left\{ \sum_{i=1}^N \mathcal{Y}_i^T \mathcal{Y}_i \right\} \geq \underline{\lambda}$ .

*Remark 5.1.* The finite excitation condition in Assumption 5.1 is easier to satisfy than the PE condition used in previous adaptive control results since excitation is only required over a finite duration of time, whereas in PE, as the name implies, excitation is required for all time. In addition, the finite excitation condition can be checked online by checking the minimum eigenvalue of the sum of the regressor in (5–12) (i.e.  $\sum_{i=1}^N \mathcal{Y}_i^T \mathcal{Y}_i$ ).

As a reminder,  $Y(x(t), t)$  is PE if  $\exists T, \alpha > 0 :$

$$\int_t^{t+T} Y^T(x(t), t) Y(x(t), t) dt \geq \alpha I > 0, \quad \forall t > 0.$$

For PE it is difficult to find the correct time window,  $T$ , to check if the integral is lower bounded, and further, check this at every time  $t$ .

The stability analysis for ICL is separated into two phases. In the first phase, before sufficient data has been collected (i.e.,  $t \in [0, T]$ ), the tracking errors and parameter estimates remain bounded, as shown in Theorem 5.1. In Theorem 5.2 it is shown that the tracking errors and parameter estimates converge once sufficient data has been collected to satisfy the finite excitation condition (i.e.,  $t \in [T, \infty)$ ), which, when combined

with the results of Theorem 5.1, can be used to develop an exponential envelope on the system trajectories.

**Theorem 5.1.** *For the system defined in (5–1) and (5–7), the controller and adaptive update law defined in (5–5) and (5–8) ensures bounded tracking and parameter estimation errors during the time interval  $t \in [0, T]$ .*

*Proof.* Let  $V : \mathbb{R}^{n+m} \rightarrow \mathbb{R}$  be a candidate Lyapunov function defined as

$$V(\eta(t)) = \frac{1}{2}e(t)^T e(t) + \frac{1}{2}\tilde{\theta}(t)^T \Gamma^{-1}\tilde{\theta}(t).$$

Taking the derivative of  $V(\eta(t))$  along the trajectories of (5–1) during  $t \in [0, T]$ , substituting the closed-loop error dynamics in (5–6) and the equivalent adaptive update law in (5–12), and simplifying yields

$$\dot{V}(\eta(t)) \leq -e(t)^T K e(t), \quad \forall t \in [0, T]$$

which implies the system states remain bounded via [123, Theorem 8.4]. Further, since  $\dot{V}(\eta(t)) \leq 0$ ,  $V(\eta(T)) \leq V(\eta(0))$ , and therefore,  $\|\eta(T)\| \leq \sqrt{\frac{\beta_2}{\beta_1}} \|\eta(0)\|$ , where  $\beta_1 \triangleq \frac{1}{2} \min\{1, \lambda_{\min}\{\Gamma^{-1}\}\}$  and  $\beta_2 \triangleq \frac{1}{2} \max\{1, \lambda_{\max}\{\Gamma^{-1}\}\}$ .  $\square$

**Theorem 5.2.** *For the system defined in (5–1) and (5–7), the controller and adaptive update law defined in (5–5) and (5–8) ensures globally exponential tracking in the sense that*

$$\|\eta(t)\| \leq \left(\frac{\beta_2}{\beta_1}\right) \exp(\lambda_1 T) \|\eta(0)\| \exp(-\lambda_1 t), \quad \forall t \in [0, \infty). \quad (5-13)$$

*Proof.* Let  $V : \mathbb{R}^{n+m} \rightarrow \mathbb{R}$  be a candidate Lyapunov function defined as

$$V(\eta(t)) = \frac{1}{2}e(t)^T e(t) + \frac{1}{2}\tilde{\theta}(t)^T \Gamma^{-1}\tilde{\theta}(t). \quad (5-14)$$

Taking the derivative of  $V$  along the trajectories of (5–1) during  $t \in [T, \infty)$ , substituting the closed-loop error dynamics in (5–6) and the equivalent adaptive update law in

(5–12), and simplifying yields

$$\dot{V}(\eta(t)) = -e(t)^T K e(t) - k_{CL} \tilde{\theta}(t)^T \sum_{i=1}^N \mathcal{Y}_i^T \mathcal{Y}_i \tilde{\theta}(t), \quad \forall t \in [T, \infty). \quad (5-15)$$

From Assumption 5.1,  $\lambda_{\min} \left\{ \sum_{i=1}^N \mathcal{Y}_i^T \mathcal{Y}_i \right\} > 0, \forall t \in [T, \infty)$ , which implies that  $\sum_{i=1}^N \mathcal{Y}_i^T \mathcal{Y}_i$  is positive definite and therefore  $\dot{V}(\eta(t))$  is upper bounded by a negative definite function of  $\eta(t)$ . Invoking [123, Theorem 4.10],  $e(t)$  and  $\tilde{\theta}(t)$  are globally exponentially stable, i.e.,  $\forall t \in [T, \infty)$ ,

$$\|\eta(t)\| \leq \sqrt{\frac{\beta_2}{\beta_1}} \|\eta(T)\| \exp(-\lambda_1(t-T))$$

where  $\lambda_1 \triangleq \frac{1}{2\beta_2} \min\{\lambda_{\min}\{K\}, k_{CL}\Delta\}$ . The composite state vector can be further upper bounded using the results of Theorem 5.1, yielding (5–13).  $\square$

*Remark 5.2.* Although the analysis only explicitly considers two periods, i.e., before and after the history stack is sufficiently rich, additional data may be added into the history stack after  $T$  as long as the data increases the minimum eigenvalue of  $\sum_{i=1}^N \mathcal{Y}_i^T \mathcal{Y}_i$ . By using the data selection algorithm in [108, Chapter 6], the minimum eigenvalue of  $\sum_{i=1}^N \mathcal{Y}_i^T \mathcal{Y}_i$  is always increasing, and therefore the Lyapunov function derivative upper bound in (5–15), is valid for all time after  $T$ . Hence (5–14) is a common Lyapunov function [101, Chapter 2].

## 5.2 Euler-Lagrange Dynamics

### 5.2.1 Control Development

Consider Euler-Lagrange dynamics of the form [136, Chapter 2.3], [137, Chapter 9.3]

$$M(q(t)) \ddot{q}(t) + V_m(q(t), \dot{q}(t)) \dot{q}(t) + F_d \dot{q}(t) + G(q(t)) = \tau(t) \quad (5-16)$$

where  $q(t), \dot{q}(t), \ddot{q}(t) \in \mathbb{R}^n$  represent position, velocity and acceleration vectors, respectively,  $M : \mathbb{R}^n \rightarrow \mathbb{R}^{n \times n}$  represents the inertial matrix,  $V_m : \mathbb{R}^n \times \mathbb{R}^n \rightarrow \mathbb{R}^{n \times n}$  represents centripetal-Coriolis effects,  $F_d \in \mathbb{R}^{n \times n}$  represents frictional effects,  $G : \mathbb{R}^n \rightarrow$

$\mathbb{R}^n$  represents gravitational effects and  $\tau(t) \in \mathbb{R}^n$  denotes the control input. The system in (5–16) has the following properties (see [136, Chapter 2.3]).

**Property 1.** The system in (5–16) can be linearly parameterized, i.e., (5–16) can be rewritten as

$$Y_1(q(t), \dot{q}(t), \ddot{q}(t))\theta = M(q(t))\ddot{q}(t) + V_m(q(t), \dot{q}(t))\dot{q}(t) + F_d\dot{q}(t) + G(q(t)) = \tau(t)$$

where  $Y_1 : \mathbb{R}^n \times \mathbb{R}^n \times \mathbb{R}^n \rightarrow \mathbb{R}^{n \times m}$  denotes the regression matrix, and  $\theta \in \mathbb{R}^m$  is a vector of uncertain parameters.

**Property 2.** The inertia matrix is symmetric and positive definite, and satisfies the following inequalities

$$m_1 \|\xi\|^2 \leq \xi^T M(q(t)) \xi \leq m_2 \|\xi\|^2, \quad \forall \xi \in \mathbb{R}^n$$

where  $m_1$  and  $m_2$  are known positive scalar constants, and  $\|\cdot\|$  represents the Euclidean norm.

**Property 3.** The inertia and centripetal-Coriolis matrices satisfy the following skew symmetric relation

$$\xi^T \left( \frac{1}{2} \dot{M}(q(t)) - V_m(q(t), \dot{q}(t)) \right) \xi = 0, \quad \forall \xi \in \mathbb{R}^n$$

where  $\dot{M}(q(t))$  is the time derivative of the inertial matrix.

To quantify the tracking objective, the position tracking error,  $e(t) \in \mathbb{R}^n$ , and the filtered tracking error,  $r(t) \in \mathbb{R}^n$ , are defined as

$$e(t) = q_d(t) - q(t)$$

$$r(t) = \dot{e}(t) + \alpha e(t) \tag{5–17}$$

where  $q_d(t) \in \mathbb{R}^n$  represents the desired trajectory, whose first and second time derivatives exist and are continuous (i.e.,  $q_d(t) \in C^2$ ). To quantify the parameter

identification objective, the parameter estimation error,  $\tilde{\theta}(t) \in \mathbb{R}^m$ , is again defined as

$$\tilde{\theta}(t) = \theta - \hat{\theta}(t) \quad (5-18)$$

where  $\hat{\theta}(t) \in \mathbb{R}^m$  represents the parameter estimate.

Taking the time derivative of (5-17), premultiplying by  $M(q(t))$ , substituting in from (5-16), and adding and subtracting  $V_m(q(t), \dot{q}(t))r(t)$  results in the following open-loop error dynamics

$$\begin{aligned} M(q(t))\dot{r}(t) &= M(q(t))\ddot{q}_d(t) - M(q(t))\ddot{q}(t) + \alpha M(q(t))\dot{e}(t) \\ &= M(q(t))\ddot{q}_d(t) + V_m(q(t), \dot{q}(t))\dot{q}(t) + F_d\dot{q}(t) + G(q(t)) \\ &\quad + \alpha M(q(t))\dot{e}(t) - \tau(t) \pm V_m(q(t), \dot{q}(t))r(t) \\ &= M(q(t))\ddot{q}_d(t) + V_m(q(t), \dot{q}(t))(\dot{q}_d(t) + \alpha e(t)) + F_d\dot{q}(t) + G(q(t)) \\ &\quad + \alpha M(q(t))\dot{e}(t) - \tau(t) - V_m(q(t), \dot{q}(t))r(t) \end{aligned}$$

$$M(q(t))\dot{r}(t) = Y_2(q(t), \dot{q}(t), q_d(t), \dot{q}_d(t), \ddot{q}_d(t))\theta - V_m(q(t), \dot{q}(t))r(t) - \tau(t) \quad (5-19)$$

where  $Y_2 : \mathbb{R}^n \times \mathbb{R}^n \times \mathbb{R}^n \times \mathbb{R}^n \times \mathbb{R}^n \rightarrow \mathbb{R}^{n \times m}$  is defined based on the relation

$$\begin{aligned} Y_2(q(t), \dot{q}(t), q_d(t), \dot{q}_d(t), \ddot{q}_d(t))\theta &\triangleq M(q(t))\ddot{q}_d(t) + V_m(q(t), \dot{q}(t))(\dot{q}_d(t) + \alpha e(t)) \\ &\quad + F_d\dot{q}(t) + G(q(t)) + \alpha M(q(t))\dot{e}(t). \end{aligned}$$

To achieve the tracking objective, the controller is designed as

$$\tau(t) = Y_2\hat{\theta}(t) + e(t) + k_1r(t) \quad (5-20)$$

where  $k_1 \in \mathbb{R}$  is a positive constant. To circumvent the need for  $\ddot{q}(t)$ , the update law can be formulated in terms of an integral, as

$$\dot{\hat{\theta}} = \Gamma Y_2(q(t), \dot{q}(t), q_d(t), \dot{q}_d(t), \ddot{q}_d(t))^T r(t) + k_2\Gamma \sum_{i=1}^N \mathcal{Y}_i^T (\mathcal{U}_i - \mathcal{Y}_i\hat{\theta}(t)) \quad (5-21)$$

where  $\mathcal{Y}_i \triangleq \mathcal{Y}(t_i)$ ,  $\mathcal{U}_i \triangleq \mathcal{U}(t_i)$ ,  $\mathcal{Y} : [0, \infty) \rightarrow \mathbb{R}^{n \times m}$  and  $\mathcal{U} : [0, \infty) \rightarrow \mathbb{R}^n$  are defined as

$$\mathcal{U}(t_i) \triangleq \int_{t-\Delta t}^t \tau(\sigma) d\sigma,$$

$$\mathcal{Y}(t_i) \triangleq Y_3(q(t), \dot{q}(t)) + \int_{t-\Delta t}^t Y_4(q(\sigma), \dot{q}(\sigma)) d\sigma,$$

and the functions  $Y_3, Y_4 : \mathbb{R}^n \times \mathbb{R}^n \rightarrow \mathbb{R}^{n \times m}$  are defined as

$$Y_3(q(t), \dot{q}(t)) \theta \triangleq M(q(t)) \dot{q}(t) - M(q(t - \Delta t)) \dot{q}(t - \Delta t),$$

$$Y_4(q(t), \dot{q}(t)) \theta \triangleq -\dot{M}(q(t)) \dot{q}(t) + V_m(q(t), \dot{q}(t)) \dot{q}(t) + F_d \dot{q}(t) + G(q(t)).$$

Note that integrating both sides of (5-16) yields

$$\int_{t-\Delta t}^t \tau(\sigma) d\sigma = \int_{t-\Delta t}^t M(q(\sigma)) \ddot{q}(\sigma) d\sigma + \int_{t-\Delta t}^t [V_m(q(\sigma), \dot{q}(\sigma)) \dot{q}(\sigma) + F_d \dot{q}(\sigma) + G(q(\sigma))] d\sigma. \quad (5-22)$$

The first term on the right hand side can be rewritten using integration by parts as

$$\begin{aligned} \int_{t-\Delta t}^t \underbrace{M(q(\sigma))}_{u} \underbrace{\ddot{q}(\sigma)}_{dv} d\sigma &= [M(q(\sigma)) \dot{q}(\sigma)]_{t-\Delta t}^t - \int_{t-\Delta t}^t \dot{M}(q(\sigma)) \dot{q}(\sigma) d\sigma \\ &= M(q(t)) \dot{q}(t) - M(q(t - \Delta t)) \dot{q}(t - \Delta t) \\ &\quad - \int_{t-\Delta t}^t \dot{M}(q(\sigma)) \dot{q}(\sigma) d\sigma. \end{aligned}$$

Substituting into (5-22) yields

$$\begin{aligned} \int_{t-\Delta t}^t \tau(\sigma) d\sigma &= \underbrace{M(q(t)) \dot{q}(t) - M(q(t - \Delta t)) \dot{q}(t - \Delta t)}_{Y_3(q(t), \dot{q}(t)) \theta} \\ &\quad + \underbrace{\int_{t-\Delta t}^t [-\dot{M}(q(\sigma)) \dot{q}(\sigma) + V_m(q(\sigma), \dot{q}(\sigma)) \dot{q}(\sigma) + F_d \dot{q}(\sigma) + G(q(\sigma))] d\sigma}_{Y_4(q(t), \dot{q}(t)) \theta} \\ \int_{t-\Delta t}^t \tau(\sigma) d\sigma &= Y_3(q(t), \dot{q}(t)) \theta + \int_{t-\Delta t}^t Y_4(q(\sigma), \dot{q}(\sigma)) d\sigma \\ \mathcal{U} &= \mathcal{Y} \theta. \end{aligned} \quad (5-23)$$

Using the relation in (5–23), (5–21) can be rewritten as

$$\dot{\hat{\theta}} = \Gamma Y_2(q(t), \dot{q}(t), q_d(t), \dot{q}_d(t), \ddot{q}_d(t))^T r(t) + k_2 \Gamma \sum_{i=1}^N \mathcal{Y}_i^T (\mathcal{Y}_i \theta - \mathcal{Y}_i \hat{\theta}(t)). \quad (5-24)$$

Substituting the controller from (5–20) into the error dynamics in (5–19) results in the following closed-loop tracking error dynamics

$$M(q) \dot{r} = Y_2(q(t), \dot{q}(t), q_d(t), \dot{q}_d(t), \ddot{q}_d(t)) \tilde{\theta}(t) - e(t) - V_m(q(t), \dot{q}(t)) r(t) - k_1 r(t). \quad (5-25)$$

Similarly, taking the time derivative of (5–18) and substituting the parameter estimate update law from (5–24) results in the following closed-loop parameter estimation error dynamics

$$\dot{\tilde{\theta}} = -\Gamma Y_2(q(t), \dot{q}(t), q_d(t), \dot{q}_d(t), \ddot{q}_d(t))^T r(t) - k_2 \Gamma \left[ \sum_{i=1}^N \mathcal{Y}_i^T \mathcal{Y}_i \right] \tilde{\theta}(t). \quad (5-26)$$

### 5.2.2 Stability Analysis

Similar to the analysis in Section 5.1, two periods of time are considered. In Theorem 5.3 it is shown that the designed controller and adaptive update law are sufficient for the system to remain bounded for all time despite the lack of data and in Theorem 5.4 exponential convergence is established given a sufficiently rich history stack. Similar to Section 5.1, an excitation condition is required to guarantee that the transition to the second phase happens in finite time, i.e.,

$$\exists \lambda, T > 0 : \forall t \geq T, \lambda_{\min} \left\{ \sum_{i=1}^N \mathcal{Y}_i^T \mathcal{Y}_i \right\} \geq \lambda.$$

**Theorem 5.3.** *For the system defined in (5–16), the controller and adaptive update law defined in (5–20) and (5–21) ensure bounded tracking and parameter estimation errors.*

*Proof.* Let  $V : \mathbb{R}^{2n+m} \rightarrow \mathbb{R}$  be a candidate Lyapunov function defined as

$$V(\eta(t)) = \frac{1}{2} e(t)^T e(t) + \frac{1}{2} r(t)^T M(q(t)) r(t) + \frac{1}{2} \tilde{\theta}(t)^T \Gamma^{-1} \tilde{\theta}(t) \quad (5-27)$$

where  $\eta(t) \triangleq \begin{bmatrix} e(t)^T & r(t)^T & \tilde{\theta}(t)^T \end{bmatrix}^T \in \mathbb{R}^{2n+m}$  is a composite state vector. Taking the time derivative of (5–27) and substituting (5–17), (5–25), and (5–26) yields

$$\begin{aligned} \dot{V}(\eta(t)) = & e(t)^T (r(t) - \alpha e(t)) + \frac{1}{2} r(t)^T \dot{M}(q(t)) r(t) - k_2 \tilde{\theta}(t)^T \left[ \sum_{i=1}^N \mathcal{Y}_i^T \mathcal{Y}_i \right] \tilde{\theta}(t) \\ & - \tilde{\theta}(t)^T Y_2(q(t), \dot{q}(t), q_d(t), \dot{q}_d(t), \ddot{q}_d(t))^T r(t) \\ & + r(t)^T \left( Y_2(q(t), \dot{q}(t), q_d(t), \dot{q}_d(t), \ddot{q}_d(t)) \tilde{\theta}(t) \right) \\ & + r(t)^T (-e(t) - V_m(q(t), \dot{q}(t))) r(t) - k_1 r(t) \end{aligned}$$

Simplifying and noting that  $\sum_{i=1}^N \mathcal{Y}_i^T \mathcal{Y}_i$  is always positive semi-definite,  $\dot{V}$  can be upper bounded as

$$\dot{V}(\eta(t)) \leq -\alpha e(t)^T e(t) - k_1 r(t)^T r(t).$$

Therefore,  $\eta(t)$  is bounded based on [123, Theorem 8.4]. Furthermore, since

$$\dot{V}(\eta(t)) \leq 0, V(\eta(T)) \leq V(\eta(0)) \text{ and therefore } \|\eta(T)\| \leq \sqrt{\frac{\beta_2}{\beta_1}} \|\eta(0)\|, \text{ where}$$

$$\beta_1 \triangleq \frac{1}{2} \min \{1, m_1, \lambda_{\min} \{\Gamma^{-1}\}\} \text{ and } \beta_2 \triangleq \frac{1}{2} \max \{1, m_2, \lambda_{\max} \{\Gamma^{-1}\}\}. \quad \square$$

**Theorem 5.4.** *For the system defined in (5–16), the controller and adaptive update law defined in (5–20) and (5–21) ensure globally exponential tracking in the sense that*

$$\|\eta(t)\| \leq \left( \frac{\beta_2}{\beta_1} \right) \exp(\lambda_1 T) \|\eta(0)\| \exp(-\lambda_1 t), \quad \forall t \in [0, \infty) \quad (5-28)$$

where  $\lambda_1 \triangleq \frac{1}{2\beta_2} \min \{\alpha, k_1, k_2 \lambda\}$ .

*Proof.* Let  $V : \mathbb{R}^{2n+m} \rightarrow \mathbb{R}$  be a candidate Lyapunov function defined as in (5–27).

Taking the time derivative of (5–27), substituting (5–17), (5–25), (5–26) and simplifying yields

$$\dot{V}(\eta(t)) = -\alpha e(t)^T e(t) - k_1 r(t)^T r(t) - k_2 \tilde{\theta}(t)^T \left[ \sum_{i=1}^N \mathcal{Y}_i^T \mathcal{Y}_i \right] \tilde{\theta}(t).$$

From the finite excitation condition,  $\lambda_{\min} \left\{ \sum_{i=1}^N \mathcal{Y}_i^T \mathcal{Y}_i \right\} > 0, \forall t \in [T, \infty)$ , which implies that  $\sum_{i=1}^N \mathcal{Y}_i^T \mathcal{Y}_i$  is positive definite, and therefore  $\dot{V}$  can be upper bounded as

$$\dot{V}(\eta(t)) \leq -\alpha e(t)^T e(t) - k_1 r(t)^T r(t) - k_2 \lambda \left\| \tilde{\theta}(t) \right\|^2, \quad \forall t \in [T, \infty).$$

Invoking [123, Theorem 4.10],  $\eta(t)$  is globally exponentially stable, i.e.,  $\forall t \in [T, \infty)$ ,

$$\|\eta(t)\| \leq \sqrt{\frac{\beta_2}{\beta_1}} \|\eta(T)\| \exp(-\lambda_1(t-T)).$$

The composite state vector can be further upper bounded using the results of Theorem 5.3, yielding (5–28). □

*Remark 5.3.* Similar to Part 5.1, using an appropriate data selection algorithm ensures the minimum eigenvalue of  $\sum_{i=1}^N \mathcal{Y}_i^T \mathcal{Y}_i$  is always increasing, and therefore the Lyapunov function (5–27) is a common Lyapunov function.

### 5.3 Simulation

A Monte Carlo simulation was performed to demonstrate the application of the theoretical results presented in Section 5.1.2 and to illustrate the increased performance and robustness to noise compared to the traditional state derivative based CL methods across a wide variety of gain selections and noise realizations. The following example system was used in the simulations:

$$\dot{x}(t) = \begin{bmatrix} x_1^2(t) & \sin(x_2(t)) & 0 & 0 \\ 0 & x_2(t) \sin(t) & x_1(t) & x_1(t) x_2(t) \end{bmatrix} \theta + u(t)$$

where  $x : [0, \infty) \rightarrow \mathbb{R}^2$ ,  $u : [0, \infty) \rightarrow \mathbb{R}^2$ , the unknown parameters were selected as

$$\theta = \begin{bmatrix} 5 & 10 & 15 & 20 \end{bmatrix}^T,$$

and the desired trajectory was selected as

$$x_d(t) = 10(1 - e^{-0.1t}) \begin{bmatrix} \sin(2t) \\ 0.4 \cos(3t) \end{bmatrix}.$$

For each of the 200 trials within the Monte Carlo simulation, the feedback and adaptation gains were selected as  $K = K_s I_2$  and  $\Gamma = \Gamma_s I_4$ , where  $K_s \in \mathbb{R}$  was sampled from a uniform distribution on  $(0.1, 15)$  and  $\Gamma_s \in \mathbb{R}$  was sampled from a uniform distribution on  $(0.3, 3)$ . Also, the concurrent learning gain,  $k_{CL}$ , and the integration window,  $\Delta t$ , were sampled from uniform distributions with support on  $(0.002, 0.2)$  and  $(0.01, 1)$ , respectively. After gain sampling, a simulation using each, the traditional state derivative based, and the integral based, CL update law was performed, with a step size of 0.0004 seconds and additive white Gaussian noise on the measured state with standard deviation of 0.3. For each integral CL simulation, a buffer, with size based on  $\Delta t$  and the step size, was used to store the values of  $x$ ,  $Y$ , and  $u$  during the time interval  $[t - \Delta t, t]$  and to calculate  $x(t)$ ,  $x(t - \Delta t)$ ,  $\mathcal{Y}(t)$  and  $\mathcal{U}(t)$ . Similarly, for the state derivative CL simulation, a buffer of the same size was used as the input to a moving average filter before calculating the state derivative via central finite difference. The size of the history stack and the simulation time span were kept constant across all trials at  $N = 20$  and 100 seconds, respectively.

Since the moving average filter window used in the state derivative CL simulations provides an extra degree of freedom, the optimal filter window size was determined *a priori* for a fair comparison. The optimal filtering window was calculated by adding Gaussian noise, with the same standard deviation as in the simulation, to the desired trajectory, and selecting the window size that minimizes the root mean square error between the estimated and true  $\dot{x}_d$ . This process yielded an optimal filtering window of 0.5 seconds; however, the filtering window was truncated to  $\Delta t$  on trials where the sampled  $\Delta t$  was less than 0.5 seconds, i.e.,  $filter\ window = \min\{0.5, \Delta t\}$ .

The mean tracking error trajectory and parameter estimation error trajectory across all trials are depicted in Figs. 5-1 and 5-2. To compare the overall performance of both methods, the RMS tracking error and the RMS parameter estimation error during the time interval  $t \in [60, 100]$  (i.e., after reaching steady state) were calculated for each trial, and then the average RMS errors across all trials was determined. The final results of the Monte Carlo simulation are shown in Table 5-1, illustrating the improved performance of integral CL versus state derivative CL.

#### 5.4 Summary

A modified concurrent learning adaptive update law was developed, resulting in guarantees on the convergence of the parameter estimation errors without requiring persistent excitation or the estimation of state derivatives. The development in this chapter represents a significant improvement in online system identification. Whereas PE is required in the majority of adaptive methods for parameter estimation convergence (usually ensured through the use of a probing signal that is not considered in the Lyapunov analysis), the technique described in this chapter does not require PE. Furthermore, the formulation of concurrent learning in this chapter circumvents the need to estimate the unmeasurable state derivatives, therefore avoiding the design and tuning of a state derivative estimator. This formulation is more robust to noise, i.e., has better tracking and estimation performance, compared to other concurrent learning designs, as demonstrated by the included Monte Carlo simulation.

A tuning parameter that results from this design is the integration time window,  $\Delta t$ . As the integration window increases, the difference between the prediction of the state evolution based on current parameter estimates (i.e.,  $\mathcal{U}_i + \mathcal{Y}_i \hat{\theta}(t)$ ) and the actual state evolution (i.e.,  $x(t_i) - x(t_i - \Delta t)$ ) should increase, therefore providing a larger error signal from which to learn. On the other hand, a larger integration window increases the effect of disturbances and noise since these signals would also be integrated, resulting in a larger ultimate error bound (cf. [109] for a discussion on the effects of disturbances

Table 5-1. Average steady state RMS tracking and RMS parameter estimation errors across all simulations, for integral concurrent learning (ICL) and traditional derivative-based concurrent learning (DCL).

	$e_1$	$e_2$	$\tilde{\theta}_1$	$\tilde{\theta}_2$	$\tilde{\theta}_3$	$\tilde{\theta}_4$
ICL	0.1078	0.2117	.0507	0.3100	0.1867	0.1121
DCL	0.2497	0.6717	0.1802	1.3376	0.3753	0.2382

on the ultimate error). Therefore, future efforts will investigate optimal selection of the integration window based on disturbance and noise characteristics.

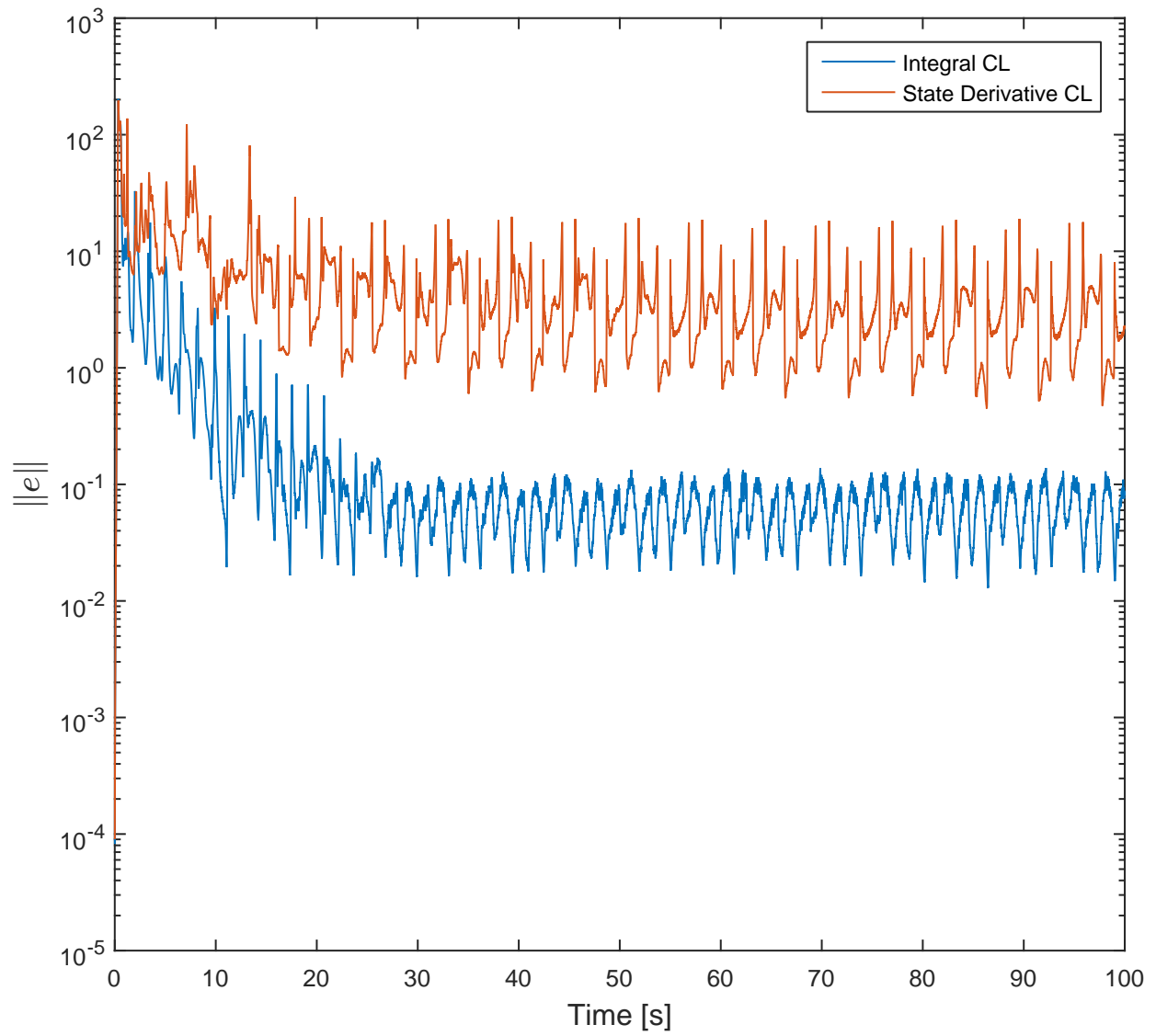


Figure 5-1. Mean state trajectory tracking errors across all trials.

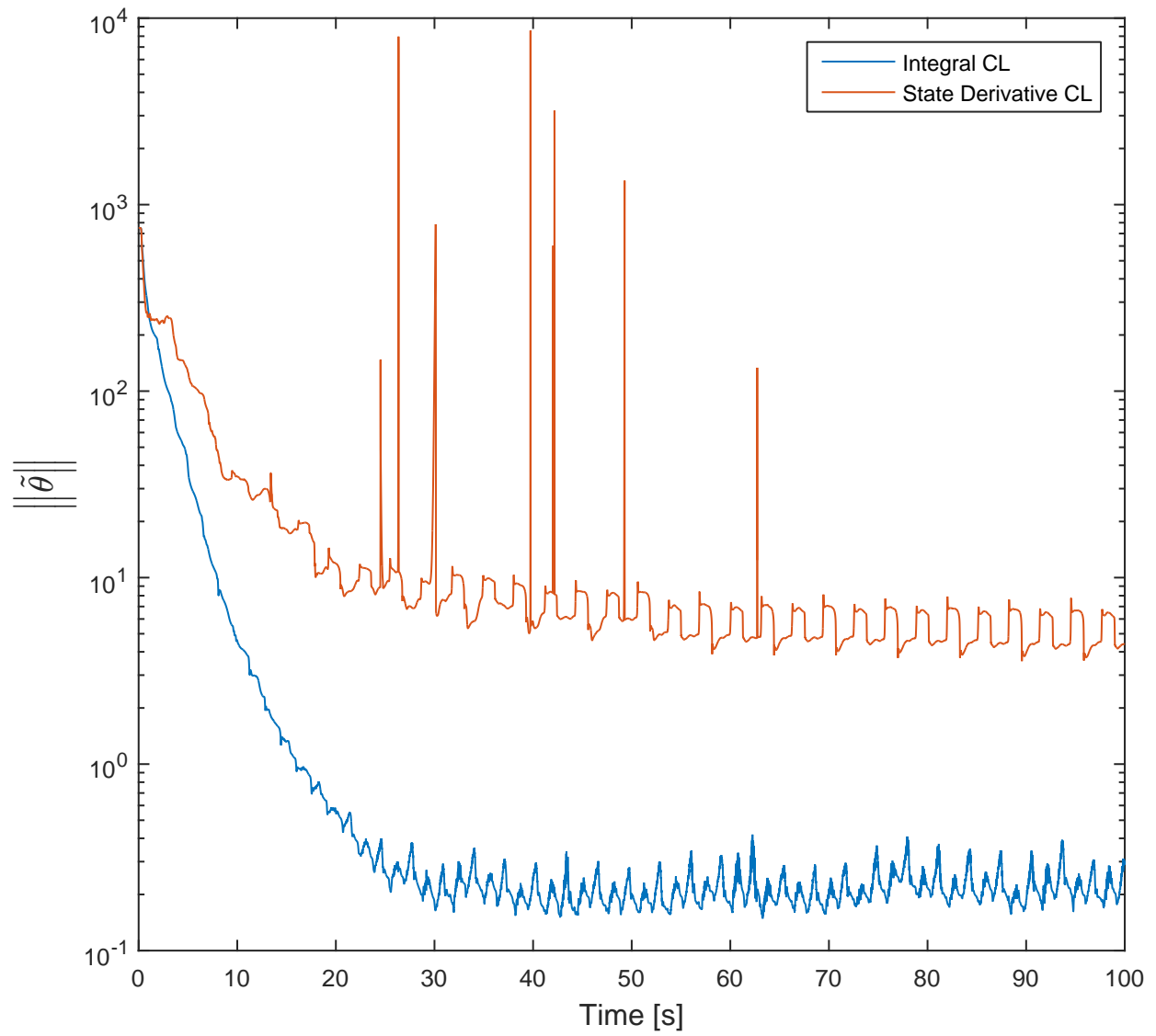


Figure 5-2. Mean parameter estimation errors across all trials.

## CHAPTER 6 ESTIMATION AND PREDICTION WITH MODEL LEARNING

This chapter combines the results of Chapters 4 and 5. In Chapter 4 it was demonstrated that estimation performance could be significantly increased, and dwell time stability conditions significantly relaxed, if a predictor was used to update state estimates when measurements are unavailable. However, implementation of the predictor required knowing a motion model of the target. In Chapter 5, a novel adaptive update law was developed to learn unknown system dynamics online. The focus of this chapter is to use the function approximation techniques of Chapter 5 to learn a motion model of the target online, which can then be used to generate target velocity estimates requires for prediction. As will be shown in the proceeding development, unlike Chapter 5, a neural network (NN) universal function approximator will be used to learn the unknown portions of the dynamics, since a parametric model for the target motion may not be available. This results in ultimately bounded convergence when measurements are available, unlike the exponential convergence provided by existing observers considered in Chapter 4, and therefore the average dwell time based stability theorems of Chapter 4 cannot be directly applied.

The full 6 DOF pose of the target with respect to the camera is estimated in this chapter. To this end, the dynamics in (2–9) can be rewritten as

$$\dot{x}(t) = v_q(t) - v_c(t) - \omega_c(t)^\times x(t) \quad (6-1)$$

where  $x(t) \in \mathbb{R}^3$  denotes the position of the origin of  $\mathcal{F}_Q$  with respect to the origin of  $\mathcal{F}_C$  (i.e., the relative position of the object with respect to the camera), and  $()^\times : \mathbb{R}^3 \rightarrow \mathbb{R}^{3 \times 3}$  represents the skew operator, defined as

$$p^\times \triangleq \begin{bmatrix} 0 & -p_3 & p_2 \\ p_3 & 0 & -p_1 \\ -p_2 & p_1 & 0 \end{bmatrix}.$$

The relative orientation dynamics of the target with respect to the camera are given in (2–13) and repeated here as

$$\dot{q}(t) = \frac{1}{2}B(q(t))(\omega_q(t) - \bar{q}(t) \cdot \omega_c(t) \cdot q(t)). \quad (6-2)$$

## 6.1 Estimation Objective

The primary goal in this work is to develop a pose estimator that is robust to intermittent measurements. The design strategy employed here is to filter the pose measurements when they are available, and predict future poses when measurements are unavailable (e.g., the object is not visible to the camera). However, a predictor based on (6–1) and (6–2) would require linear and angular velocities of the object to be known. The novelty in this work is to learn a model of the object velocities when measurements are available, and use the model in the predictor when measurements are not available. To this end, a stacked pose state,  $\eta(t) \in \mathbb{R}^7$ , is defined as  $\eta(t) \triangleq \begin{bmatrix} x^T(t) & q^T(t) \end{bmatrix}^T$  and the following assumptions are utilized.

**Assumption 6.1.** Measurements of the relative pose of the target are available from camera images when the target is in view.

*Remark 6.1.* The projection of a 3D scene onto a 2D sensor during the imaging process results in scale ambiguity [112, Chapter 5.4.4]. In typical SfM observers, target velocity is used to inject scale into the system and recover the full Euclidean coordinates of the target (as done in Chapters 3 and 4). However, in the scenario considered in this chapter, the target velocities are unknown. To resolve the ambiguity, a known length scale on the target can be used, and by exploiting Perspective-n-Point (e.g., [138–144]) or homography (e.g., [145] and [126]) solvers, the pose of the target can be recovered.

**Assumption 6.2.** The object velocities are a time-invariant, locally Lipschitz function of the object pose, i.e.,  $v_q(t) = \phi_1(\rho(\eta(t), t))$  and  $\omega_q(t) = \phi_2(\rho(\eta(t), t))$ , where  $\phi_1, \phi_2 : \mathbb{R}^7 \rightarrow \mathbb{R}^3$  are bounded and  $\rho : \mathbb{R}^7 \times [0, \infty) \rightarrow \mathbb{R}^7$  is a known, bounded, and locally Lipschitz function.

*Remark 6.2.* In some applications, the velocity field of the target is expected to be dependent on the target's pose with respect to the world, rather than its relative pose with respect to the camera. The function  $\rho$  is used to transform the relative pose to its world pose by using the camera pose with respect to the world. In other applications, the velocity field is expected to rely solely on the relative pose (e.g., a pursuit-evasion scenario in an obstacle free environment, where the evader's motion would only be dependent on its pose with respect to the pursuer/camera) or the camera pose is unknown, in which case  $\rho$  can be taken as the identity function on  $\eta(t)$ .

**Assumption 6.3.** The state  $\eta(t)$  is bounded, i.e.  $\eta(t) \in \mathcal{X}$ , where  $\mathcal{X} \subset \mathbb{R}^7$  is a convex, compact set.

*Remark 6.3.* In estimation, for the state estimates to converge to the states while remaining bounded, the states themselves must remain bounded. This is analogous to the requirement of bounded desired trajectories in control problems.

In this development, the unknown motion model functions,  $\phi_1$  and  $\phi_2$ , are approximated with a neural network, i.e.,

$$\begin{bmatrix} v_q(t) \\ \frac{1}{2}B(q(t))\omega_q(t) \end{bmatrix} = \begin{bmatrix} \phi_1(\rho(\eta(t), t)) \\ \frac{1}{2}B(q(t))\phi_2(\rho(\eta(t), t)) \end{bmatrix} = W^T\sigma(\rho(\eta, t)) + \varepsilon(\rho(\eta, t))$$

where  $\sigma : \mathbb{R}^7 \rightarrow \mathbb{R}^p$  is a known, bounded, locally Lipschitz, vector of basis functions,

$W \in \mathbb{R}^{p \times 7}$  is a matrix of the unknown ideal weights, and  $\varepsilon : \mathbb{R}^7 \rightarrow \mathbb{R}^7$  is the function approximation residual, which is locally Lipschitz based on the locally Lipschitz

properties of  $v_q(t)$ ,  $\omega_q(t)$ ,  $B(q(t))$  and  $\sigma(\cdot)$ , and is *a priori* bounded with a bound that can be made arbitrarily small based on the Stone-Weierstrass theorem, i.e.,

$\bar{\varepsilon} \triangleq \sup_{\eta \in \mathcal{X}, t \in [0, \infty)} \|\varepsilon(\rho(\eta, t))\|$ , where  $\|\cdot\|$  denotes the Euclidean norm. Note that if  $W$  is known,  $\phi_2(\rho(\eta(t), t))$  can be approximated by premultiplying by  $2B^T(q(t))$  and utilizing the pseudoinverse property of  $B(q(t))$ .

To quantify the estimation objective, let

$$\tilde{\eta}(t) \triangleq \eta(t) - \hat{\eta}(t) \quad (6-3)$$

denote the estimation error, where  $\hat{\eta}(t) \in \mathbb{R}^7$  contains the position and orientation estimates. Also, let

$$\tilde{W}(t) \triangleq W - \hat{W}(t),$$

denote the parameter estimation error, where  $\hat{W}(t) \in \mathbb{R}^{p \times 7}$  is the estimate of the ideal function approximation weights. Based on these definitions, the kinematics in (6-1) and (6-2) can be rewritten as

$$\dot{\eta}(t) = W^T \sigma(\rho(\eta(t), t)) + \varepsilon(\rho(\eta(t), t)) + f(\eta(t), t), \quad (6-4)$$

where  $f: \mathbb{R}^7 \times [0, \infty) \rightarrow \mathbb{R}^7$  is a known function defined as

$$f(\eta(t), t) \triangleq - \begin{bmatrix} v_c(t) + \omega_c(t)^\times x(t) \\ \frac{1}{2} B(q(t)) (\bar{q}(t) \cdot \omega_c(t) \cdot q(t)) \end{bmatrix}.$$

## 6.2 Estimator Design

Taking the transpose of (6-4) and integrating yields

$$\int_{t-\Delta t}^t \dot{\eta}^T(\tau) d\tau = \int_{t-\Delta t}^t \sigma^T(\rho(\eta(\tau), \tau)) W d\tau + \int_{t-\Delta t}^t \varepsilon^T(\rho(\eta(\tau), \tau)) d\tau + \int_{t-\Delta t}^t f^T(\eta(\tau), \tau) d\tau$$

where  $\Delta t \in \mathbb{R}$  is a positive constant denoting the size of the window of integration. Using the Fundamental Theorem of Calculus and simplifying yields

$$\eta^T(t) - \eta^T(t - \Delta t) = \mathcal{Y}(t) W + \mathcal{E}(t) + \mathcal{F}(t), \quad \forall t \in [\Delta t, \infty) \quad (6-5)$$

where,  $\forall t \in [\Delta t, \infty)$ ,  $\mathcal{Y}(t) \triangleq \int_{t-\Delta t}^t \sigma^T(\rho(\eta(\tau), \tau)) d\tau$ ,  $\mathcal{E}(t) \triangleq \int_{t-\Delta t}^t \varepsilon^T(\rho(\eta(\tau), \tau)) d\tau$ , and  $\mathcal{F}(t) \triangleq \int_{t-\Delta t}^t f^T(\eta(\tau), \tau) d\tau$ .

### 6.2.1 Estimator

Based on the subsequent stability analysis, during the periods in which measurements are available, the position and orientation estimate update laws are designed as

$$\dot{\hat{\eta}}(t) = \hat{W}(t)^T \sigma(\rho(\eta(t), t)) + f(\eta(t), t) + k_1 \tilde{\eta}(t) + k_2 \text{sgn}(\tilde{\eta}(t)), \quad (6-6)$$

where  $\text{sgn}(\cdot)$  is the signum function. The update law for the motion model approximation parameters is based on ICL and is designed as

$$\dot{\hat{W}} = \text{proj} \left( \Gamma \sigma(\rho(\eta(t), t)) \tilde{\eta}(t)^T + k_{CL} \Gamma \sum_{i=1}^N \mathcal{Y}_i^T (\Delta \eta_i - \mathcal{F}_i - \mathcal{Y}_i \hat{W}(t)) \right) \quad (6-7)$$

where  $\text{proj}(\cdot)$  is a smooth projection operator (see [133, Appendix E], [134, Remark 3.7]) with bounds based on the state bounds and velocity bounds of Assumptions 6.2 and 6.3,  $N \in \mathbb{N}_0$ ,  $k_{CL} \in \mathbb{R}$  and  $\Gamma \in \mathbb{R}^{p \times p}$  are constant, positive definite and symmetric control gains,  $\Delta \eta_i \triangleq \eta^T(t_i) - \eta^T(t_i - \Delta t)$ ,  $\mathcal{F}_i \triangleq \mathcal{F}(t_i)$ ,  $\mathcal{Y}_i \triangleq \mathcal{Y}(t_i)$ , and  $t_i$  represents past time points, i.e.,  $t_i \in [\Delta t, t]$ , at which measurements are available. The principle goal behind this design is to incorporate recorded input and trajectory data to identify the ideal weights. The time points  $t_i$ , and the corresponding  $\Delta \eta_i$ ,  $\mathcal{F}_i$ , and  $\mathcal{Y}_i$  that are recorded and used in (6-7) are referred to as the history stack. As shown in the subsequent stability analysis, the parameter estimate learning rate is related to the minimum eigenvalue of  $\sum_{i=1}^N \mathcal{Y}_i^T \mathcal{Y}_i$ , motivating the use of the singular value maximization algorithm in [108, Chapter 6] for adding data to the history stack.

Using the relation in (6-5), the update law in (6-7) can be simplified to

$$\dot{\hat{W}} = \text{proj} \left( \Gamma \sigma(\rho(\eta(t), t)) \tilde{\eta}(t)^T + k_{CL} \Gamma \sum_{i=1}^N \mathcal{Y}_i^T \mathcal{Y}_i \tilde{W}(t) + k_{CL} \Gamma \sum_{i=1}^N \mathcal{Y}_i^T \mathcal{E}_i \right), \quad (6-8)$$

for all  $t > \Delta t$ , where  $\mathcal{E}_i \triangleq \mathcal{E}(t_i)$ . Taking the time derivative of (6-3), substituting (6-4) and (6-6), and simplifying, yields the following closed-loop error dynamics when

measurements are available

$$\dot{\hat{\eta}}(t) = \tilde{W}(t)^T \sigma(\rho(\eta(t), t)) - k_1 \tilde{\eta}(t) + \varepsilon(\rho(\eta(t), t)) - k_2 \text{sgn}(\tilde{\eta}(t)). \quad (6-9)$$

### 6.2.2 Predictor

During periods when measurements are not available, the state estimates are simulated forward in time using

$$\dot{\hat{\eta}}(t) = \text{proj} \left( \hat{W}(t)^T \sigma(\rho(\hat{\eta}(t), t)) + f(\hat{\eta}(t), t) \right). \quad (6-10)$$

Similarly, the recorded data continues to provide updates to the ideal weight estimates via

$$\dot{\hat{W}}(t) = \text{proj} \left( k_{CL} \Gamma \sum_{i=1}^N \mathcal{Y}_i^T \left( \Delta \eta_i - \mathcal{F}_i - \mathcal{Y}_i \hat{W}(t) \right) \right), \quad (6-11)$$

which can be simplified as

$$\dot{\hat{W}}(t) = \text{proj} \left( k_{CL} \Gamma \sum_{i=1}^N \mathcal{Y}_i^T \mathcal{Y}_i \tilde{W}(t) + k_{CL} \Gamma \sum_{i=1}^N \mathcal{Y}_i^T \mathcal{E}_i \right). \quad (6-12)$$

Taking the time derivative of (6-3), substituting (6-4) and (6-10), and simplifying yields the following closed-loop dynamics when measurements are not available

$$\begin{aligned} \dot{\hat{\eta}}(t) = & \tilde{W}(t)^T \sigma(\rho(\eta(t), t)) + \hat{W}(t)^T (\sigma(\rho(\eta(t), t)) - \sigma(\rho(\hat{\eta}(t), t))) + f(\eta(t), t) \\ & - f(\hat{\eta}(t), t) + \varepsilon(\rho(\eta(t), t)). \end{aligned} \quad (6-13)$$

## 6.3 Analysis

The system considered in this work operates in two modes. The evolution of a Lyapunov-like function is developed in Lemma 6.1 for the mode when measurements are available and the estimator is used. Similarly, the evolution of a Lyapunov-like function is developed in Lemma 6.2 for the mode when measurements are unavailable and the predictor is active.

In addition to the switching that occurs as measurements become intermittently unavailable, in the following stability analysis, time is partitioned into two phases. During the initial phase, insufficient data has been collected to satisfy a richness condition on the history stack. In Theorem 6.1 it is shown that the designed estimator and adaptive update law are still sufficient for the system to remain bounded for all time despite the lack of data. After a finite period of time, the system transitions to the second phase, where the history stack is sufficiently rich and the estimator and adaptive update law are shown, in Theorem 6.2, to asymptotically converge to an arbitrarily small bound. To guarantee that the transition to the second phase happens in finite time, and therefore the overall system trajectories are ultimately bounded, we require the history stack be sufficiently rich after a finite period of time, as specified in the following assumption.

**Assumption 6.4.**

$$\exists \underline{\lambda}, T > 0 : \forall t \geq T, \lambda_{\min} \left\{ \sum_{i=1}^N \mathcal{Y}_i^T \mathcal{Y}_i \right\} \geq \underline{\lambda}, \quad (6-14)$$

where  $\lambda_{\min} \{ \cdot \}$  refers to the minimum eigenvalue of  $\{ \cdot \}$ .

The condition in (6-14) requires that the system be sufficiently excited, though is weaker than the persistence of excitation condition since excitation is unnecessary once  $\sum_{i=1}^N \mathcal{Y}_i^T \mathcal{Y}_i$  is full rank.

To facilitate the following analysis, let  $t_n^{\text{on}}$  and  $t_n^{\text{off}}$  denote the  $n^{\text{th}}$  instance at which measurements become available and unavailable, respectively. Then during  $t \in [t_n^{\text{on}}, t_n^{\text{off}})$  measurements are available and the estimator is active, whereas during  $t \in [t_n^{\text{off}}, t_{n+1}^{\text{on}})$  measurements are unavailable and the predictor is active. The duration of contiguous time each of these modes are active is denoted  $\Delta t_n^{\text{on}} \triangleq t_n^{\text{off}} - t_n^{\text{on}}$  and  $\Delta t_n^{\text{off}} \triangleq t_{n+1}^{\text{on}} - t_n^{\text{off}}$ , respectively, and the total amount of time each of these modes is active between switching instances  $a$  and  $b$  are denoted  $T^{\text{on}}(a, b) \triangleq \sum_{i=a}^b \Delta t_i^{\text{on}}$  and  $T^{\text{off}}(a, b) \triangleq \sum_{i=a}^b \Delta t_i^{\text{off}}$ , respectively. Also,  $\xi(t) \triangleq \begin{bmatrix} \tilde{\eta}(t)^T & \text{vec}(\tilde{W}(t))^T \end{bmatrix}^T \in \mathbb{R}^{7+7p}$  denotes a stacked state and parameter error vector, where  $\text{vec}(\cdot)$  denotes a stack of the columns of  $(\cdot)$ . Finally,

$V : \mathbb{R}^{7+7p} \rightarrow \mathbb{R}$  is a Lyapunov-like function defined as

$$V(\xi(t)) \triangleq \frac{1}{2} \tilde{\eta}(t)^T \tilde{\eta}(t) + \frac{1}{2} \text{tr} \left( \tilde{W}(t)^T \Gamma^{-1} \tilde{W}(t) \right), \quad (6-15)$$

which can be bounded as  $\beta_1 \|\xi(t)\|^2 \leq V(\xi(t)) \leq \beta_2 \|\xi(t)\|^2$ , where  $\text{tr}(\cdot)$  denotes the matrix trace operator,  $\beta_1 \triangleq \frac{1}{2} \min \{1, \lambda_{\min}(\Gamma^{-1})\}$ , and  $\beta_2 \triangleq \frac{1}{2} \max \{1, \lambda_{\max}(\Gamma^{-1})\}$ . Also, due to the projection operator in (6-7) and (6-11), and since  $W$  is a constant,  $\tilde{W}(t)$  is bounded and  $V(\xi(t)) \leq c_2 + c_3 \|\tilde{\eta}(t)\|^2$ , where  $c_2, c_3 \in \mathbb{R}_{>0}$  are positive constants.

**Lemma 6.1.** *The estimator in (6-6) and (6-7) remains bounded during  $t \in [t_n^{\text{on}}, t_n^{\text{off}})$ .*

*Proof.* Taking the time derivative of (6-15) during  $t \in [t_n^{\text{on}}, t_n^{\text{off}})$ , substituting (6-8) and (6-9), and simplifying yields

$$\dot{V}(\xi(t)) \leq -k_1 \|\tilde{\eta}(t)\|^2 + c_1,$$

where  $c_1 \in \mathbb{R}_{>0}$  is a positive constant. Using the bounds on  $V$ ,  $\dot{V}$  can be bounded as

$$\dot{V}(\xi(t)) \leq -\frac{k_1}{c_3} V(\xi(t)) + \left( \frac{k_1 c_2 + c_1}{c_3} \right).$$

Using the Comparison Lemma in [123, Lemma 3.4],

$$V(\xi(t)) \leq V(\xi(t_n^{\text{on}})) \exp[-\lambda(t - t_n^{\text{on}})] + \left( c_2 + \frac{c_1}{k_1} \right), \quad \forall t \in [t_n^{\text{on}}, t_n^{\text{off}}) \quad (6-16)$$

where  $\lambda \triangleq \frac{k_1}{c_3}$ .

Similarly, after sufficient data has been gathered (i.e.,  $t \in [t_n^{\text{on}}, t_n^{\text{off}}) \cap [T, \infty)$ , where  $T$  was defined in Assumption 6.4)

$$V(\xi(t)) \leq V(\xi(t_n^{\text{on}})) \exp[-\lambda_T(t - t_n^{\text{on}})] + c_{UB}, \quad \forall t \in [t_n^{\text{on}}, t_n^{\text{off}}) \cap [T, \infty), \quad (6-17)$$

where  $\lambda_T \triangleq \frac{\min\{k_1, \lambda_{CL}\}}{\beta_2}$ ,  $c_{UB} \triangleq \frac{c_1 \beta_2}{\min\{k_1, \lambda_{CL}\}}$ ,  $\lambda_{CL} \triangleq k_{CL} \lambda_{\min} \left\{ \sum_{i=1}^N \mathcal{Y}_i^T \mathcal{Y}_i \right\}$  and  $\lambda_{CL} > 0$  based on Assumption 6.4.  $\square$

*Remark 6.4.* Note that  $c_1$  is based on a bound on the data in the history stack,  $\mathcal{Y}_i$ , the concurrent learning gain,  $k_{CL}$ , and the bound on function approximation error,  $\bar{\varepsilon}$ , and

therefore cannot be decreased through gain tuning. However,  $c_1$ , and hence the ultimate error bound after sufficient data has been gathered, can be made arbitrarily small by decreasing  $\bar{\varepsilon}$ , e.g., increasing the number of neurons in the NN.

**Lemma 6.2.** *The predictor in (6–10) and (6–11) remains bounded during  $t \in [t_n^{\text{off}}, t_{n+1}^{\text{on}})$ .*

*Proof.* Taking the time derivative of (6–15) during  $t \in [t_n^{\text{off}}, t_{n+1}^{\text{on}})$ , substituting (6–12) and (6–13), and simplifying yields

$$\dot{V}(\xi(t)) \leq c_4 \|\xi(t)\|^2 + c_5$$

where  $c_4, c_5 \in \mathbb{R}_{>0}$  are positive constants. Using bounds on  $V$ ,  $\dot{V}$  can be bounded as

$$\dot{V}(\xi(t)) \leq \frac{c_4}{\beta_1} V(\xi(t)) + c_5.$$

Using the Comparison Lemma in [123, Lemma 3.4],

$$V(\xi(t)) \leq V(\xi(t_n^{\text{off}})) \exp\left[\frac{c_4}{\beta_1}(t - t_n^{\text{off}})\right], \quad \forall t \in [t_n^{\text{off}}, t_{n+1}^{\text{on}}) \quad (6-18)$$

which remains bounded for all bounded  $t$ . □

**Theorem 6.1.** *The estimator and predictor in (6–6), (6–7), (6–10), and (6–11) remain bounded provided there exists a  $k < \infty$ , and sequences  $\{\Delta t_n^{\text{on}}\}_{n=0}^{\infty}$  and  $\{\Delta t_n^{\text{off}}\}_{n=0}^{\infty}$  such that*

$$\frac{c_4}{\beta_1} T^{\text{off}}(nk, (n+1)k) < \lambda_T T^{\text{on}}(nk, (n+1)k), \quad \forall n \in \mathbb{N}. \quad (6-19)$$

*Proof.* Consider a single cycle of losing and regaining measurements, i.e.,  $t \in [t_n^{\text{on}}, t_{n+1}^{\text{on}})$ .

Based on (6–16) and (6–18)

$$V(\xi(t_{n+1}^{\text{on}})) \leq V(\xi(t_n^{\text{on}})) \exp\left[\frac{c_4}{\beta_1} \Delta t_n^{\text{off}} - \lambda \Delta t_n^{\text{on}}\right] + \left(c_2 + \frac{c_1}{k_1}\right) \exp\left[\frac{c_4}{\beta_1} \Delta t_n^{\text{off}}\right]. \quad (6-20)$$

Using (6–20), the evolution of  $V$  over  $k$  cycles is

$$V\left(\xi\left(t_{(n+1)k}^{\text{on}}\right)\right) \leq c_6 V(\xi(t_{nk}^{\text{on}})) + c_7$$

where  $c_6, c_7 \in \mathbb{R}_{>0}$  are positive, bounded constants, and  $c_6 < 1$  based on (6–19). Let  $\{s_n\}_{n=0}^{\infty}$  be a sequence defined by the recurrence relation

$$s_{n+1} = M(s_n),$$

with initial condition  $s_0 = V(\xi(t_0^{\text{on}}))$ , where  $M : \mathbb{R} \rightarrow \mathbb{R}$  is defined as  $M(s) \triangleq c_6 s + c_7$ .

Since  $c_6 < 1$ ,  $M$  is a contraction [124, Definition 9.22], and therefore all initial conditions,

$s_0$ , approach the fixed point  $s = \frac{c_7}{1-c_6}$  [124, Theorem 9.23]. Since the sequence  $\{s_n\}$

upper bounds  $V$  in the sense that  $V(\xi(t_{nk}^{\text{on}})) \leq s_n$ ,  $V$  is also ultimately bounded.

However,  $V$  may grow within  $[t_{nk}^{\text{on}}, t_{(n+1)k}^{\text{on}}]$  since the dwell time condition (6–19) is specified over  $k$  cycles rather than a single cycle, and therefore the ultimate bound of  $\xi$ , which is based on the ultimate bound of  $V$ , is

$$\limsup_t \|\xi(t)\| \leq \beta_1 \frac{c_7}{1-c_6} \exp\left(\frac{c_4}{\beta_1} T_{\max}^{\text{off}}\right),$$

where  $T_{\max}^{\text{off}} \triangleq \sup_n T^{\text{off}}(nk, (n+1)k)$ . □

**Theorem 6.2.** *After sufficient data is collected, i.e.,  $t \in [T, \infty)$ , the estimator and predictor in (6–6), (6–7), (6–10), and (6–11) converge to a bound that can be made arbitrarily small provided there exists a  $k < \infty$ , and sequences  $\{\Delta t_n^{\text{on}}\}_{n=0}^{\infty}$  and  $\{\Delta t_n^{\text{off}}\}_{n=0}^{\infty}$  such that (6–19) is satisfied.*

*Proof.* The proof follows similarly to the proof of Theorem 6.1. Consider a single cycle of losing and regaining measurements after sufficient data has been collected, i.e.,  $t \in [t_n^{\text{on}}, t_{n+1}^{\text{on}}) \cap [T, \infty)$ . Based on (6–17) and (6–18)

$$V(\xi(t_{n+1}^{\text{on}})) \leq V(\xi(t_n^{\text{on}})) \exp\left[\frac{c_4}{\beta_1} \Delta t_n^{\text{off}} - \lambda_T \Delta t_n^{\text{on}}\right] + c_{UB} \exp\left[\frac{c_4}{\beta_1} \Delta t_n^{\text{off}}\right]. \quad (6-21)$$

Using (6–21), the evolution of  $V$  over  $k$  cycles is

$$V\left(\xi\left(t_{(n+1)k}^{\text{on}}\right)\right) \leq c_8 V(\xi(t_{nk}^{\text{on}})) + c_9$$

where  $c_8, c_9 \in \mathbb{R}_{>0}$  are positive, bounded constants, and  $c_8 < 1$  based on (6–19). Let  $\{s_n\}_{n=0}^{\infty}$  be a sequence defined by the recurrence relation

$$s_{n+1} = M(s_n),$$

with initial condition  $s_0 = V(\xi(t_q^{\text{on}}))$ , where  $q \triangleq \underset{n}{\operatorname{argmin}} \{t_n^{\text{on}} > T\}$  and  $M : \mathbb{R} \rightarrow \mathbb{R}$  is defined as  $M(s) \triangleq c_8 s + c_9$ . Since  $c_8 < 1$ ,  $M$  is a contraction [124, Definition 9.22], and therefore all initial conditions,  $s_0$ , approach the fixed point  $s = \frac{c_9}{1-c_8}$  [124, Theorem 9.23]. Similar to Theorem 6.2, the sequence  $\{s_n\}$  upper bounds  $V$  in the sense that  $V(\xi(t_{nk}^{\text{on}})) \leq s_n$ , but  $V$  may grow within  $[t_{nk}^{\text{on}}, t_{(n+1)k}^{\text{on}}]$  since the dwell time condition (6–19) is specified over  $k$  cycles rather than a single cycle, and therefore the ultimate bound of  $\xi$ , is

$$\limsup_t \|\xi(t)\| \leq \beta_1 \frac{c_9}{1-c_8} \exp\left(\frac{c_4}{\beta_1} T_{\max}^{\text{off}}\right),$$

where  $T_{\max}^{\text{off}} \triangleq \sup_n T^{\text{off}}(nk, (n+1)k)$ . □

*Remark 6.5.* The fundamental difference between Theorem 6.1 and Theorem 6.2, and hence the need for sufficiently rich data, is the control over the ultimate error bound. In Theorem 6.1,  $c_7$  is based on  $c_2$ , which is based on a bound on the ideal function approximation weight errors, which is *a priori* determined, and therefore the ultimate error bound cannot be decreased. In Theorem 6.2,  $c_9$  is based on  $c_{UB}$  which can be made arbitrarily small by, for example, increasing the number of neurons in the NN.

## 6.4 Experiments

Experiments were performed to verify the theoretical results and demonstrate the performance of the developed estimation and prediction scheme with online model learning. In the first experiment, a stationary camera observed a target moving in a vector field of the form shown in Figure 6-1. An IDS UI-3060CP was used to capture 1936x1216 pixel resolution images at a rate of 60 frames per second. A Clearpath Robotics TurtleBot 2 with a Kobuki base was utilized as a mobile vehicle simulant (i.e., the target). A fiducial marker was mounted on the mobile robot, and a corresponding

tracking software library (see [131] and [132]) was used to repeatably track the image feature pixel coordinates, as well as provide target pose measurements, when the target was in the camera FOV. A NaturalPoint, Inc. OptiTrack motion capture system was used to record the ground truth pose of the camera and target at a rate of 360 Hz. The pose provided by the motion capture system was also used to estimate the linear and angular velocities of the camera necessary for the estimator, where the current camera velocity estimates were taken to be the slope of the linear regression of the 20 most recent pose data points. The same procedure was used to calculate the linear and angular velocities of the target for ground truth and comparison with the learned model.

For both experiments, radial basis functions were used in the NN, with covariance  $\Sigma_k = 0.3I$ . Estimator gains were selected as  $k_1 = 3$ ,  $k_2 = 0.1$ ,  $k_{CL} = 1$  and  $\Gamma = I$ , and the integration window was selected as  $\Delta t = 0.1$  s.

In the first experiment, the function  $\rho(\eta, t)$  was used to determine the estimated 2D position of the target in the world coordinate system using the camera pose (see Remark 6.2). For this experiment, 81 kernels were used in the NN, with means arranged in a uniform 9x9 grid across the vector field (Figure 6-1), and a total of  $N = 600$  data points were saved in the CL history stack. During the first 60 seconds of the experiment, target visibility was maintained in order to quickly fill the CL history stack. Data was added at a rate of approximately 1 sample per second, resulting in 10% of the history stack filled at the end of the initial learning phase. After the initial phase, periodic measurement loss was induced artificially by intermittently disregarding pose measurements and switching to the predictor. The dwell times for each period were selected randomly as  $t_n^{\text{on}} \sim U(15, 30)$  and  $t_n^{\text{off}} \sim U(10, 20)$ . The results of this experiment are shown in Figures 6-2 through 6-6. As shown in Figures 6-2 and 6-3, the predictor initially performs poorly; however, prediction significantly improves as more data is acquired. Boundedness of the unknown parameter estimates is validated in Figure 6-4. Figures 6-5 and 6-6 demonstrate that once sufficient data is acquired, the NN output

tracks the motion of the target well, therefore reducing the need for large feedback and sliding mode gains, as well as accurately predicting target motion when measurements are unavailable.

A second experiment was performed to demonstrate the application of the results developed in this chapter to a more realistic scenario. Specifically, the goal of this experiment was to use a single moving camera to estimate the pose of two targets independently moving along a road network (shown in Figure 6-7). At intersections in the road network, the targets randomly selected a direction to travel, hence violating Assumption 6.2. In this experiment, a camera on-board a Parrot Bebop 2 quadcopter platform was used to capture 640x368 pixel resolution images, which were wirelessly streamed to an off-board computer at 30 frames per second. The function  $\rho(\eta, t)$  was augmented to also output the estimated target heading in the world coordinate system, and the NN was composed of 172 kernels with means distributed along the road network. Two independent instances of the estimator developed in this chapter were used to estimate the target poses, one for each target, however, since the targets share a common road network, the CL history stack was shared between the two estimators, with a total of  $N = 2000$  data points saved in the stack, thus allowing for the following strategy. During the initial phase, the quadcopter was commanded to follow a single target for approximately 300 seconds, therefore acquiring enough data to reasonably approximate a motion model of the targets along the road network. After the initial phase, the quadcopter was commanded to follow whichever target was closest to an intersection, since this is where the assumptions are violated, i.e., a deterministic function approximator would not be expected to accurately approximate a stochastic function. After the target has selected a direction, and left the intersection, the predictor for this target is activated, and the quadcopter can follow the other target. This strategy matches a reasonable strategy one might employ in a real world scenario: observe a target at intersections or other areas where the target can act randomly, but once the

target has chosen a direction, a sufficiently learned predictor is expected to perform well, and the observer can move on to other targets.

The results of this experiment are shown in Figures 6-8 through 6-15. Figures 6-8, 6-9, 6-12 and 6-13 show the true and estimated pose of the targets in world coordinates, thus demonstrating that after sufficient data is collected, target pose can be accurately estimated even if the target remains outside the camera FOV for significant durations, despite significant delay due to the wireless transmission of the images, as well as the decreased measurement accuracy compared to the first experiment due to the low resolution camera. Figures 6-10 and 6-14 demonstrate the accuracy of the learned parameters.

## **6.5 Summary**

An adaptive observer and predictor were developed to estimate the relative pose of a target from a camera in the presence of intermittent measurements. While measurements are available, data is recorded and used to update an estimate of the target motion model. When measurements are not available, the motion model is used in a predictor to update state estimates. The overall framework is shown to yield ultimately bounded estimation errors, where the bound can be made arbitrarily small through gain tuning, increasing data richness, and function approximation tuning. Experimental results demonstrate the performance of the developed estimator.

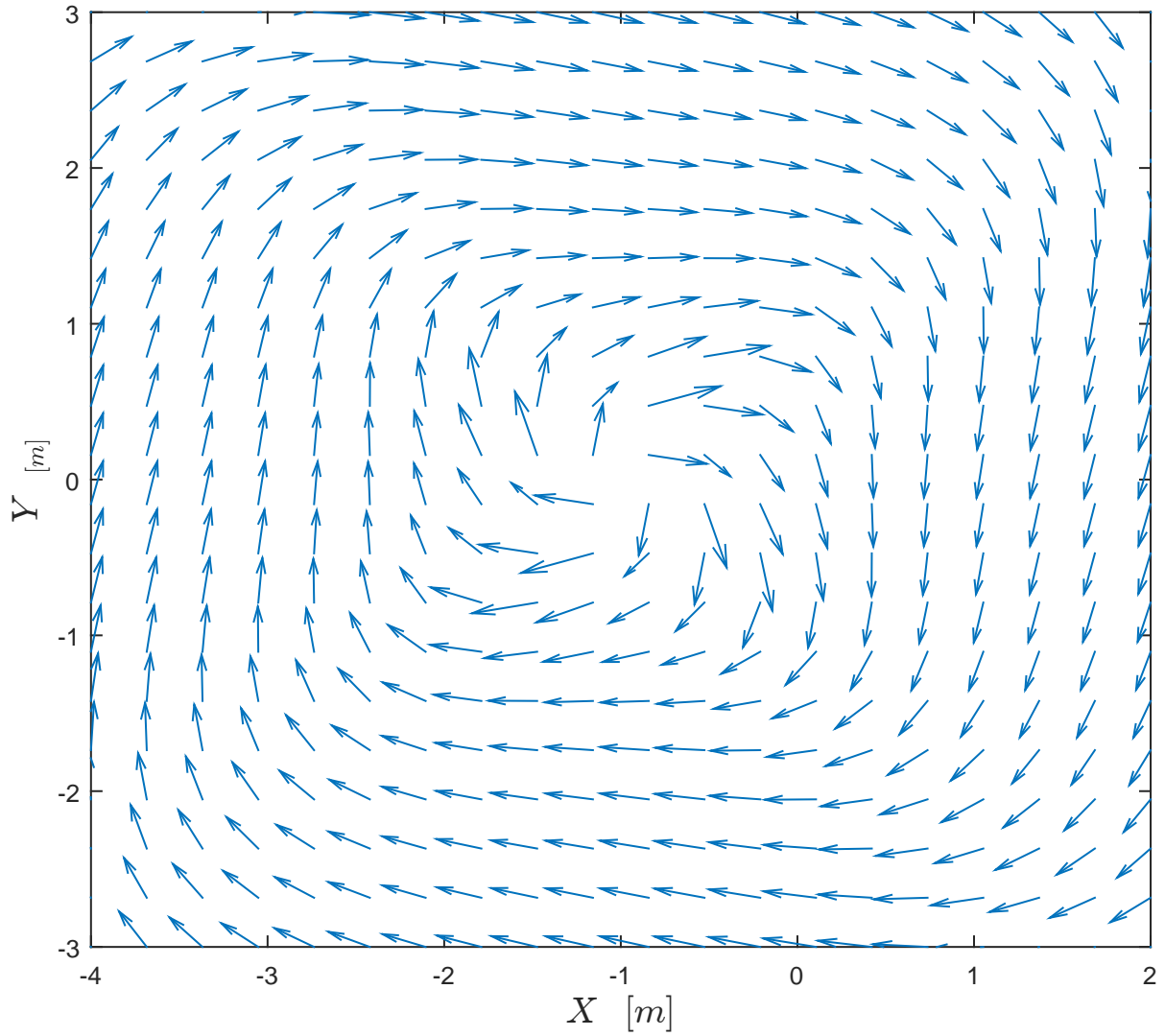


Figure 6-1. During the first experiment, the target was commanded to follow a vector field of this form.

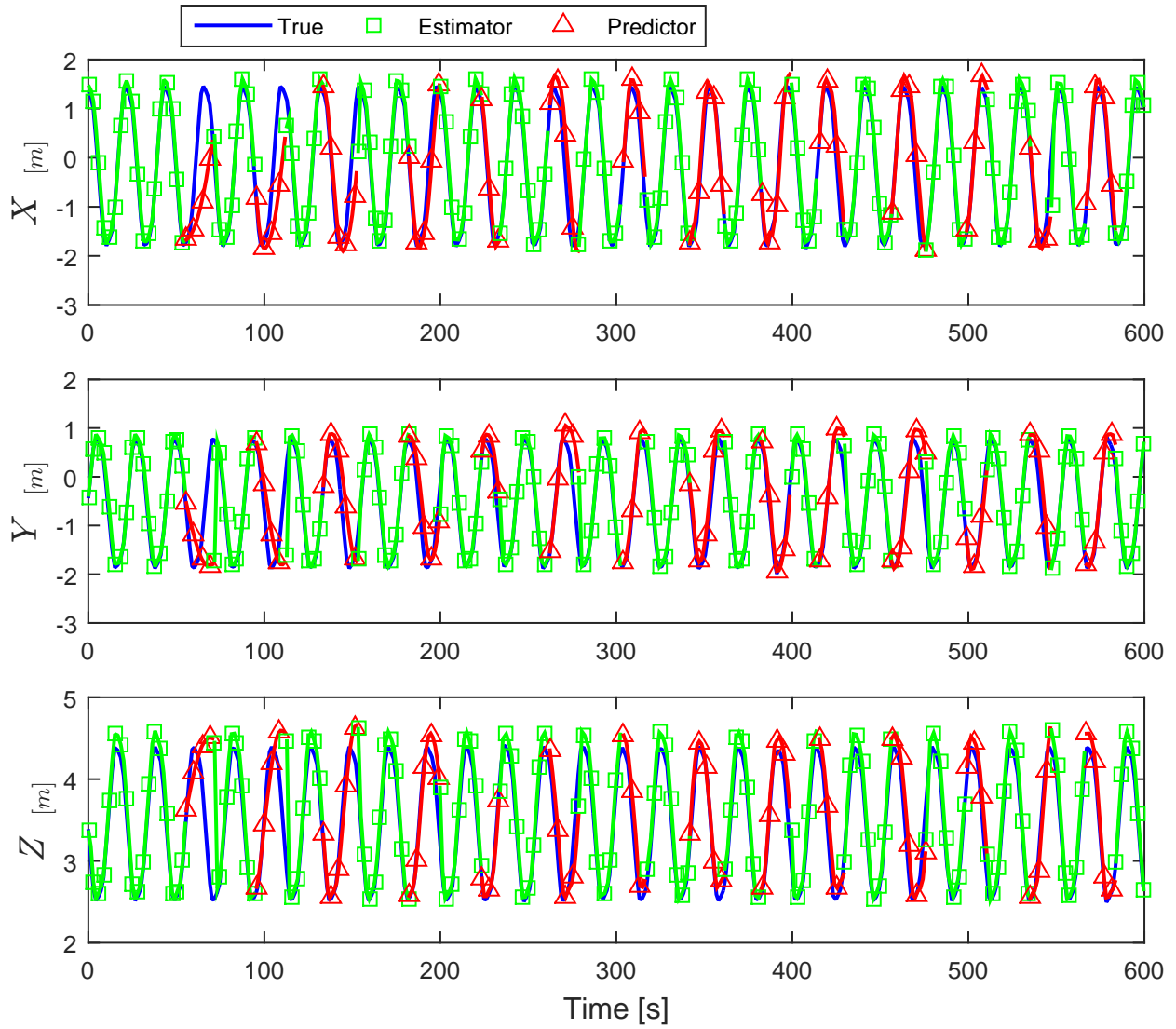


Figure 6-2. Relative position estimates for the first experiment with a stationary camera.

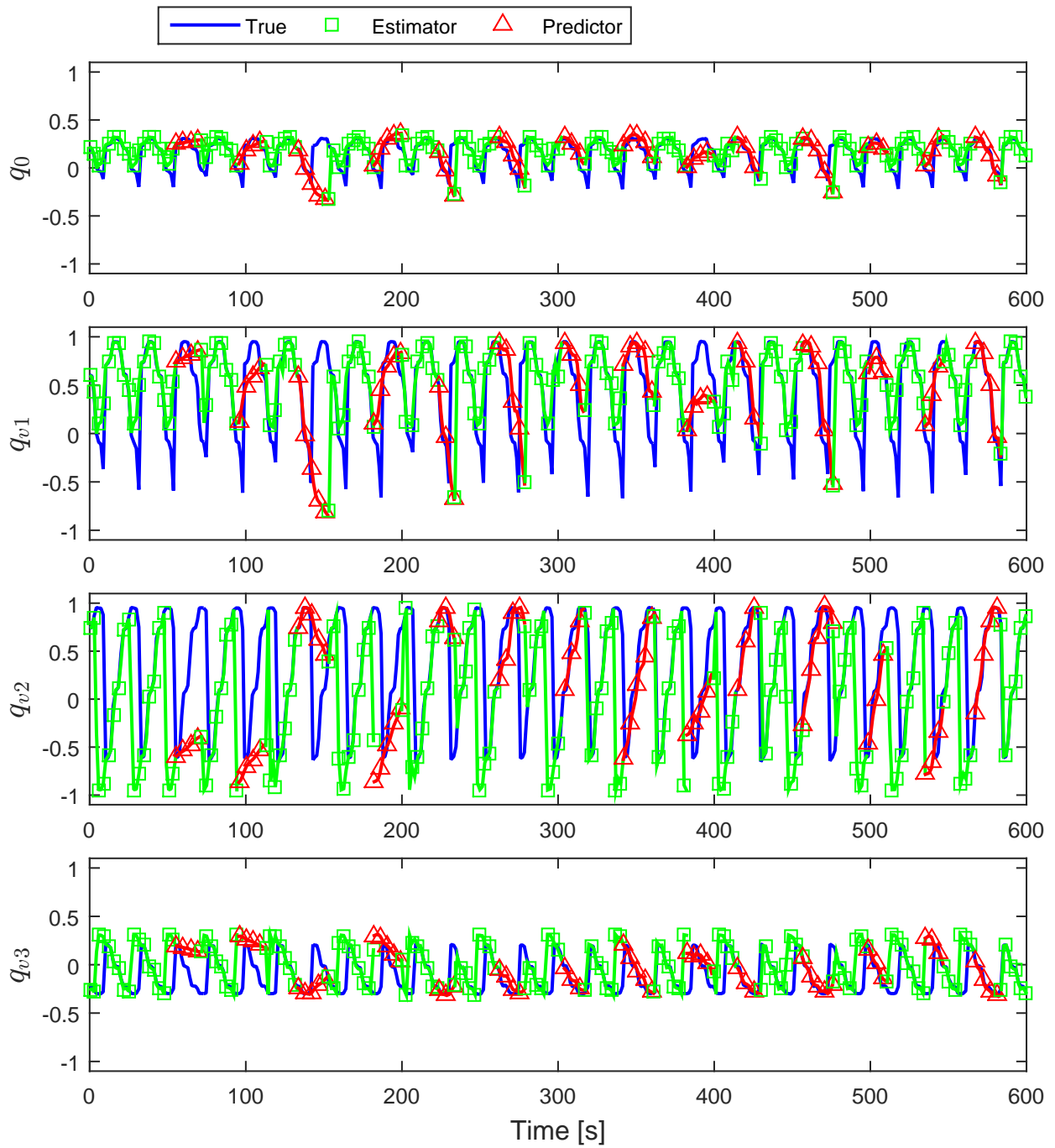


Figure 6-3. Relative orientation estimates for the first experiment with a stationary camera.

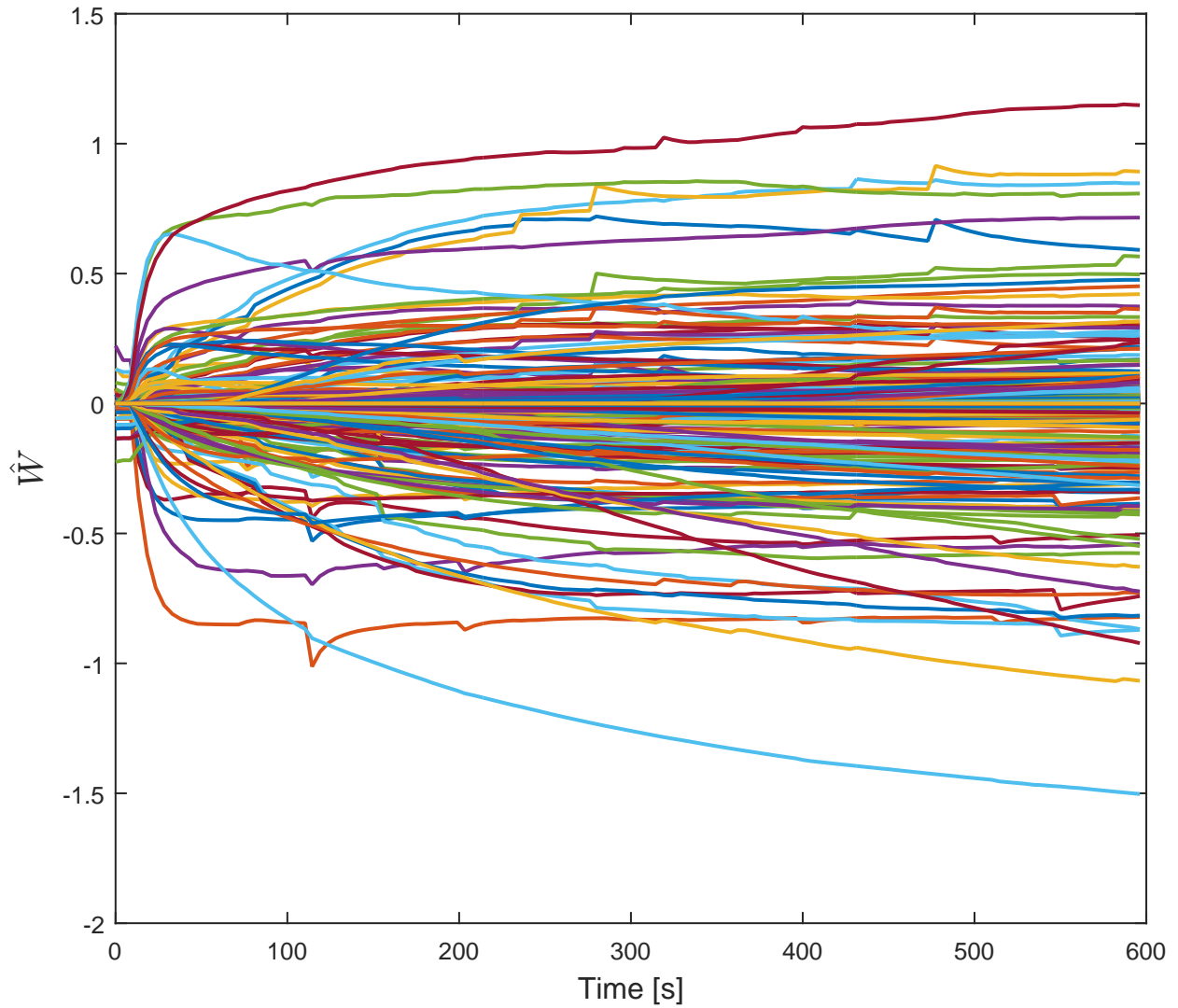


Figure 6-4. Evolution of the NN ideal weight estimates during the first experiment with a stationary camera.

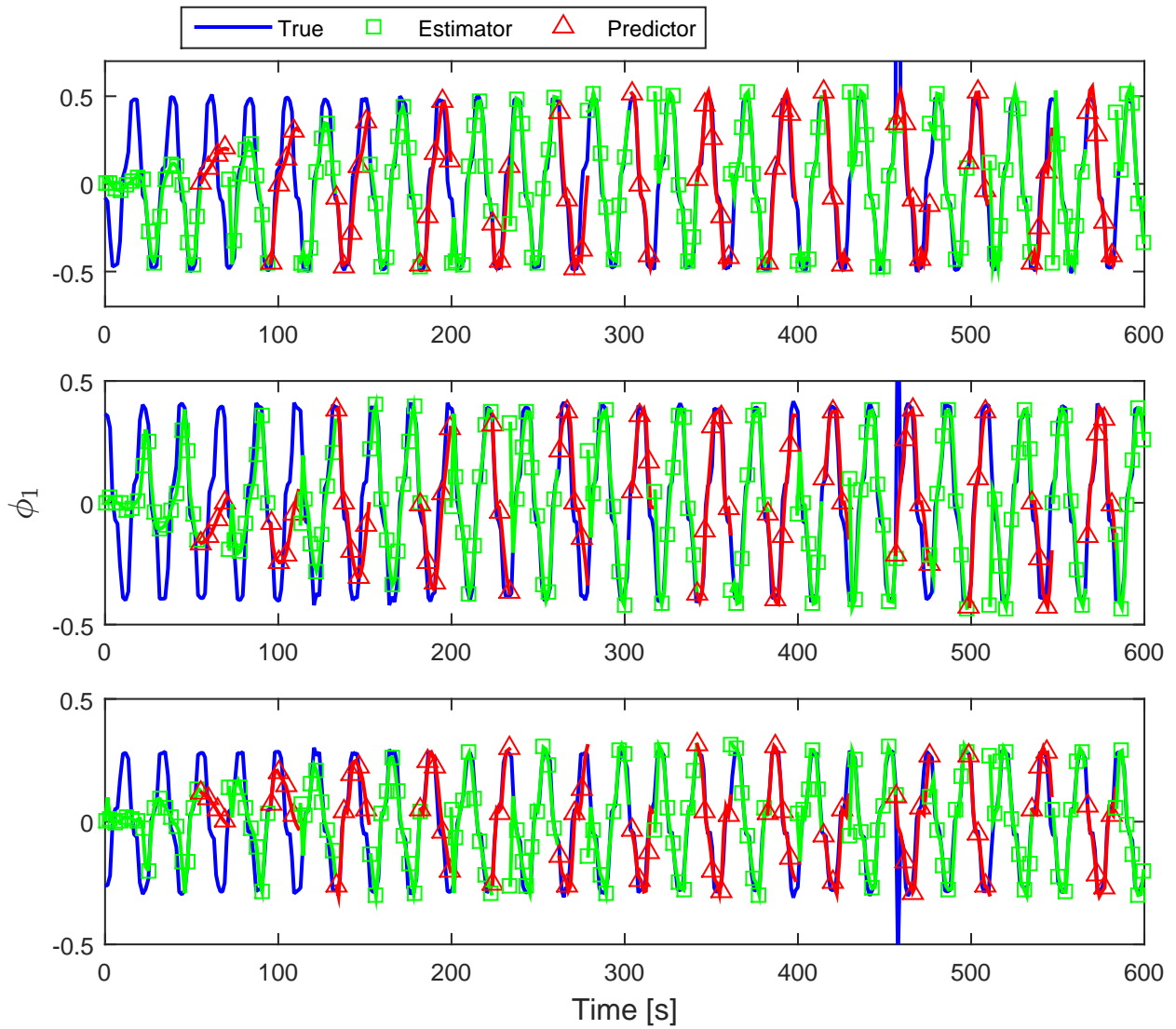


Figure 6-5. Output of the NN compared with ground truth linear velocities for the first experiment with a stationary camera.

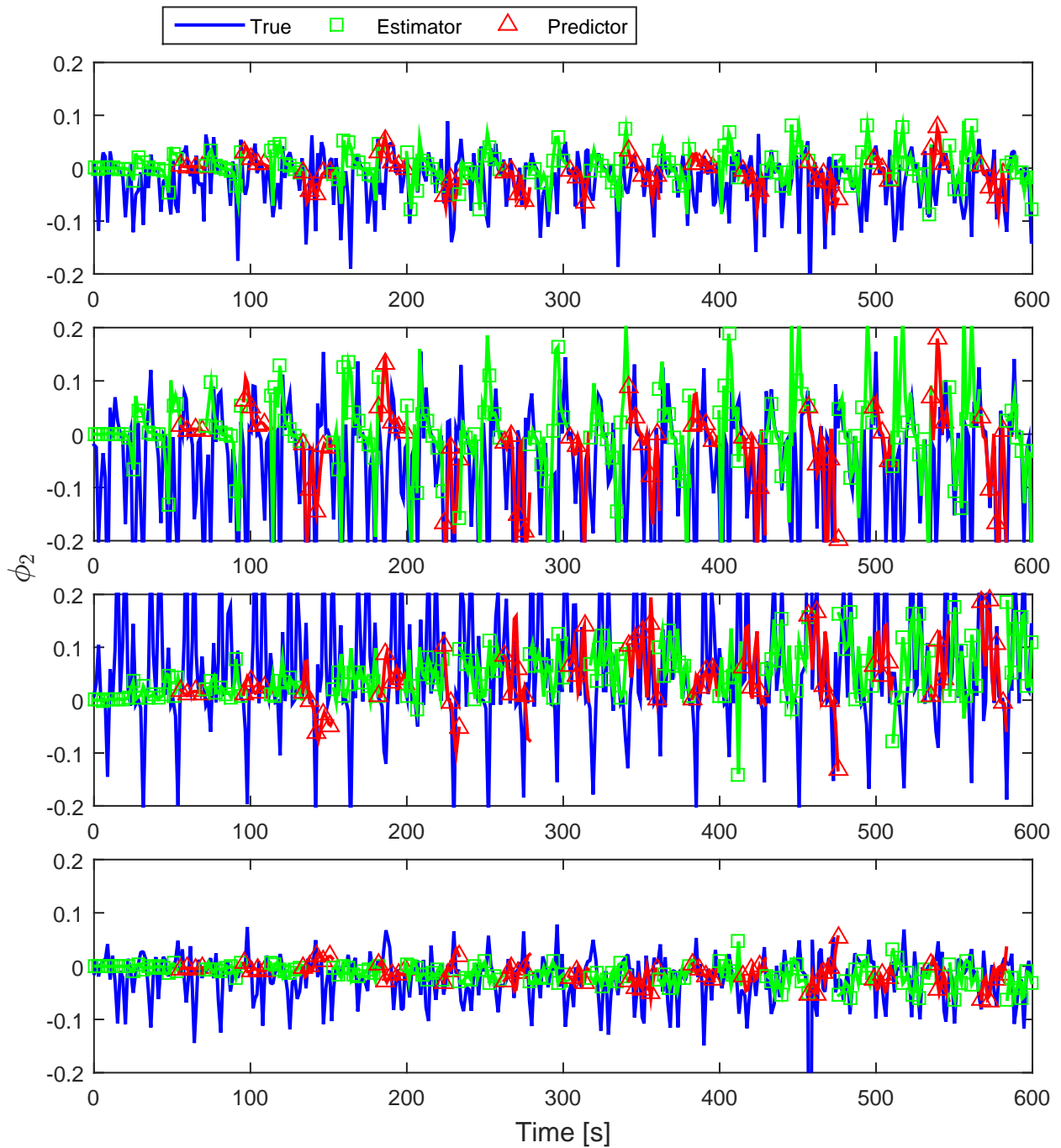


Figure 6-6. Output of the NN compared with ground truth orientation rates (i.e.,  $\frac{1}{2}B(q(t))\omega_q(t)$ ) for the first experiment with a stationary camera.

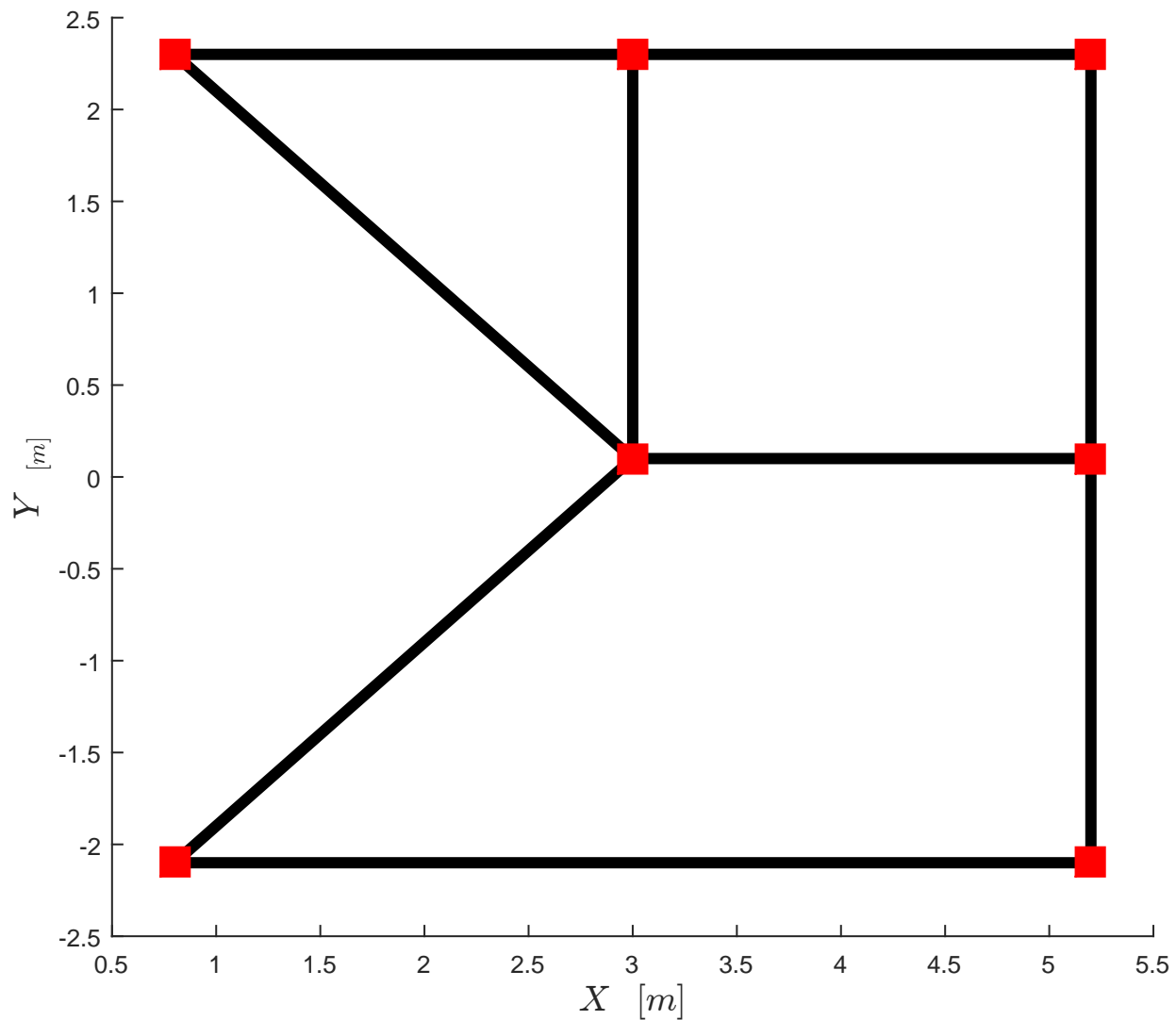


Figure 6-7. During the second experiment, both targets traveled along this network, randomly selecting turns at intersections

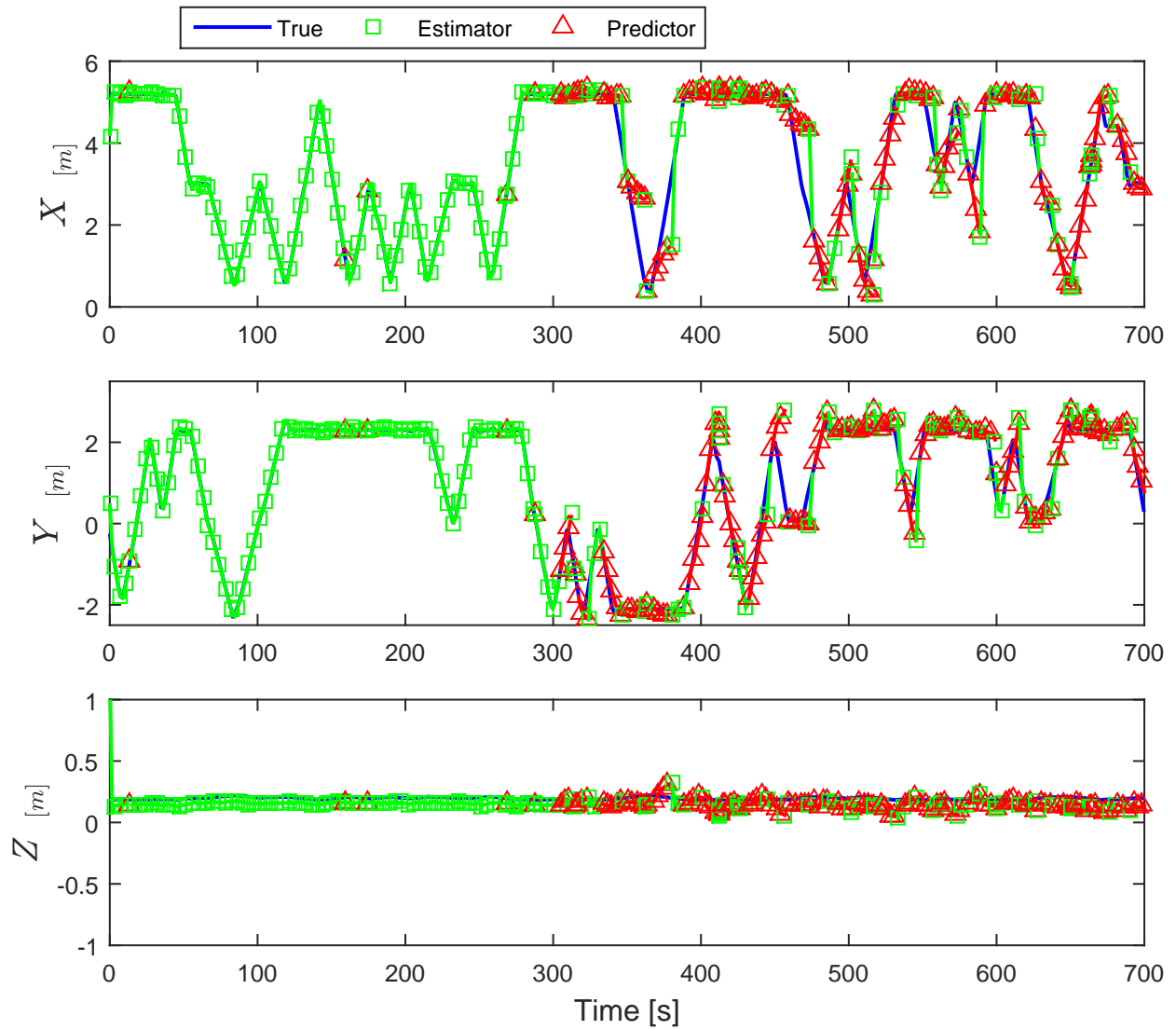


Figure 6-8. Position estimates of target 1 expressed in world coordinates for the second experiment with a quadcopter observing two moving targets.

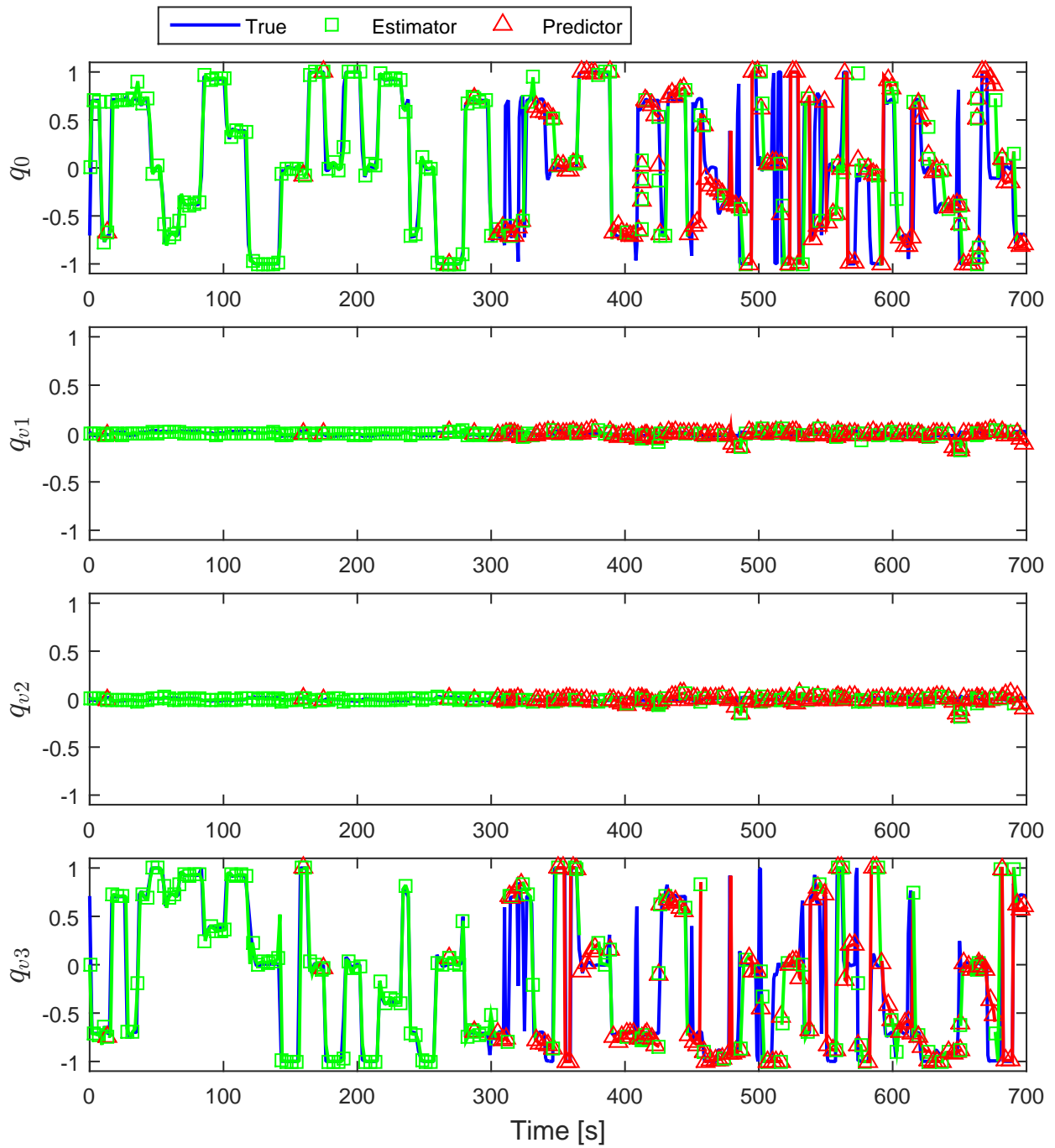


Figure 6-9. Orientation estimates of target 1 relative to the world coordinate system for the second experiment with a quadcopter observing two moving targets.

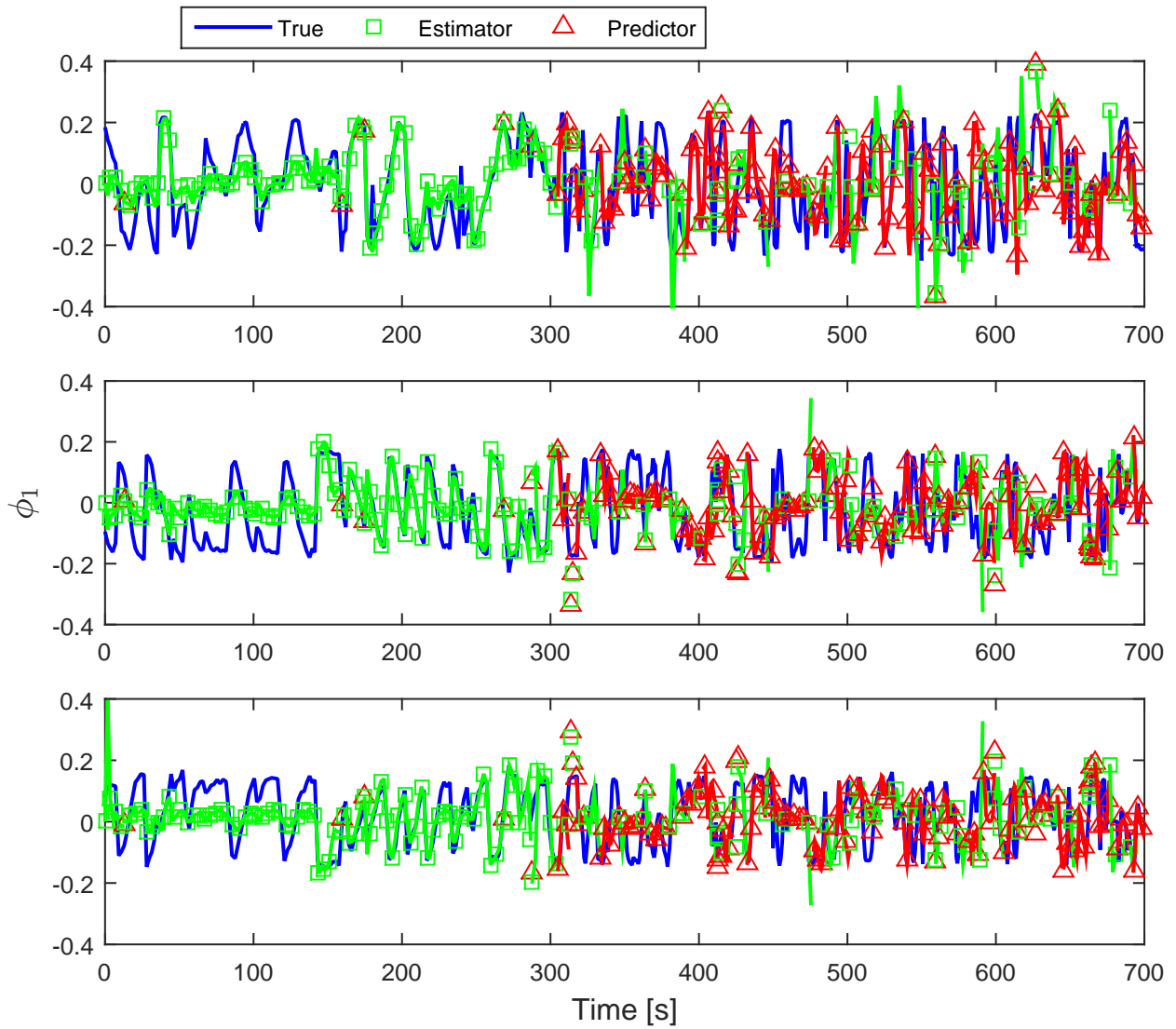


Figure 6-10. Output of the NN compared with ground truth linear velocities of target 1 for the second experiment with a quadcopter observing two moving targets.

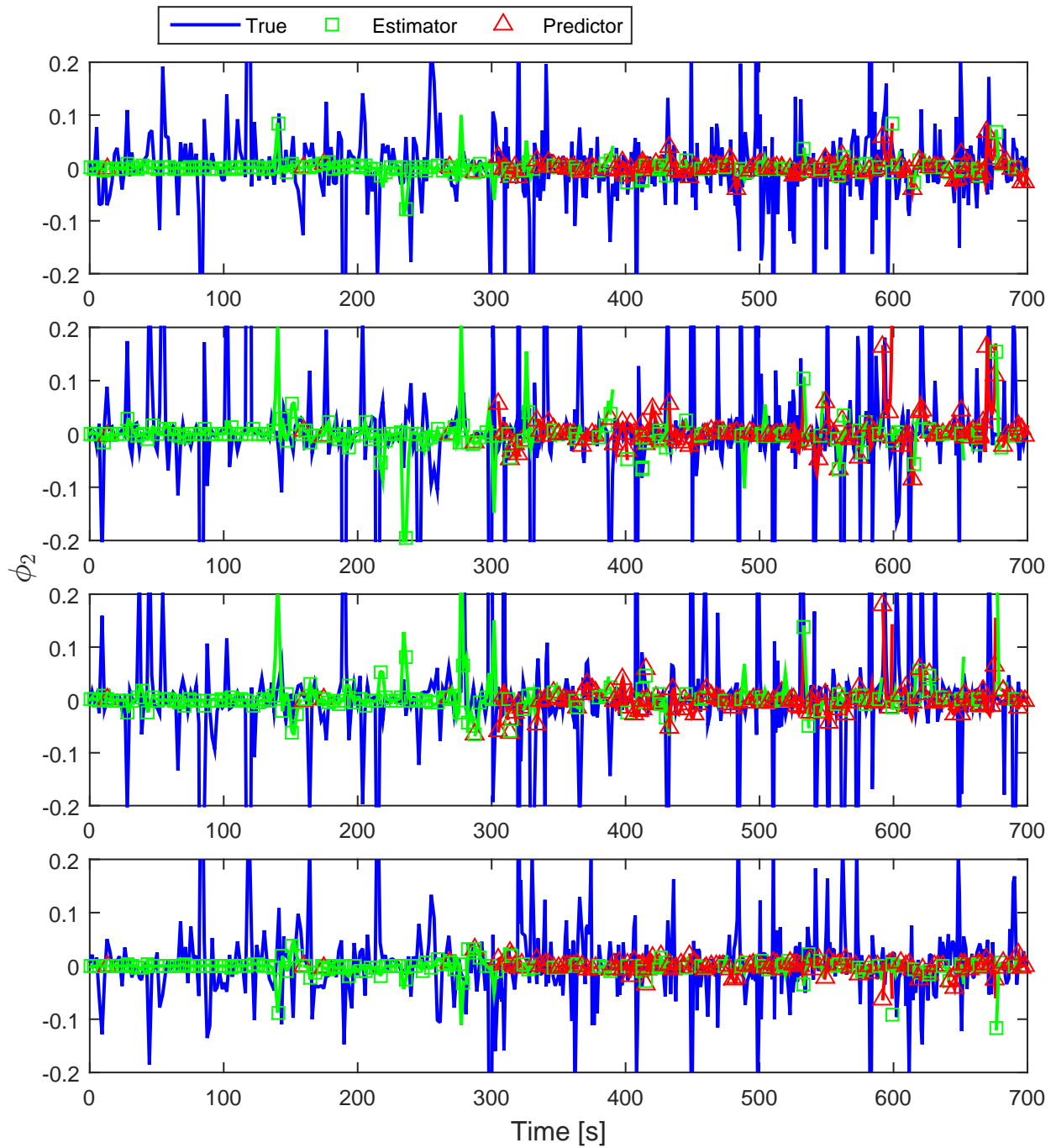


Figure 6-11. Output of the NN compared with ground truth orientation rates (i.e.,  $\frac{1}{2}B(q(t))\omega_q(t)$ ) of target 1 for the second experiment with a quadcopter observing two moving targets.

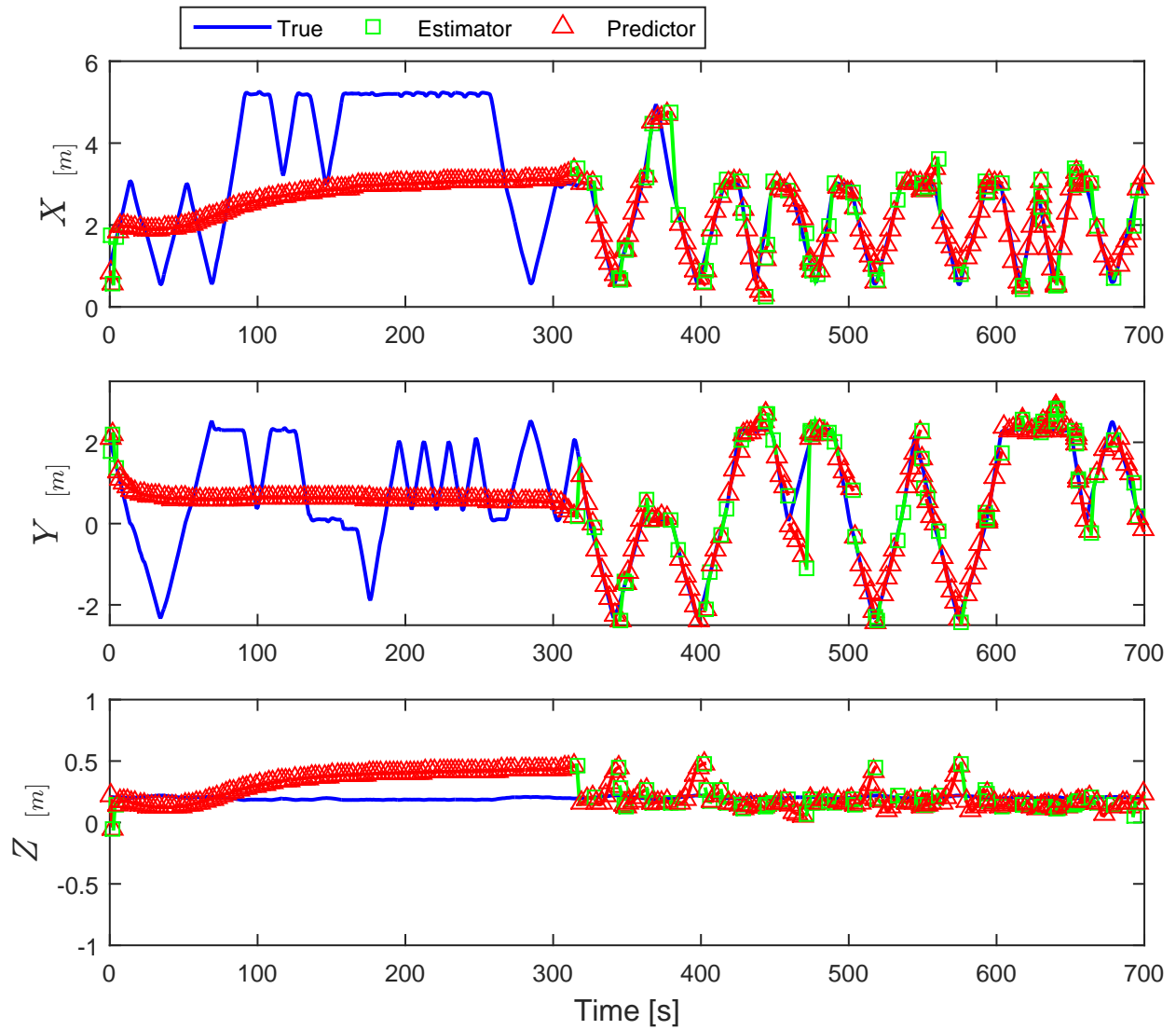


Figure 6-12. Position estimates of target 2 expressed in world coordinates for the second experiment with a quadcopter observing two moving targets.

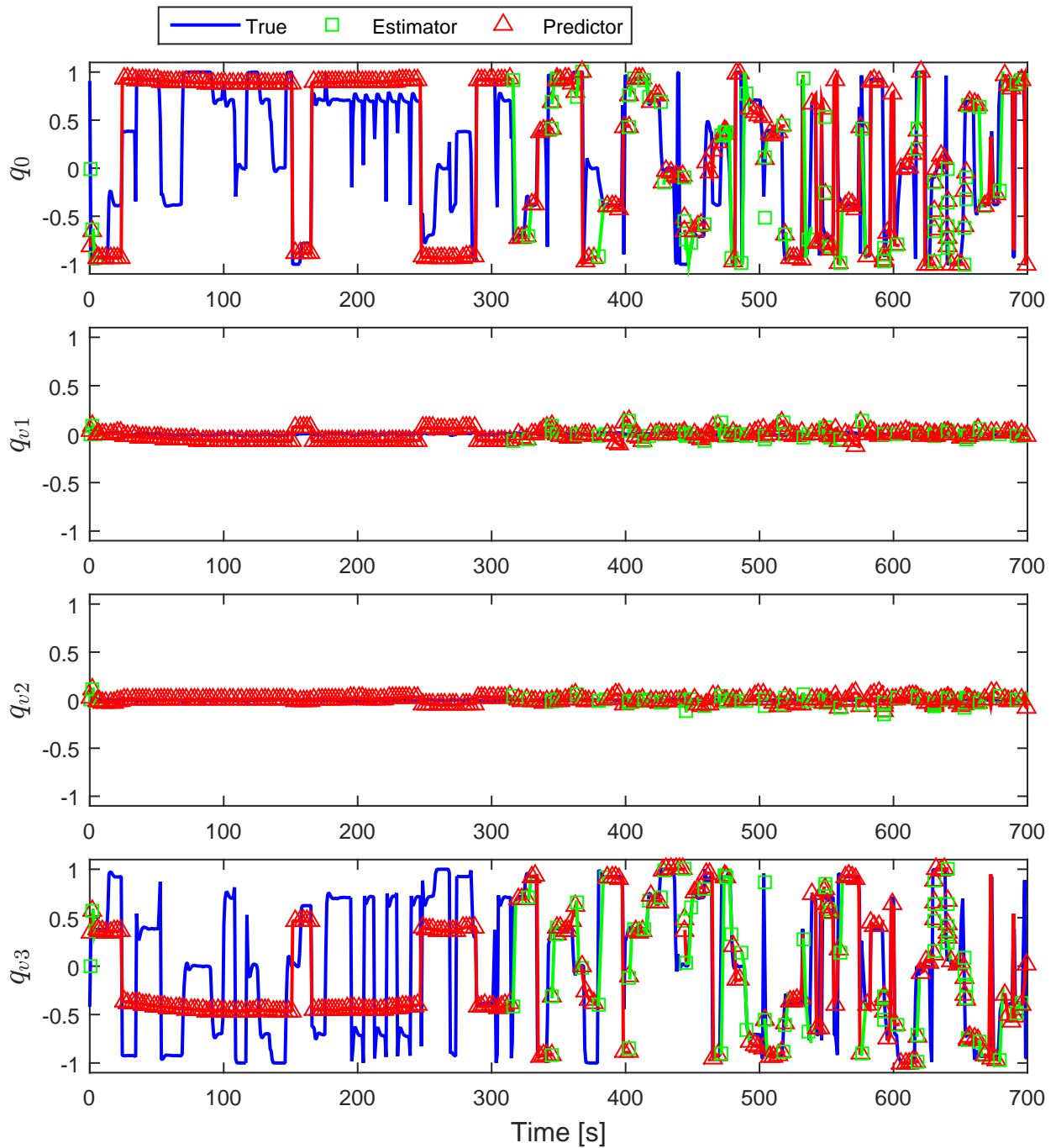


Figure 6-13. Orientation estimates of target 2 relative to the world coordinate system for the second experiment with a quadcopter observing two moving targets.

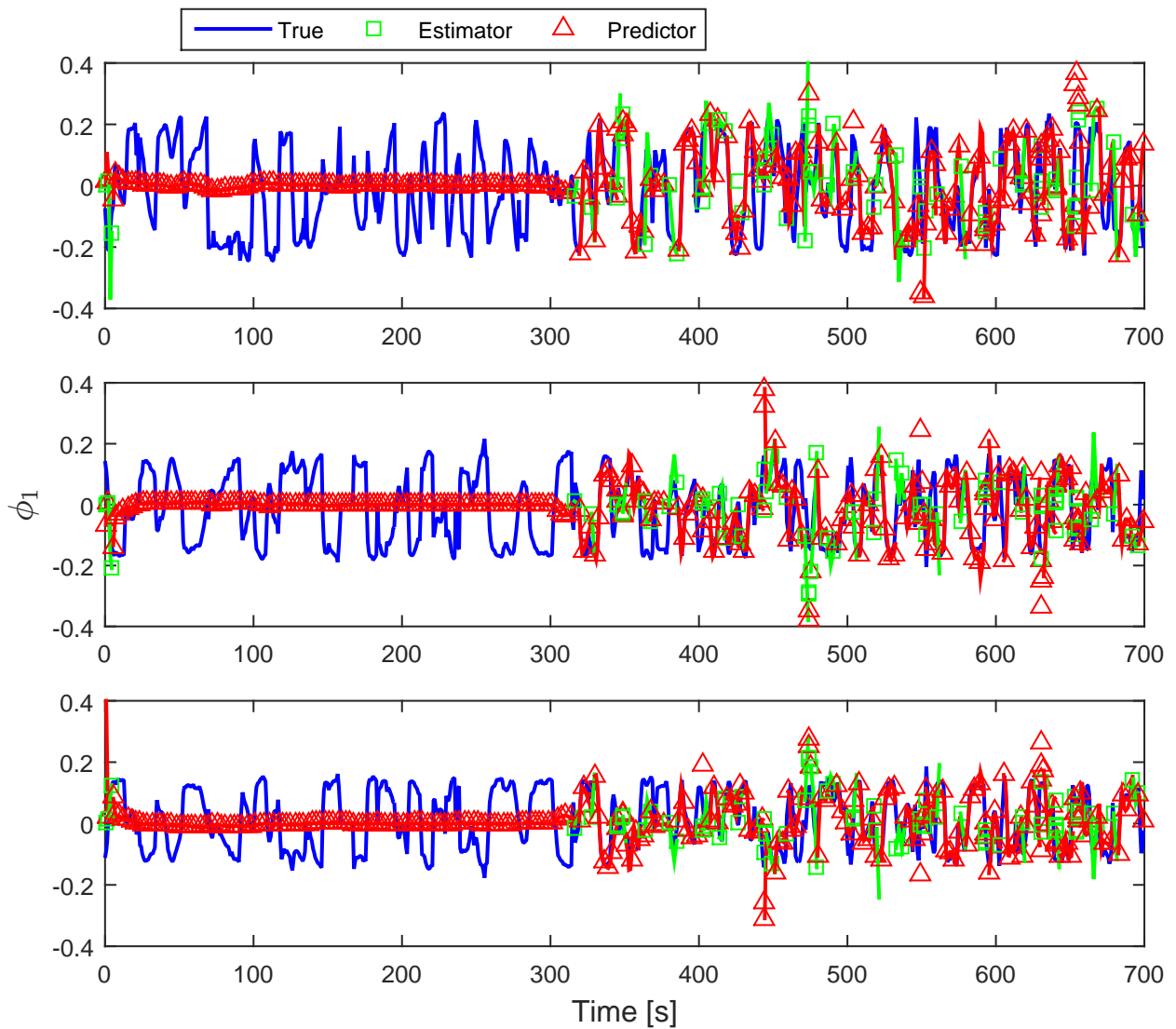


Figure 6-14. Output of the NN compared with ground truth linear velocities of target 2 for the second experiment with a quadcopter observing two moving targets.

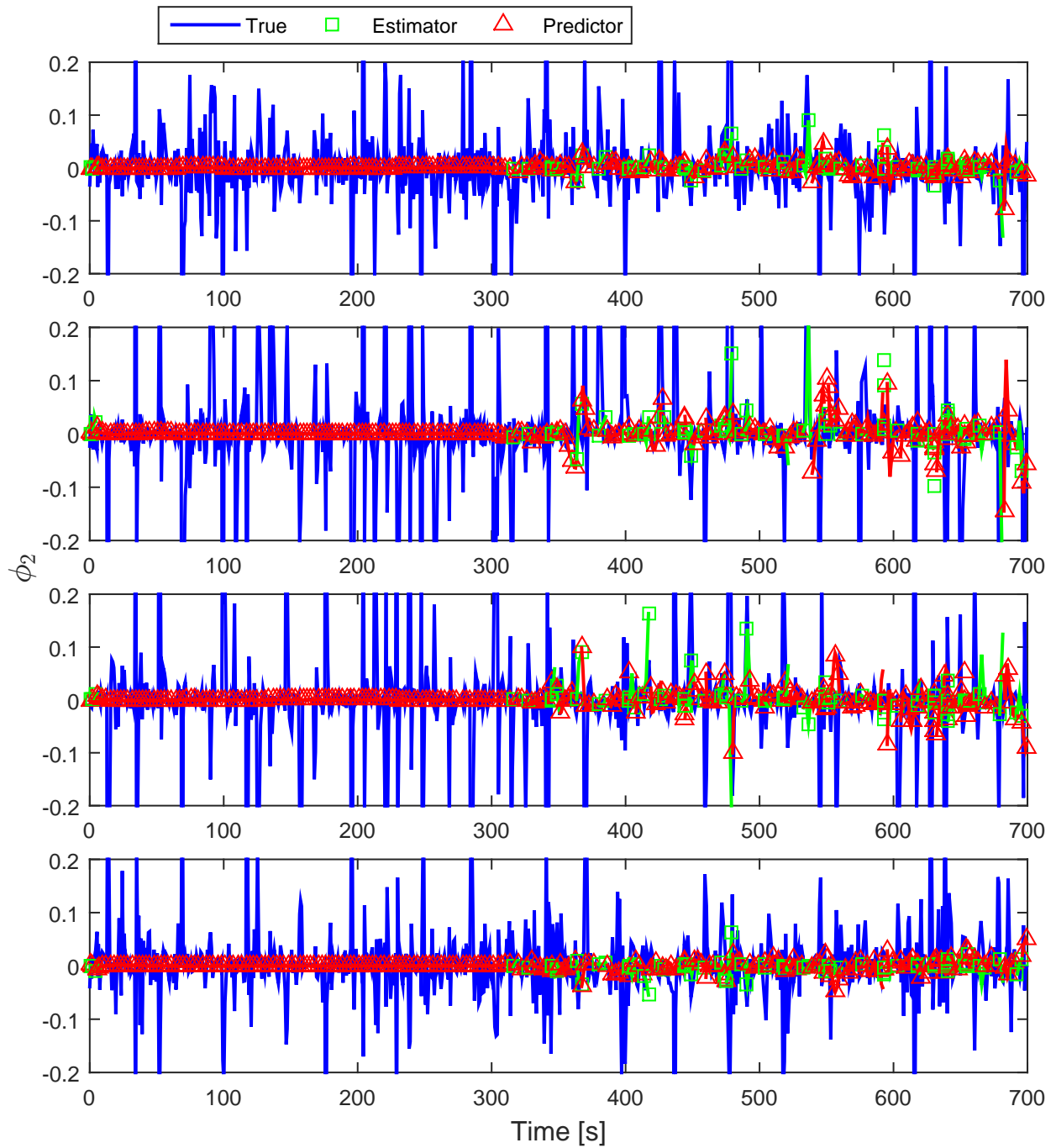


Figure 6-15. Output of the NN compared with ground truth orientation rates (i.e.,  $\frac{1}{2}B(q(t))\omega_q(t)$ ) of target 2 for the second experiment with a quadcopter observing two moving targets.

## CHAPTER 7 CONCLUSIONS

With the advent of technological improvements in imaging systems and computational resources, as well as the development of image-based reconstruction techniques, it is necessary to understand algorithm performance when subject to real world conditions. Specifically, this dissertation focuses on the stability and performance of a class of image-based observers in the presence of intermittent measurements, caused by e.g., occlusions, limited FOV, feature tracking losses, communication losses, or finite frame rates.

Chapter 3 represents a first cut engineering approach to dealing with intermittent measurements. When measurements are available, an observer is used to estimate the full state. The estimate is held constant when measurements are not available, until feedback is reestablished, at which point the observer is reinitialized with the last estimate. This models especially well the real world implementation of continuous image based observer using cameras with finite frame rates. In this general scenario, the estimation error was shown to grow based on the trigonometric tangent function when measurements are unavailable, resulting in a finite escape time and therefore reverse dwell time conditions on each period in which measurements are unavailable to ensure stability. Provided dwell time conditions on the periods in which measurements are available are also met, the estimation errors were shown to converge to an ultimate bound, which can be made arbitrarily small through adjustment of the observer gains and dwell times.

In Chapter 4, a predictor was added to the framework to update state estimates during periods in which measurements are unavailable. As shown in the analysis, this resulted in slower error growth during these periods (i.e., exponential increases versus tangential increase with finite escape when using ZOH), and therefore relaxed dwell time conditions (i.e., average dwell time conditions versus (reverse) dwell time

conditions using ZOH) to ensure stability. Further, provided the average dwell time conditions were satisfied, the estimation error were shown to exponentially converge. However, a motion model of the target must be available in order to implement the predictor, limiting the applicability of this approach. Both Chapters 3 and 4 focused on analyzing a general framework in which a wide class of observers can be utilized to estimate the states when measurements are available, therefore generalizing the results.

To overcome the limitation in requiring a known motion model in order to implement a predictor and benefit from relaxed dwell time conditions and increased performance, the remainder of the dissertation focused on using adaptive control techniques to learn the motion model online. Typical adaptive methods achieve a control objective without actually learning; although the tracking errors are shown to asymptotically converge, parameter estimation errors are only shown to be bounded. Ensuring parameter estimation convergence, and hence system identification, requires the PE assumption. This assumption is restrictive for two reasons: 1) excitation must be persistent, and 2) excitation is unmeasurable. Since typical adaptive methods that utilize PE only update parameter estimates based on current measurements, the system must be excited in perpetuity to ensure the parameter estimates continue to converge. Typically excitation is accomplished by injecting a perturbation signal in the controller or desired trajectory, but perturbing the system for all time runs counter to the original control objective. Also, the PE condition is based on the integral of a matrix over an unknown time window, and methods do not currently exist to *a priori* ensure PE for general nonlinear systems. CL techniques have been developed to ensure parameter convergence, and hence exponential convergence of the overall system, under relaxed finite excitation conditions that can be trivially verified online; however, these techniques require estimation of state derivatives, which are typically not measured and require extensive filter tuning. The primary contribution of Chapter 5 is in the development of an adaptive update law that

ensure parameter convergence without PE or state derivatives, and with a measurable excitation condition, and a Monte Carlo simulation is presented to demonstrate the improved performance of this method compared to traditional CL techniques. This represents a major step forward in adaptive control methods.

The concepts developed in Chapter 5 are utilized in Chapter 6 to implement a framework similar to that developed in Chapter 4 in scenarios where the motion model of the target is unknown. Unlike Chapter 5 where the example systems have a known parametric model with unknown parameters, the form of the target motion model would be unknown in many applications, and therefore a neural network universal function approximator is utilized in this chapter. This results in ultimately bounded convergence when measurements are available, unlike the exponential convergence utilized in Chapters 3 and 4. Despite these complexities, estimation errors are shown to converge to an ultimate bound that can be made arbitrarily small through function approximation tuning, provided  $k$ -average dwell time conditions are satisfied.

One of the limitations of the development in Chapter 6 is the assumption that the target motion model can be represented by an autonomous function (i.e., only explicitly dependent on the states), whereas actual target motion may also be time dependent. This assumption is due to the theoretical results that bound function approximation errors; error bounds can only be established on a compact set, therefore excluding time-varying functions with infinite support. A subject for future research is the use of stochastic models and predictors, from which richer behaviors may be covered while still being limited to autonomous models.

## APPENDIX AUGMENTED STATE OBSERVER

In [122], an observer is designed for the unmeasurable state,  $x_3$ , whereas it is assumed the estimates for the first two states,  $x_1$  and  $x_2$ , are directly measurable. If this design were directly implemented, the state estimates may discontinuously jump whenever the target comes into view, violating the continuity assumption of Theorem 4.1. By using filtered measurements for the complete state estimate, the continuity assumption can be satisfied. The observer used in the experiments in Chapters 3 and 4 is a modified version of the observer in [122] and is defined by the update laws

$$\begin{aligned}\dot{\hat{x}}_1(t) &= h_1(t) \hat{x}_3(t) + p_1(t) + k_1 e_1(t) \\ \dot{\hat{x}}_2(t) &= h_2(t) \hat{x}_3(t) + p_2(t) + k_2 e_2(t) \\ \dot{\hat{x}}_3(t) &= -b_3(t) \hat{x}_3^2(t) - (x_1(t) \omega_2(t) - x_2(t) \omega_1(t)) \hat{x}_3(t) - k_3 (h_1^2(t) + h_2^2(t)) \hat{x}_3(t) \\ &\quad + k_3 h_1(t) (\dot{x}_1(t) - p_1(t)) + k_3 h_2(t) (\dot{x}_2(t) - p_2(t)) + h_1(t) e_1(t) + h_2(t) e_2(t)\end{aligned}$$

where the error signals,  $e(t) \triangleq \begin{bmatrix} e_1(t) & e_2(t) & e_3(t) \end{bmatrix}^T \in \mathbb{R}^3$ , are defined as

$$\begin{aligned}e_1(t) &\triangleq x_1(t) - \hat{x}_1(t), \\ e_2(t) &\triangleq x_2(t) - \hat{x}_2(t), \\ e_3(t) &\triangleq x_3(t) - \hat{x}_3(t),\end{aligned}$$

the linear velocity signal is defined as  $b(t) \triangleq v_q(t) - v_c(t) \in \mathbb{R}^3$ ,  $k_1, k_2, k_3 \in \mathbb{R}$  are positive constants, and the auxiliary signals  $h_1(t), h_2(t), p_1(t), p_2(t) \in \mathbb{R}$  are defined as

$$\begin{aligned}h_1(t) &\triangleq b_1(t) - x_1(t) b_3(t), \\ h_2(t) &\triangleq b_2(t) - x_2(t) b_3(t), \\ p_1(t) &\triangleq x_1(t) x_2(t) \omega_1(t) - (1 + x_1^2(t)) \omega_2(t) + x_2(t) \omega_3(t), \\ p_2(t) &\triangleq (1 + x_2^2(t)) \omega_1(t) - x_1(t) x_2(t) \omega_2(t) - x_1(t) \omega_3(t).\end{aligned}$$

Using the Lyapunov function candidate

$$V(e(t)) = \frac{1}{2}e_1^2(t) + \frac{1}{2}e_2^2(t) + \frac{1}{2}e_3^2(t)$$

it can be shown that

$$\dot{V}(e(t)) \leq -k_1e_1^2(t) - k_2e_2^2(t) - k_4e_3^2(t)$$

for some positive constant  $k_4 \in \mathbb{R}$ , using the same bounding arguments and gain conditions as in [122]. Thus, the augmented observer is exponentially convergent.

## REFERENCES

- [1] A. Yilmaz, O. Javed, and M. Shah, "Object tracking: A survey," *ACM Comput. Surv.*, vol. 38, no. 4, pp. 1–45, 2006.
- [2] W. Hu, T. Tan, L. Wang, and S. Maybank, "A survey on visual surveillance of object motion and behaviors," *IEEE Trans. Syst. Man Cybern.-Part C: Appl. Rev.*, vol. 34, no. 3, pp. 334–352, Aug. 2004.
- [3] S. M. Seitz, B. Curless, J. Diebel, D. Scharstein, and R. Szeliski, "A comparison and evaluation of multi-view stereo reconstruction algorithms," in *Proc. IEEE Comput. Soc. Conf. Comput. Vis. Pattern Recognit.*, vol. 1, Jun. 2006, pp. 519–528.
- [4] T. B. Moeslund, A. Hilton, and V. Krüger, "A survey of advances in vision-based human motion capture and analysis," *Comput. Vis. Image Understand.*, vol. 104, no. 2-3, pp. 90–126, Nov. 2006.
- [5] G. Slabaugh, B. Culbertson, T. Malzbender, and R. Schafer, "A survey of methods for volumetric scene reconstruction from photographs," in *Proc. 2001 Eurographics Conf. Vol. Graph.*, 2001, pp. 81–101.
- [6] O. Russakovsky, J. Deng, H. Su, J. Krause, S. Satheesh, S. Ma, Z. Huang, A. Karpathy, A. Khosla, M. Bernstein, A. C. Berg, and L. Fei-Fei. (2014) Imagenet large scale visual recognition challenge. arXiv:1409.0575.
- [7] M. Everingham, S. M. A. Eslami, L. V. Gool, C. K. I. Williams, J. Winn, and A. Zisserman, "The pascal visual object classes challenge - a retrospective," *Int. J. Comput. Vision*, 2014.
- [8] X. Tan, S. Chen, Z.-H. Zhou, and F. Zhang, "Face recognition from a single image per person: A survey," *Pattern Recognit.*, vol. 39, no. 9, pp. 1725–1745, Sep. 2006.
- [9] W. Zhao, R. Chellappa, P. J. Phillips, and A. Rosenfeld, "Face recognition: A literature survey," *ACM Comput. Surv.*, vol. 35, no. 4, pp. 399–458, Dec. 2003.
- [10] E. Hjelmås and B. K. Low, "Face detection: A survey," *Comput. Vis. Image Understand.*, vol. 83, no. 3, pp. 236–274, Sep. 2001.
- [11] R. J. Radke, S. Andra, O. Al-Kofahi, and B. Roysam, "Image change detection algorithms: A systematic survey," *IEEE Trans. Image Process.*, vol. 14, no. 3, pp. 294–307, Mar. 2005.
- [12] A. Mitiche and P. Bouthemy, "Computation and analysis of image motion: A synopsis of current problems and methods," *Int. J. Comput. Vision*, vol. 19, no. 1, pp. 29–55, Jul. 1996.

- [13] A. J. Davison, I. D. Reid, N. D. Molton, and O. Stasse, "Monoslam: Real-time single camera slam," *IEEE Trans. Pattern Anal. Mach. Intell.*, vol. 29, no. 6, pp. 1052–1067, Jun. 2007.
- [14] S. Y. Chen, "Kalman filter for robot vision: A survey," *IEEE Trans. Ind. Electron.*, vol. 59, no. 11, pp. 4409–4420, Aug. 2011.
- [15] F. Bonin-Font, A. Ortiz, and G. Oliver, "Visual navigation for mobile robots: A survey," *J. Intell. Rob. Syst.*, vol. 53, no. 3, pp. 263–296, Nov. 2008.
- [16] T. Lemaire, C. Berger, I.-K. Jung, and S. Lacroix, "Vision-based slam: Stereo and monocular approaches," *Int. J. Comput. Vision*, vol. 74, no. 3, pp. 343–364, Sep. 2007.
- [17] R. Sim, P. Elinas, and J. J. Little, "A study of the rao-blackwellised particle filter for efficient and accurate vision-based slam," *Int. J. Comput. Vision*, vol. 74, no. 3, pp. 303–318, 2007.
- [18] N. R. Gans and S. A. Hutchinson, "A stable vision-based control scheme for nonholonomic vehicles to keep a landmark in the field of view," in *Proc. IEEE Int. Conf. Robot. Autom.*, Roma, Italy, Apr. 2007, pp. 2196–2201.
- [19] B. Triggs, P. McLauchlan, R. Hartley, and A. Fitzgibbon, "Bundle adjustment - a modern synthesis," in *Vision Algorithms: Theory and Practice*, ser. Lecture Notes in Computer Science. Springer Berlin / Heidelberg, 2000, vol. 1883/2000.
- [20] C. Tomasi and T. Kanade, "Shape and motion from image streams under orthography: a factorization method," *Int. J. Comput. Vision*, vol. 9, no. 2, pp. 137–154, Nov. 1992.
- [21] P. Sturm and B. Triggs, "A factorization based algorithm for multi-image projective structure and motion," *Lect. Notes Comput. Sci.*, vol. 1065, pp. 709–720, 1996.
- [22] O. Dahl and A. Heyden, "Dynamic structure from motion based on nonlinear adaptive observers," in *Int. Conf. Pattern Recognit.*, 2008, pp. 1–4.
- [23] D. Braganza, D. M. Dawson, and T. Hughes, "Euclidean position estimation of static features using a moving camera with known velocities," in *Proc. IEEE Conf. Decis. Control*, New Orleans, LA, USA, Dec 2007, pp. 2695–2700.
- [24] O. Dahl, F. Nyberg, J. Holst, and A. Heyden, "Linear design of a nonlinear observer for perspective systems," in *Proc. IEEE Int. Conf. Robot. Autom.*, Barcelona, Spain, Apr. 2005, pp. 429–435.
- [25] O. Dahl, F. Nyberg, and A. Heyden, "Nonlinear and adaptive observers for perspective dynamic systems," in *Proc. Am. Control Conf.*, New York City, USA, Jul. 2007, pp. 966–971.

- [26] O. Dahl, Y. Wang, A. F. Lynch, and A. Heyden, "Observer forms for perspective systems," *Automatica*, vol. 46, no. 11, pp. 1829–1834, Nov. 2010.
- [27] N. Zarrouati, E. Aldea, and P. Rouchon, "So(3)-invariant asymptotic observers for dense depth field estimation based on visual data and known camera motion," in *Proc. Am. Control Conf.*, Fairmont Queen Elizabeth, Montreal, Canada, Jun. 2012, pp. 4116–4123.
- [28] A. Chiuso, P. Favaro, H. Jin, and S. Soatto, "Structure from motion causally integrated over time," *IEEE Trans. Pattern Anal. Mach. Intell.*, vol. 24, no. 4, pp. 523–535, Apr. 2002.
- [29] D. Karagiannis and A. Astolfi, "A new solution to the problem of range identification in perspective vision systems," *IEEE Trans. Autom. Control*, vol. 50, no. 12, pp. 2074–2077, 2005.
- [30] X. Chen and H. Kano, "A new state observer for perspective systems," *IEEE Trans. Autom. Control*, vol. 47, no. 4, pp. 658–663, 2002.
- [31] L. Ma, C. Cao, N. Hovakimyan, C. Woolsey, and W. E. Dixon, "Fast estimation and range identification in the presence of unknown motion parameters," *IMA J. of App. Math.*, vol. 75, no. 2, pp. 165–189, 2010. [Online]. Available: <http://ncr.mae.ufl.edu/papers/IMA10.pdf>
- [32] S. Gupta, D. Aiken, G. Hu, and W. E. Dixon, "Lyapunov-based range and motion identification for a nonaffine perspective dynamic system," in *Proc. Am. Control Conf.*, Minneapolis, Minnesota, Jun. 2006, pp. 4471–4476.
- [33] W. E. Dixon, Y. Fang, D. M. Dawson, and T. J. Flynn, "Range identification for perspective vision systems," *IEEE Trans. Autom. Control*, vol. 48, pp. 2232–2238, 2003.
- [34] L. Ma, C. Cao, N. Hovakimyan, W. E. Dixon, and C. Woolsey, "Range identification in the presence of unknown motion parameters for perspective vision systems," in *Proc. Am. Control Conf.*, New York, NY, Jul. 2007, pp. 972–977.
- [35] X. Chen and H. Kano, "State observer for a class of nonlinear systems and its application to machine vision," *IEEE Trans. Autom. Control*, vol. 49, no. 11, pp. 2085–2091, 2004.
- [36] A. Dani, Z. Kan, N. Fischer, and W. E. Dixon, "Structure and motion estimation of a moving object using a moving camera," in *Proc. Am. Control Conf.*, Baltimore, MD, 2010, pp. 6962–6967.
- [37] F. Xiong, O. I. Camps, and M. Sznaier, "Dynamic context for tracking behind occlusions," in *Proc. Eur. Conf. Comput. Vis.*, Florence, Italy, Oct. 2012, pp. 580–593.

- [38] T. Ding, M. Sznaier, and O. Camps, "Receding horizon rank minimization based estimation with applications to visual tracking," in *Proc. IEEE Conf. Decis. Control*, Cancun, Mexico, Dec 2008, pp. 3446–3451.
- [39] M. Ayazoglu, B. Li, C. Dicle, M. Sznaier, and O. I. Camps, "Dynamic subspace-based coordinated multicamera tracking," in *Proc. IEEE Int. Conf. Comput. Vis.*, Barcelona, Spain, Nov. 2011, pp. 2462–2469.
- [40] M. Yang, Y. Wu, and G. Hua, "Context-aware visual tracking," *IEEE Trans. Pattern Anal. Mach. Intell.*, vol. 31, no. 7, pp. 1195–1209, Jul. 2009.
- [41] H. Grabner, J. Matas, L. V. Gool, and P. Cattin, "Tracking the invisible: Learning where the object might be," in *Proc. IEEE Conf. Comput. Vis. Pattern Recognit.*, San Francisco, CA, Jun. 2010, pp. 1285–1292.
- [42] L. Cerman, J. Matas, and V. Hlavac, "Sputnik tracker: Having a companion improves robustness of the tracker," in *Proc. Scand. Conf.*, Oslo, Norway, Jun. 2009, pp. 291–300.
- [43] B. R. Fransen, O. I. Camps, and M. Sznaier, "Robust structure from motion and identified dynamics," in *Proc. IEEE Int. Conf. Comput. Vis.*, October 2005, pp. 772–777.
- [44] J. Liang, Z. Wang, and X. Liu, "Distributed state estimation for discrete-time sensor networks with randomly varying nonlinearities and missing measurements," *IEEE Trans. Neural Netw.*, vol. 22, no. 3, pp. 486–496, Mar. 2011.
- [45] L. Ma, F. Da, and K.-J. Zhang, "Exponential  $H_\infty$  filter design for discrete time-delay stochastic systems with Markovian jump parameters and missing measurements," *IEEE Trans. Circuits Syst.*, vol. 58, no. 5, pp. 994–1007, 2011.
- [46] J. Hu, Z. Wang, H. Gao, and L. K. Stergioulas, "Extended Kalman filtering with stochastic nonlinearities and multiple missing measurements," *Automatica*, vol. 48, no. 9, pp. 2007–2015, Sep 2012.
- [47] X. Yao, L. Wu, and W. X. Zheng, "Fault detection filter design for Markovian jump singular systems with intermittent measurements," *IEEE Trans. Signal Process.*, vol. 59, no. 7, pp. 3099–3109, 2011.
- [48] Y. Zhao, J. Lam, and H. Gao, "Fault detection for fuzzy systems with intermittent measurements," *IEEE Trans. Fuzzy Syst.*, vol. 17, no. 2, pp. 398–410, 2009.
- [49] J. You and S. Yin, " $H_\infty$  filtering for time-delay t-s fuzzy systems with intermittent measurements and quantization," *J. Franklin Inst.*, Feb 2013.
- [50] Z. Wang, B. Shen, and X. Liu, " $H_\infty$  filtering with randomly occurring sensor saturations and missing measurements," *Automatica*, vol. 48, no. 3, pp. 556–562, Mar. 2012.

- [51] H. Gao, Y. Zhao, J. Lam, and K. Chen, " $H_\infty$  fuzzy filtering of nonlinear systems with intermittent measurements," *IEEE Trans. Fuzzy Syst.*, vol. 17, no. 2, pp. 291–300, Apr. 2009.
- [52] S. Dey, A. S. Leong, and J. S. Evans, "Kalman filtering with faded measurements," *Automatica*, vol. 45, no. 10, pp. 2223–2233, Oct 2009.
- [53] B. Sinopoli, L. Schenato, M. Franceschetti, K. Poolla, M. Jordan, and S. Sastry, "Kalman filtering with intermittent observations," *IEEE Trans. Autom. Control*, vol. 49, no. 9, pp. 1453–1464, 2004.
- [54] K. You, M. Fu, and L. Xie, "Mean square stability for Kalman filtering with Markovian packet losses," *Automatica*, vol. 47, no. 12, pp. 2647–2657, Dec 2011.
- [55] H. Zhang and Y. Shi, "Observer-based  $H_\infty$  feedback control for arbitrarily time-varying discrete-time systems with intermittent measurements and input constraints," *J. Dyn. Syst., Meas., and Control*, vol. 134, no. 6, Sep. 2012.
- [56] B. Shen, Z. Wang, H. Shu, and G. Wei, "On nonlinear  $H_\infty$  filtering for discrete-time stochastic systems with missing measurements," *IEEE Trans. Autom. Control*, vol. 53, no. 9, pp. 2170–2180, 2008.
- [57] S. C. Smith and P. Seiler, "Optimal pseudo-steady-state estimators for systems with markovian intermittent measurements," in *Proc. Am. Control Conf.*, vol. 4, 2002, pp. 3021–3027.
- [58] H. M. Faridani, "Performance of kalman filter with missing measurements," *Automatica*, vol. 22, no. 1, pp. 117–120, 1986.
- [59] L. K. Carvalho, J. C. Basilio, and M. V. Moreira, "Robust diagnosis of discrete event systems against intermittent loss of observations," *Automatica*, vol. 48, no. 9, pp. 2068–2078, 2012.
- [60] J. You, S. Yin, and H. R. Karimi, "Robust estimation for discrete markov system with time-varying delay and missing measurements," *Math. Probl. Eng.*, 2013.
- [61] Z. Wang, F. Yang, D. W. C. Ho, and X. Liu, "Robust finite-horizon filtering for stochastic systems with missing measurements," *IEEE Signal Process. Lett.*, vol. 12, no. 6, pp. 437–440, Jun. 2005.
- [62] Z. Wang, D. W. Ho, Y. Liu, and X. Liu, "Robust  $H_\infty$  control for a class of nonlinear discrete time-delay stochastic systems with missing measurements," *Automatica*, vol. 45, no. 3, pp. 684–691, 2009.
- [63] Z. Wang, F. Yang, D. W. Ho, and X. Liu, "Robust  $H_\infty$  filtering for stochastic time-delay systems with missing measurements," *IEEE Trans. Signal Process.*, vol. 54, no. 7, pp. 2579–2587, 2006.

- [64] F. O. Hounkpevi and E. E. Yaz, "Robust minimum variance linear state estimators for multiple sensors with different failure rates," *Automatica*, vol. 43, no. 7, pp. 1274–1280, 2007.
- [65] H. Liang and T. Zhou, "Robust state estimation for uncertain discrete-time stochastic systems with missing measurements," *Automatica*, vol. 47, no. 7, pp. 1520–1524, 2011.
- [66] L. Ma, Z. Wang, J. Hu, Y. Bo, and Z. Guo, "Robust variance-constrained filtering for a class of nonlinear stochastic systems with missing measurements," *Signal Process.*, vol. 90, no. 6, pp. 2060–2071, Jun 2010.
- [67] J. Liang, Z. Wang, and X. Liu, "State estimation for coupled uncertain stochastic networks with missing measurements and time-varying delays: the discrete-time case," *IEEE Trans. Neural Netw.*, vol. 20, no. 5, pp. 781–793, 2009.
- [68] S. Kluge, K. Reif, and M. Brokate, "Stochastic stability of the extended Kalman filter with intermittent observations," *IEEE Trans. Autom. Control*, vol. 55, no. 2, pp. 514–518, 2010.
- [69] L. Li and Y. Xia, "Stochastic stability of the unscented kalman filter with intermittent observations," *Automatica*, vol. 48, no. 5, pp. 978–981, 2012.
- [70] S. Deshmukh, B. Natarajan, and A. Pahwa, "Stochastic state estimation for smart grids in the presence of intermittent measurements," in *IEEE Lat.-Am. Conf. Commun.*, 2012, pp. 1–6.
- [71] Z. Wang, D. W. Ho, and X. Liu, "Variance-constrained filtering for uncertain stochastic systems with missing measurements," *IEEE Trans. Autom. Control*, vol. 48, no. 7, pp. 1254–1258, 2003.
- [72] E. Garcia and P. J. Antsaklis, "Adaptive stabilization of model-based networked control systems," in *Proc. Am. Control Conf.*, San Francisco, CA, USA, Jul. 2011, pp. 1094–1099.
- [73] N. E. Leonard and A. Olshevsky, "Cooperative learning in multi-agent systems from intermittent measurements," in *Proc. IEEE Conf. Decis. Control*, Florence, Italy, Dec. 2013, pp. 7492–7497.
- [74] Y. Shi, H. Fang, and M. Yan, "Kalman filter-based adaptive control for networked systems with unknown parameters and randomly missing outputs," *Int. J. Robust Nonlinear Control*, vol. 19, no. 18, pp. 1976–1992, Dec. 2009.
- [75] E. Garcia and P. J. Antsaklis, "Model-based event-triggered control for systems with quantization and time-varying network delays," *IEEE Trans. Autom. Control*, vol. 58, no. 2, pp. 422–434, Feb. 2013.
- [76] S. S. Mehta, W. MacKunis, S. Subramanian, E. L. Pasiliao, and J. W. Curtis, "Stabilizing a nonlinear model-based networked control system with communication

- constraints,” in *Proc. Am. Control Conf.*, Washington, DC, Jun. 2013, pp. 1570–1577.
- [77] M. J. McCourt, E. Garcia, and P. J. Antsaklis, “Model-based event-triggered control of nonlinear dissipative systems,” in *Proc. Am. Control Conf.*, Portland, Oregon, USA, Jun. 2014, pp. 5355–5360.
- [78] H. Durrant-Whyte and T. Bailey, “Simultaneous localization and mapping: Part I,” *IEEE Robot. Autom. Mag.*, vol. 13, no. 2, pp. 99–110, 2006.
- [79] T. Bailey and H. Durrant-Whyte, “Simultaneous localization and mapping (SLAM): Part II,” *IEEE Robot. Autom. Mag.*, vol. 13, no. 3, pp. 108–117, September 2006.
- [80] M. W. M. G. Dissanayake, P. Newman, S. Clark, H. F. Durrant-Whyte, and M. Csorba, “A solution to the simultaneous localization and map building (SLAM) problem,” *IEEE Trans. Robot. Autom.*, vol. 17, no. 3, pp. 229–241, 2001.
- [81] G. P. Huang, A. I. Mourikis, and S. I. Roumeliotis, “A quadratic-complexity observability-constrained unscented Kalman filter for SLAM,” *IEEE Trans. Robot.*, vol. 29, no. 5, pp. 1226–1243, October 2013.
- [82] J. Sola, A. Monin, M. Devy, and T. Vidal-Calleja, “Fusing monocular information in multicamera SLAM,” *IEEE Trans. Robot.*, vol. 24, no. 5, pp. 958–968, October 2008.
- [83] J. A. Hesch, D. G. Kottas, S. L. Bowman, and S. I. Roumeliotis, “Consistency analysis and improvement of vision-aided inertial navigation,” *IEEE Trans. Robot.*, vol. 30, no. 1, pp. 158–176, Feb. 2014.
- [84] T. Lupton and S. Sukkarieh, “Visual-inertial-aided navigation for high-dynamic motion in built environments without initial conditions,” *IEEE Trans. Robot.*, vol. 28, no. 1, pp. 61–76, February 2012.
- [85] M. Kaess, A. Ranganathan, and F. Dellaert, “iSAM: Incremental smoothing and mapping,” *IEEE Trans. Robot.*, vol. 24, no. 6, pp. 1365–1378, December 2008.
- [86] M. Montemerlo, S. Thrun, D. Koller, and B. Wegbreit, “FastSLAM 2.0: An improved particle filtering algorithm for simultaneous localization and mapping that provably converges,” in *Proc. Int. Joint Conf. Artif. Intell.*, 2003, pp. 1151–1156.
- [87] G. Grisetti, C. Stachniss, and W. Burgard, “Improved techniques for grid mapping with rao-blackwellised particle filters,” *IEEE Trans. Robot.*, vol. 23, no. 1, pp. 34–46, Feb. 2007.
- [88] E. Mazor, A. Averbuch, Y. Bar-Shalom, and J. Dayan, “Interacting multiple model methods in target tracking: A survey,” *IEEE Trans. Aerosp. Electron. Syst.*, vol. 34, no. 1, pp. 103–123, January 1998.

- [89] S. S. Blackman, *Multiple-target Tracking with Radar Applications*. Artech House, 1986.
- [90] K. Granstrom and U. Orguner, "A PHD filter for tracking multiple extended targets using random matrices," *IEEE Trans. Signal Process.*, vol. 60, no. 11, pp. 5657–5671, November 2012.
- [91] K. Wyffels and M. Campbell, "Negative observations for multiple hypothesis tracking of dynamic extended objects," in *Proc. Am. Control Conf.*, 2014.
- [92] —, "Negative information for occlusion reasoning in dynamic extended multiobject tracking," *IEEE Trans. Robot.*, vol. 31, no. 2, pp. 425–442, April 2015.
- [93] A. Andriyenko, S. Roth, and K. Schindler, "An analytical formulation of global occlusion reasoning for multi-target tracking," in *Proc. IEEE Int. Conf. Comput. Vis. Workshop*, 2011, pp. 1839–1846.
- [94] H. Wei, W. Lu, P. Zhu, S. Ferrari, R. H. Klein, S. Omidshafiei, and J. P. How, "Camera control for learning nonlinear target dynamics via bayesian nonparametric dirichlet-process gaussian-process (dp-gp) models," in *Proc. IEEE/RSJ Int. Conf. Intell. Robot. Syst.*, 2014, pp. 95–102.
- [95] W. Lu, G. Zhang, S. Ferrari, and I. Palunko, "An information potential approach for tracking and surveilling multiple moving targets using mobile sensor agents," in *Proc. SPIE 8045 Unmanned Syst. Technol. XIII*, 2011.
- [96] J. Joseph, F. Doshi-Velez, A. S. Huang, and N. Roy, "A bayesian nonparametric approach to modeling motion patterns," *Auton. Robot.*, vol. 31, no. 4, pp. 383–400, 2011.
- [97] M. K. C. Tay and C. Laugier, *Field and Service Robotics*, ser. Springer Tracts in Advanced Robotics. Springer Berlin Heidelberg, 2008, vol. 42, ch. Modelling Smooth Paths Using Gaussian Processes, pp. 381–390.
- [98] J. Ko and D. Fox, "Gp-bayesfilters: Bayesian filtering using gaussian process prediction and observation models," *Auton. Robot.*, vol. 27, no. 1, pp. 75–90, 2009.
- [99] D. Ellis, E. Sommerlade, and I. Reid, "Modelling pedestrian trajectory patterns with gaussian processes," in *Proc. IEEE Int. Conf. Comput. Vis. Workshops*, 2009, pp. 1229–1234.
- [100] R. Goebel, R. Sanfelice, and A. Teel, *Hybrid Dynamical Systems*. Princeton University Press, 2012.
- [101] D. Liberzon, *Switching in Systems and Control*. Birkhauser, 2003.
- [102] G. Zhai, B. Hu, K. Yasuda, and A. N. Michel, "Stability analysis of switched systems with stable and unstable subsystems: An average dwell time approach," *Int. J. Syst. Sci.*, vol. 32, no. 8, pp. 1055–1061, Nov. 2001.

- [103] M. A. Müller and D. Liberzon, "Input/output-to-state stability and state-norm estimators for switched nonlinear systems," *Automatica*, vol. 48, no. 9, pp. 2029–2039, 2012.
- [104] P. Ioannou and J. Sun, *Robust Adaptive Control*. Prentice Hall, 1996.
- [105] K. Narendra and A. Annaswamy, *Stable Adaptive Systems*. Prentice-Hall, Inc., 1989.
- [106] S. Sastry and M. Bodson, *Adaptive Control: Stability, Convergence, and Robustness*. Upper Saddle River, NJ: Prentice-Hall, 1989.
- [107] G. V. Chowdhary and E. N. Johnson, "Theory and flight-test validation of a concurrent-learning adaptive controller," *J. Guid. Control Dynam.*, vol. 34, no. 2, pp. 592–607, Mar. 2011.
- [108] G. Chowdhary, "Concurrent learning for convergence in adaptive control without persistency of excitation," Ph.D. dissertation, Georgia Institute of Technology, Dec. 2010.
- [109] G. Chowdhary, T. Yucelen, M. Mühlegg, and E. N. Johnson, "Concurrent learning adaptive control of linear systems with exponentially convergent bounds," *Int. J. Adapt. Control Signal Process.*, vol. 27, no. 4, pp. 280–301, 2013.
- [110] H. Schaub and J. Junkins, *Analytical Mechanics of Space Systems*, AIAA, Ed. New York: AIAA Education Series, 2003.
- [111] D. H. Titterton and J. L. Weston, *Strapdown Inertial Navigation Technology*, 2nd ed., ser. IEE Radar, Sonar, Navigation and Avionics Series. The Institution of Electrical Engineers and The American Institute of Aeronautics and Astronautics, 2004.
- [112] Y. Ma, S. Soatto, J. Kosecka, and S. Sastry, *An Invitation to 3-D Vision*. Springer, 2004.
- [113] C. Tomasi and T. Kanade, "Detection and tracking of point features," Carnegie Mellon University, Tech. Rep. CMU-CS-91-132, Apr. 1991.
- [114] D. Lowe, "Distinctive image features from scale-invariant keypoints," in *IJCV*, 2004.
- [115] H. Bay, A. Ess, T. Tuytelaars, and L. Van Gool, "Speeded-up robust features (surf)," *Computer vision and image understanding*, vol. 110, no. 3, pp. 346–359, 2008.
- [116] O. Russakovsky, J. Deng, H. Su, J. Krause, S. Satheesh, S. Ma, Z. Huang, A. Karpathy, A. Khosla, M. Bernstein, A. Berg, and L. Fei-Fei, "Imagenet large scale visual recognition challenge," *Int. J. Comput. Vision*, pp. 1–42, 2015.
- [117] Z. Kalal, K. Mikolajczyk, and J. Matas, "Tracking-learning-detection," *IEEE Trans. Pattern Anal. Mach. Intell.*, vol. 34, no. 7, pp. 1409–1422, July 2012.

- [118] T. Tuytelaars and K. Mikolajczyk, *Local Invariant Feature Detectors: A Survey*, ser. Foundations and Trends in Computer Graphics and Vision. Now Publishers Inc, 2008, vol. 10.
- [119] A. Dani, Z. Kan, N. Fischer, and W. E. Dixon, "Structure estimation of a moving object using a moving camera: An unknown input observer approach," in *Proc. IEEE Conf. Decis. Control*, Orlando, FL, 2011, pp. 5005–5012.
- [120] A. De Luca, G. Oriolo, and P. Robuffo Giordano, "Feature depth observation for image-based visual servoing: Theory and experiments," *Int. J. Robot. Res.*, vol. 27, no. 10, pp. 1093–1116, 2008.
- [121] F. Morbidi and D. Prattichizzo, "Range estimation from a moving camera: an immersion and invariance approach," in *Proc. IEEE Int. Conf. Robot. Autom.*, Kobe, Japan, May 2009, pp. 2810–2815.
- [122] A. Dani, N. Fischer, Z. Kan, and W. E. Dixon, "Globally exponentially stable observer for vision-based range estimation," *Mechatron.*, vol. 22, no. 4, pp. 381–389, Special Issue on Visual Servoing 2012.
- [123] H. K. Khalil, *Nonlinear Systems*, 3rd ed. Upper Saddle River, NJ: Prentice Hall, 2002.
- [124] W. Rudin, *Principles of Mathematical Analysis*. McGraw-Hill, 1976.
- [125] S. S. Mehta, T. Burks, and W. E. Dixon, "A theoretical model for vision-based localization of a wheeled mobile robot in greenhouse applications: A daisy chaining approach," *Computers Electron. Agric.*, vol. 63, pp. 28–37, 2008. [Online]. Available: <http://ncr.mae.ufl.edu/papers/ag08.pdf>
- [126] K. Dupree, N. R. Gans, W. MacKunis, , and W. E. Dixon, "Euclidean calculation of feature points of a rotating satellite: A daisy chaining approach," *AIAA J. Guid. Control Dyn.*, vol. 31, pp. 954–961, 2008.
- [127] R. Sharma, S. Quebe, R. W. Beard, and C. N. Taylor, "Bearing-only cooperative localization," *J. Intell. Robot. Syst.*, vol. 72, no. 3-4, pp. 429–440, December 2013.
- [128] S. I. Roumeliotis and G. A. Bekey, "Distributed multirobot localization," *IEEE Trans. Robot. Autom.*, vol. 18, no. 5, pp. 781–795, Oct. 2002.
- [129] A. I. Mourikis and S. I. Roumeliotis, "Performance analysis of multirobot cooperative localization," *IEEE Trans. Robot.*, vol. 22, no. 4, pp. 666–681, Aug. 2006.
- [130] X. S. Zhou and S. I. Roumeliotis, "Robot-to-robot relative pose estimation from range measurements," *IEEE Trans. Robot.*, vol. 24, no. 6, pp. 1379–1393, December 2008.

- [131] S. Garrido-Jurado, R. Muñoz-Salinas, F. Madrid-Cuevas, and M. Marin-Jimenez, "Automatic generation and detection of highly reliable fiducial markers under occlusion," *Pattern Recognit.*, vol. 47, no. 6, pp. 2280–2292, Jun. 2014.
- [132] "Aruco library," <http://www.uco.es/investiga/grupos/ava/node/26>. [Online]. Available: <http://www.uco.es/investiga/grupos/ava/node/26>
- [133] M. Krstic, I. Kanellakopoulos, and P. V. Kokotovic, *Nonlinear and Adaptive Control Design*. New York, NY, USA: John Wiley & Sons, 1995.
- [134] W. E. Dixon, A. Behal, D. M. Dawson, and S. Nagarkatti, *Nonlinear Control of Engineering Systems: A Lyapunov-Based Approach*. Birkhauser: Boston, 2003.
- [135] J. P. Hespanha and A. S. Morse, "Stability of switched systems with average dwell-time," in *Proc. IEEE Conf. Decis. Control*, Dec. 1999, pp. 2655–2660.
- [136] F. L. Lewis, D. M. Dawson, and C. Abdallah, *Robot Manipulator Control Theory and Practice*. CRC, 2003.
- [137] M. Spong and M. Vidyasagar, *Robot Dynamics and Control*. New York: John Wiley & Sons Inc., 1989.
- [138] B. M. Haralick, C.-N. Lee, K. Ottenberg, and M. Niçølle, "Review and analysis of solutions of the three point perspective pose estimation problem," *Int. J. Comput. Vision*, vol. 13, no. 3, pp. 331–356, December 1994.
- [139] R. Horaud, B. Conio, O. Le Boulleux, and B. Lacolle, "An analytic solution for the perspective 4-point problem," in *Proc. IEEE Conf. Comput. Vis. Pattern Recog.*, 1989, pp. 500–507.
- [140] D. DeMenthon and L. S. Davis, "Exact and approximate solutions of the perspective-three-point problem," *IEEE Trans. Pattern Anal. Mach. Intell.*, vol. 14, no. 11, pp. 1100–1105, 1992.
- [141] X.-S. Gao, X.-R. Hou, J. Tang, and H.-F. Cheng, "Complete solution classification for the perspective-three-point problem," *IEEE Trans. Pattern Anal. Mach. Intell.*, vol. 25, no. 8, pp. 930–943, 2003.
- [142] L. Quan and Z. Lan, "Linear n-point camera pose determination," *IEEE Trans. Pattern Anal. Mach. Intell.*, vol. 21, no. 8, pp. 774–780, 1999.
- [143] T. Q. Phong, R. Horaud, A. Yassine, and P. D. Tao, "Object pose from 2-d to 3-d point and line correspondences," *Int. J. Comput. Vision*, vol. 15, no. 3, pp. 225–243, 1995.
- [144] D. DeMenthon and L. Davis, "Model-based object pose in 25 lines of code," *Int. J. Comput. Vision*, vol. 15, pp. 123–141, 1995.

- [145] N. R. Gans, A. Dani, and W. E. Dixon, "Visual servoing to an arbitrary pose with respect to an object given a single known length," in *Proc. Am. Control Conf.*, Seattle, WA, USA, Jun. 2008, pp. 1261–1267.

## BIOGRAPHICAL SKETCH

Anup Parikh received his Bachelor of Science degree in mechanical and aerospace engineering from the University of Florida in 2008. He continued his graduate studies at UF, joined the Nonlinear Controls and Robotics (NCR) group, and received his Master of Science degree (2014) as well as his Doctor of Philosophy degree (2016) under the supervision of Dr. Warren E. Dixon. His research interests include switched systems, vision based estimation, and adaptive control of nonlinear dynamical systems.